A Dental Assisting System for Procedures Performed by Air–Turbine Handpieces

by

Vahid Zakeri

M.Sc., Shiraz University, 2008
B.Sc., Shiraz University, 2005

Thesis Submitted in Partial Fulfillment of the

Requirements for the Degree of

Doctor of Philosophy

in the

School of Mechatronic Systems Engineering

Faculty of Applied Sciences

SIMON FRASER UNIVERSITY

Fall 2013

Approval

Name: **Vahid Zakeri**

Degree: **Doctor of Philosophy**

Title of Thesis: ***A Dental Assisting System for Procedures Performed by Air–Turbine Handpieces***

Examining Committee: **Chair:** Krishna Vijayaraghavan
Position: Assistant Professor

Siamak Arzanpour
Senior Supervisor
Assistant Professor

Mehrdad Moallem
Supervisor
Professor

Carolyn Sparrey
Supervisor
Assistant Professor

Greg Mori
Internal Examiner
Associate Professor
School of Computing Science

Farrokh Sassani
External Examiner
Professor
Department of Mechanical Engineering
University of British Columbia

Date Defended/Approved: August 13, 2013

Partial Copyright Licence

Ethics Statement

The author, whose name appears on the title page of this work, has obtained, for the research described in this work, either:

a. human research ethics approval from the Simon Fraser University Office of Research Ethics,

or

b. advance approval of the animal care protocol from the University Animal Care Committee of Simon Fraser University;

or has conducted the research

c. as a co-investigator, collaborator or research assistant in a research project approved in advance,

or

d. as a member of a course approved in advance for minimal risk human research, by the Office of Research Ethics.

A copy of the approval letter has been filed at the Theses Office of the University Library at the time of submission of this thesis or project.

The original application for approval and letter of approval are filed with the relevant offices. Inquiries may be directed to those authorities.

Simon Fraser University Library
Burnaby, British Columbia, Canada

update Spring 2010

Abstract

The present thesis introduces a dental assisting system (DAS) for procedures that are performed by air–turbine dental handpieces. Dental restoration is a process that begins with removing carries and affected tissues to retain the functionality of tooth structures. Air–turbine dental handpieces are high–speed rotary cutting tools that are widely used by dentists during this operation. The next stage in the process is filling the cavity with appropriate restorative materials. “Amalgam” and “composite” are two dental restorative materials that are extensively used by dentists. Most old restorations eventually fail and need to be replaced. One of the difficulties in replacing failing restorations is discerning the boundary of the restorative materials. Dentists may remove healthy tooth structures while replacing tooth–colored composites. Although the visibility issue is less challenging for amalgam materials, replacing them still results in loss of healthy tooth layers.

Developing an objective and sensor–based method is a promising approach to monitor restorative operations and prevent removal of healthy tooth structures. The designed DAS uses the audio signals of ATDH during the cutting process. Audio signals are rich sources of information and can be analysed to identify a particular zone of cutting. Support vector machine (SVM), a powerful algorithm for classification, is employed to differentiate the tooth structures from composite/amalgam samples based on their cutting sounds. The averaged short–time Fourier transform coefficients are selected as the features; and the performance of the SVM classifier is evaluated from different aspects such as number of features, feature scaling methods, and the utilized kernels. The obtained results indicated capability and efficiency of the proposed scheme.

The developed DAS can also measure the speed of ATDH, and maintain it during loaded conditions. An indirect speed measurement method is introduced based on the vibration/sound of ATDH. This measurement technique is explained theoretically based on the rotating unbalance concept and the vibration of a fixed–free beam. To control the speed, a proportional–integral controller is designed and tested. The feasibility of this controller in maintaining the speed in the loaded conditions was confirmed by simulations and experiments.

Keywords: Air–turbine dental handpieces; dental materials monitoring scheme; dental restoration; sound classification; speed measurement; speed control

To my parents, Ahmad and Fathieh,

for their unconditional support

and

To the city where I was born and raised:

Shiraz, Iran

Acknowledgements

I believe no achievement is made individually, and rather than a person's effort, perseverance, hope, and commitment, the others' direct and indirect assistance are always involved too. Therefore, my great thanks go to all those who made it possible for me to complete this thesis.

Firstly, I must express my warmest gratitude to my senior supervisor, Dr. Siamak Arzanpour, who granted me the opportunity to continue my studies as a PhD candidate. He allowed me to freely explore different aspects of this research. Through his supervision and encouragement, I was able to develop leadership and management skills in conducting my research. I am sincerely thankful for his guidance, generous support, fairness, and understanding

I am also very grateful to Dr. Babak Chehroudi from UBC's faculty of dentistry, for his invaluable advice and assistance during my PhD research. Some of the experimental parts of this thesis would not have been accomplished without his support and guidance. I am deeply thankful to Dr. Greg Mori for teaching me the machine learning algorithms used in this thesis. My utmost gratitude goes to Dr. Mehrdad Moallem for his great help, supervision, and for the valuable discussions we had. I am very thankful to Dr. Carolyn Sparrey for her supervision and kind advice on the ethics of conducting the research. I truly appreciate Dr. Farrokh Sassani for his support and for reviewing the thesis. Furthermore, I would like to extend my sincere gratitude to Dr. Krishna Vijayaraghavan for his time and energy as my session defence chair.

I am very grateful for the financial support from Natural Sciences and Engineering Research Council of Canada (NSERC), and Sable Industries Inc. I also would like to express my appreciation to the helpful MSE staff; particularly Jennifer Leone, Taha Al–Khudairi, Mustafa Sajid, Kinga Muntener, Julibeth Fernandez, Quincy Wang, and Gloria Leung.

I am really thankful to my friends and lab mates for providing me a friendly and intellectually rich environment: Azim Keshtkar, Reza Harirforoush, Ehsan Asadi, Ehsan Arjmand, Hossein Dehghani, Soroush Norouzi, Soheil Sadeqi, Hossein Mansour, Masih Hosseini, Amr Marzouk, Parvind Grewal, Farbod Khameneifar, Alireza Hekmati, and Sina Doroudgar.

Table of Contents

List of Tables

List of Figures

List of Acronyms

ATDH	Air–Turbine Dental Handpiece
DAS	Dental Assisting System
DAQ	Data Acquisition Card
HSEH	High Speed Electrical Handpiece
ANN	Artificial Neural Network
PI	Proportional Integral
PWM	Pulse Width Modulation
RBF	Radial Basis Function
RPS	Revolutions per Second
STFT	Short Time Fourier Transform
SVM	Support Vector Machine
TAN	Tooth/Amalgam/Noncontact
TCN	Tooth/Composite/Noncontact

1. Introduction

Tooth decay is one of the most prevalent disorders, and dentists need to remove infected parts to restore tooth functionality. A tooth is one of the body parts with little healing ability and any loss will be permanent. Earlier investigations concluded that with the current dental restoration and treatment protocols, the loss of healthy tooth structures is inevitable. Moreover, for cavities that are developed close to the nerves, a minor mistake in cutting extra healthy tooth can turn a routine dental filling to a root canal. Dentists rely on their tactile, auditory, and visual senses to navigate a dental handpiece, but these senses are limited due to the high speed of the dental handpiece, visual limitation in the oral cavity, inadequate precision of tactile senses, uncontrolled patient factors, color resemblance of tooth and “white” fillings, and remotely located caries and collapsed old dental fillings. The main objective of this research is to develop a dental assistive system (DAS) for procedures that are performed by air-turbine handpieces to improve the quality and efficiency of operations. In order to do that, knowledge regarding tooth layers, dental handpieces, and restorative materials is needed.

A tooth is an inhomogeneous body part which is composed of different layers including enamel, dentin, pulp, cementum (Figure 1.1). Enamel is the hardest component of the human body which consists of 96% mineral, 1% organic material, and 3% water, [1]. Dentin is a calcified tissue, and is harder than bone. It is located between enamel or cementum and pulp. Cementum is a bone like tissue that covers the root of a tooth, and finally the dental pulp is the central part of a tooth filled with soft tissues containing blood vessels and nerves, [2].

Dental handpieces are high–speed rotary cutting tools that are widely used in dental operations. These devices are categorized as electrical and air–turbine (Figure 1.2). Electrical handpieces work by electrical motors; whereas air handpieces are driven by air–turbines.

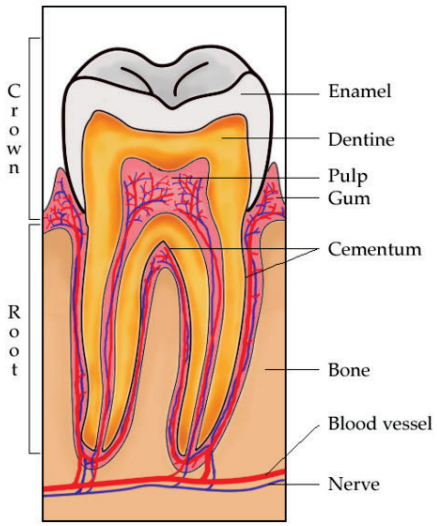

Figure 1.1 Different parts of a tooth, [2]

Figure 1.2 Dental handpieces; (a) air–turbine handpiece, (b) high–speed electrical handpiece

Air–turbine and electrical handpieces have been compared to each other in many studies. High speed electrical handpieces are known to have high–speed/high–torque (maximum speed: 40k–200k rpm, maximum torque: 3–6 Ncm, [3]), and are equipped with a control system that allows them to regulate their speed. During a cutting process, the controller of electrical handpieces provides more torque to maintain the speed. Air–turbine handpieces are high–speed/low–torque devices (maximum speed: over 300k

rpm, [4]), and their speed would reduce during a cutting process, because they do not have a speed control mechanism.

The main consequence of speed reduction in dental operations is the reduction of the cutting efficiency (machinability), defined as the ratio of removed mass over the cutting duration (gram/seconds). Eikenberg, [5], made a comparison, and indicated that the cutting efficiency of the electrical handpiece was significantly more than the air–turbine. Choi, et al., [6], also evaluated the cutting efficiencies of air–turbine and electrical handpieces. They used different dental materials such as amalgam and metal alloys, and indicated that the electrical handpiece cut those materials more efficiently than air–turbine.

Despite of this disadvantage, air–turbine handpieces possess privileges that make them still a popular choice for many dentists, [4]. These handpieces run at a higher speed than electrical handpieces which makes them capable of removing tooth structures with only a light touch. Moreover, they are less sensitive to damages caused by sterilization techniques, and are easier to repair, [7]. In addition, unlike electrical handpieces, air–turbine handpieces have good ergonomic weight and size. This characteristic is considered as a significant advantage for these handpieces, because it makes their manoeuvre easier, and provides better visibility and access for dentists during dental operations, [8].

Considering all the advantages of air–turbine handpieces, it would be highly beneficial to overcome their speed reduction and enhance their efficiency and effectiveness. To achieve this goal, one of the main objectives of this thesis is designing a dental assisting system (DAS) which is capable of controlling the speed of air–turbine handpieces.

1.1. Dental Restoration

Dental restoration is a process that begins with removing carries and affected tissues to retain the functionality of tooth structures. Air–turbine dental handpieces are high–speed rotary cutting tools that are widely used by dentists during this operation (Figure 1.2).

The next stage in the process is filling the cavity with appropriate restorative materials. There are different materials such as amalgam, composite, glass ionomer cement, etc. that are commercially available for restorations, [9]. Among these materials, amalgam and composite are extensively used by dentists. The main advantage of composite over amalgam is its aesthetical capabilities, because it can be produced in many tooth colors, which makes its appearance very similar to a real tooth (Figure 1.3)

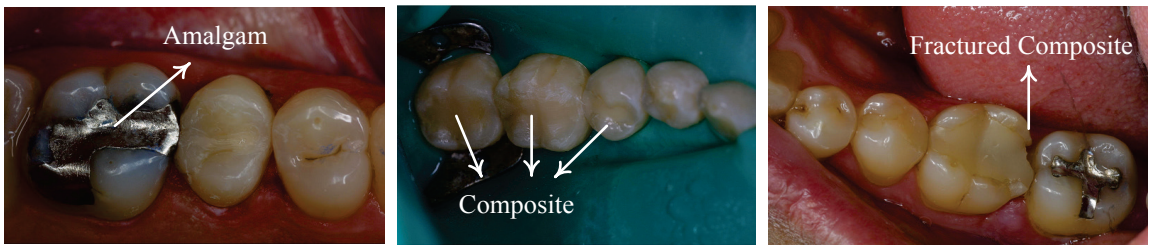

(a) (b) (c)

Figure 1.3 ***Two commonly used dental restorations; (a) amalgam; (b) composite; (c) a fractured (broken) composite which should be replaced***

The mechanical properties of dental materials and tooth layers are different, which suggest that their automatic detection should be feasible, [10]. Table 1.1 compares the modulus of elasticity, fracture toughness, compressive strength, and hardness of enamel, dentin, composite, and amalgam.

Table 1.1 ***Some Mechanical Properties of Tooth Layers (Enamel, Dentin) and Restorative Materials (Composite, Amalgam),*** [9]

Material	Modulus of Elasticity [i]	Fracture Toughness [ii]	Compressive Strength [iii]	Hardness [iv]
Enamel	84.1	0.6–1.8	384	343
Dentin	18.3	3.1	297	68
Composite	16.6	0.8–2.2	277	22–80
Amalgam	27.6	1.3	388	110

[i]: Units are in GPa (Giga Pascal)

[ii]: Units are in MN $m^{-3/2}$ (Mega Newton × $meter^{-3/2}$)

[iii]: Units are in MPa (Mega Pascal)

[iv]: Knoop Hardness Number, Kg/mm^2 (Kilo gram/milli $meter^2$)

The modulus of elasticity is a property that depends on the stress and strain of a material. Stress is the material resistance to the external force, and is defined as the force per unit of area. Strain is described as the length–change per unit of length. The modulus of elasticity represents the stiffness of a material within its elastic range, and can be calculated as the ratio of stress to strain, [9].

Fracture toughness indicates the ability of cracks or flaws in the material to cause fracture, and is dependent on the energy consumed in plastic (irreversible) deformation, [9]. The compressive strength is the maximum compressive stress that a material can tolerate before its failure. Hardness characterizes the resistance of a material to the permanent surface indentation or penetration. There are different testing methods to formulate hardness. Table 1.1 shows the Knoop hardness number which can be calculated based on the ratio of the applied load to the area of indentation, [9].

1.1.1. Restoration Replacement

The performance of dental restorations is subject to several factors such as type of restorative material, type and position of the tooth, and number of restored surfaces as investigated in the literature.

Mjör, et al., [11], studied performance of restorations in permanent teeth using amalgam, glass ionomer, and composite for five years, and concluded that the failure in the amalgam and glass ionomer was only due to bulk fractures, whereas the composite failed because of secondary caries and bulk fractures. Similarly, Collins, et al., [12], evaluated the performance of composite restorations in a five–year study, and concluded that composite failures were because of bulk fractures and secondary caries, which supported the findings of Mjör, et al., [11]. They reported the rate of failed composites two or three times more than amalgam restorations. Soncini, et al., [13], also compared the longevity of amalgam and composite restorations in primary and permanent teeth, and indicated that the longevity of amalgam was more than composite.

As for the position of tooth, Dake, [14], reported no difference in the longevity of restorations in molars and premolars teeth, whereas Johnson, et al., [15], indicated composite restorations filled in premolar teeth were more durable than molars. Dake,

[14], also showed that restorations in mandibular incisor teeth stayed more intact compared to maxillary incisors.

The surface condition of the restoration can also affect its performance. Adegbembo, et al., [16], reported that increasing the number of surfaces in amalgam restorations decreased the survival rate. Bernardo, et al., [17], reported a similar finding for composite restorations. They also concluded that longevity of amalgam was more than composite, and the difference was even more significant for higher number of surfaces.

Considering these reports, it can be concluded that although current restorative materials are very durable, most of them eventually fail (Figure 1.3c). If an existing restoration collapses, there is a high chance for developing new decay that requires replacing the old restoration and removal of all newly developed carries. Replacing of old restorations is one of the most frequent procedures (60%) in dental clinical practices, [18]. This rate has not been declined despite of the advancements in dental restoration materials, [19].

During the replacement process, discerning the boundary of tooth layers and restorative materials is challenging, in particular with tooth–colored composites. In fact, to conduct dental operations, dentists receive training to become experts of interpreting their tactile, auditory, and visual senses as their diagnosis tools, [20]. They transfer such sensory information to the actual practice through their perception. This perceptual procedure is highly subjective, and is dependent on the individual abilities and experience of dentists, [21]. The main problem with these approaches is that human senses have limited functionality, and sometimes are insufficient for dentists to rely on.

During the removal of old composite restorations (which have the same color as tooth), limited functionality of human senses causes removal of healthy tooth layers in adjacent areas. Gordan, et al., [22], evaluated the margins of replaced composite restorations, and indicated that a significant amount of tooth layers was lost during the replacement process. In another study, Gordan, [23], showed that replacement of composite restorations resulted in the loss of tooth layers in areas distant from the site of failure. Gordan, et al., [24], also investigated the effect of different cavity designs during

the replacement of composite restorations, and indicated that deeper original cavity preparation resulted in greater tooth losses. Although the visibility issue is less challenging for amalgam, replacing it still results in tooth losses. Sardenberg, et al., [25], studied replacement of old amalgam restoration, and indicated that it resulted in the loss of healthy tooth layers.

Loosing healthy dental structures is a major concern in all restorative procedures, because it reduces the longevity of restored teeth, [23]. In addition, a tooth is one of the few human body parts that has very limited healing ability, and almost all structural losses are permanent. Developing an objective and sensor–based method for restorative procedures is a promising approach to overcome the limited functionality of human senses. Therefore, designing a dental assisting system (DAS) that provides real–time information about restorative materials and tooth layers during the cutting process will be highly valuable. Depending on the dentists demand and the accuracy of DAS, the designed system can also be given autonomy to take appropriate actions such as controlling the speed of air–turbine handpieces. Such a control can prevent removing healthy tooth layers by reducing the speed or completely stopping the operation. Controlling the speed can also enhance the efficiency of air–turbine handpieces by enabling them to cut the right material easier. Thus, the objectives of the dental assisting system (DAS) are classification between tooth layers and restorative material, and controlling the speed of air–turbine handpieces (Figure 1.4).

1.2. Literature Review of Air–Turbine Handpieces

The literature was reviewed thoroughly, and no prior works were found on either classification of tooth layers and dental materials, or automatic speed control of air–turbine dental handpieces (ATDH). However, since the introduction of air–turbine handpieces in 1957, [26], they have been studied from different aspects, and subjected to a variety of investigations as follow.

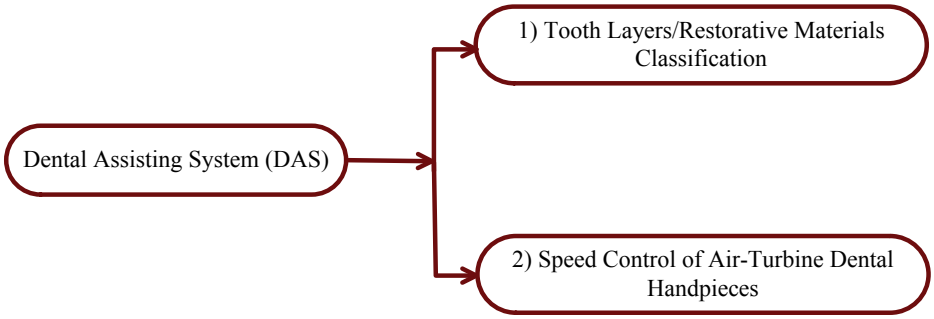

Figure 1.4 The objectives of the proposed dental assisting system

1.2.1. ATDH Comparison

The performance of air–turbine handpieces in terms of tooth cracking, temperature changes, the quality of cavity preparation, etc. has been compared to one another, electrical handpieces, and other dental devices.Watson, et al., [27], compared the cutting dynamics of electrical and air–turbine handpieces, and studied the effect of handpiece torque and bur type on the tooth cracking and temperature changes. They concluded that when the loads and cutting rates were increased, electrical handpieces better coped with increased loading. Moreover, no effects of cracking or heating were found for these handpieces and their cutting burs.

Nishimura, et al., [28], used an air–turbine handpiece, and evaluated the effect of different burs on the generation of marginal and surface cracks in enamel. They concluded that regular–grid diamond and carbide burs caused more cracks in the marginal enamel, whereas superfine–grit diamond bur generated fewer cracks in the enamel surface. Ercoli, et al., [29], studied the relation of air–turbine handpiece/bur types and the temperature variation during cutting procedures. They concluded that in case of providing adequate water flow, no harmful temperature changes would occur in the pulp chamber, regardless of the handpiece/cutting bur types. Leonard, et al., [30], compared different commercially available air–turbine handpieces which were subjected to simulated clinical uses and sterilizations. The comparison criteria included different clinical performance parameters such as longevity, power, turbine speed, visibility angle, etc. They found no difference among the handpieces considering the performance

parameters, and showed that all the devices could be expected to perform at least 500 clinical use/sterilizations.

Firoozmand, et al., [31], compared the temperature rise in cavities prepared by electrical handpiece, air–turbine handpiece, and Er:YAG laser. They concluded that electrical and air–turbine handpieces had similar temperature response, whereas Er:YAG laser generated lower temperature rise. In another study, Kenyon, et al., [8], compared the cavity preparation quality using electrical and air–turbine handpieces, and concluded that the quality was the same for both handpieces. Dyson, et al., [32], provided different aspects such as bearings, chucks, hoses/connectors, and rotors for designing air–turbine handpieces. They compared the handpieces regarding these aspects, and made general recommendation for selecting a handpiece in the clinical practice. For example, they suggested an air–turbine handpiece should be able to withstand to repeated and routine autoclaving; or it is better to have an air–turbine handpiece that has multiple coolant nozzles. In another study, Dyson, et al., [33], compared two brands of disposable air–turbine handpieces, and concluded that both brands had poor performance, vibration, excessive noise, variability of behaviour, and poor bearings.

1.2.2. Infections and Other Side Effects

Use of ATDH for dental procedures can cause some side effects such as contamination and infection. The cutting action can create small particles of blood and aerosols that may enter the environment or the handpiece and then be transferred to the next patient (cross infection).

Ishihama, et al., [34], provided evidence of blood–contaminated aerosols in a room where oral surgery was performed with air–turbine handpieces. Similarly, Toroğlu, et al., [35], indicated that use of air–turbine handpieces resulted in generation of high levels of aerosols, and even utilizing mouth rinse was ineffective. So, they suggested barrier equipment to prevent aerosol contamination. In another study, Pong, et al., [36], demonstrated the discharge of lubricating oil from air–turbine handpieces, and suggested using detergent for decontamination and preventing risky operations.

The contaminated air can be drawn into the handpiece when it stops rotating (suck–back), and then be discharged during the next usage which causes cross–infection. Checchi, et al., [37], showed the entrance of contaminating fluid into the air chamber of air–turbine handpieces when the handpiece stopped rotating. As a result, a significant cross–infection potential existed; and mandatory internal cleaning and sterilization between patients was suggested as the solution. In another study, Lewis, et al., [38], also provided evidence for contamination of internal air–turbine chambers. They suggested heat–treating of handpieces between each patient to reduce the cross–infection risks.

Masuda, et al., [39], introduced the air flushing clean system (AFCS) for ATDH to prevent cross–infection in dental procedures. AFCS could prevent contamination of the internal water and air lines of the handpiece by maintaining an internal positive pressure even after the turbine was stopped. Ohsuka et al., [40], evaluated the performance of AFCS, and indicated its effectiveness in reducing the contamination level of air–turbine handpieces. Similarly, Matsuyama, et al., [41], also tested the performance of AFCS, and indicated its capability in decreasing the bacterial contamination within the air–turbine handpiece. Montebugnoli, et al., [42], compared the performance of air–turbine handpieces that were equipped with anti–suction devices for preventing retraction of contaminated fluid into the air chamber. They concluded that anti–suction devices could reduce the contamination, and the performance would enhance if such devices were installed inside the unit.

Another side effect can be caused from the handpiece air which is forced into soft tissues through the reflections, and may result in gum swelling. This complication is called “subcutaneous emphysema”, which is a rare side effect; however, it has been observed during some dental operations. Romeo, et al., [43], reported a case that subcutaneous emphysema occurred during extraction of a mandibular third molar with the use of an air turbine handpiece. Kim, et al., [34], reported two cases of subcutaneous emphysema that were developed after opening a cavity for endodontic retreatment.

1.2.3. Machinability

Machinability (cutting efficiency) is defined as the removed mass/volume of the cutting material over a fixed quantity (i.e. time, force, etc.). Although this topic can be considered under “ATDH Comparison” title, it is more beneficial to introduce it as a new topic; because the main focus is on machinability, and not comparison of air–turbine handpieces.

Watanabe, et al., [44], studied the relation of heat treatment and machinability, and indicated that heat treatment had no effect on the machinability of cast gold alloy using an air–turbine handpiece with carbide and diamond burs. Miyawaki, et al., [45], used an air–turbine handpiece, and cut different cast alloys materials. They reported that the cutting volumes of soft alloys were significantly larger than hard alloys. They also found that the machinability of carbide bur was more than the diamond bur; however with continuing use, the machinability of carbide bur decreased, whereas that of the diamond bur remained almost constant.

Miyawaki, et al., [46], also compared the machinability of composite and dentin while they were cut by an air–turbine handpiece using a diamond bur. They showed that machinability of composite was more than dentin. In a similar study, Tanaka, et al., [47], studied the feasibility of using machinable ceramics in dentistry. Among different types of ceramics, they indicated that the machinability of mica–based ceramic had similar machinability to dentin, and so it was recommended for future production of dental prostheses.

1.2.4. Measurement and Characterization

Different descriptive parameters of ATDH such as torque, speed, flow, etc. have been measured and characterized in various reports. Brockhurs, et al., [48], determined the torque, speed, and power of air–turbine handpieces. They tested forty–one new and used handpieces, and reported the maximum speed 500k rpm, the maximum torque 2.33 N.mm, and the maximum power 29.6 watt. The maximum power was obtained between 49%–79% of the free–running speed.

Dyson and Darvel measured flow and free running speed, [4], as well as torque, power and efficiency, [49], of air–turbine handpieces. They demonstrated that the free running speed was dependent on gas properties, pressure, and rotor radius. In addition, they indicated that stall torque was related to rotor position, whereas dynamic torque had a linear relationship over the range from stall to free running. In another study, Dyson and Darvel introduced a portable testing machine to determine free–running speed, stall torque and bearing resistance of air–turbine handpieces, [50]. This machine was suggested to be used for verifying the claimed characteristics, monitoring the performance, and conducting laboratory tests.

Elias, et al., [51], investigated the magnitude of cutting forces of two air–turbine handpieces with different torques. They showed that the higher torque handpiece required a higher cutting force. The mean cutting force for the higher torque handpiece was 1.44 N whereas for the lower torque one was 1.2 N (The overall mean was 1.30). They concluded that the magnitude of forces was related both to the type of the handpiece, and to the forces applied by clinical operators. In addition, there were no difference between plain and cross–cut burs, and cutting wet or dry.

Yin, et al., [52], also evaluated the performance of an air–turbine handpiece. They developed a 2 degree–of–freedom (DOF) apparatus for conducting in vitro tests. They indicated that at a constant supplied air pressure and water flow–rate, the handpiece speed decreased by increasing depth of cut, feed rate, and cutting forces. Monagahn, et al., [53], evaluated the performance of air–turbine handpieces, and indicated that the variation in the free–running speed, bearing resistance, illuminance and sound pressure level could monitor changes in air–turbine handpieces. Norkiewicz, et al., [54], also studied the factors that were related to the air–turbine handpiece wear and breakdown, and discussed maintenance and repair options for these handpieces.

1.2.5. Computer–Aided Technologies/Manufacturing

As Figure 1.4 shows, the objectives of this research is developing a dental assisting system (DAS) for air–turbine handpieces to help dentists in identifying tooth layers from restorative materials, and to control the speed of the handpiece. To achieve these objectives, DAS employs sensors and reliable computer–aided technologies

(CAT). Computer–aided technologies/manufacturing (CAD/CAM) have been used in different fields of dental research.

Miyazaki, et al., [55], provided a survey on the history of CAD/CAM technologies for the fabrication of crowns and fixed partial dentures. Kapos, et al., [56], systematically reviewed the application of CAD/CAM technologies for fabrication of frameworks and abutments in restorative implant dentistry. They concluded that although proofs of concept were established for those technologies, they were too preliminary to provide meaningful outcomes regarding their performance in routine clinical operations.

Buchanan, [57], provided a review on dental educational technologies that were either available or were in the developmental stage. She concluded that further evaluations were needed for such technologies to dramatically improve student learning. Al–Jewair, et al., [58], reviewed the computer assisted learning (CAL) in endodontics education (study and treatment of the dental pulp). They found some evidence that suggested CAL could enhance the time spent for learning. They also concluded that the effect of CAL and traditional methods in improving knowledge were the same. Lechner, et al., [59], presented a computer–assisted learning (CAL) program for planning of oral rehabilitation in the clinical dentistry. They reported the positive responses and feedbacks; however, some students preferred to have the program as an additional resource rather than a substitution to the traditional methods.

Considering the above applications, it can be concluded that although CAT/CAM have been used in different areas such as designing/manufacturing of restorative materials, training/learning tools, etc., their applications have not been explored for air–turbine handpieces, which is the purpose of this dissertation

1.3. Classification of Tooth Layers and Restorative Materials

As Figure 1.4 shows, the first objective of DAS is classifying between tooth layers and restorative materials. Generally, to conduct such a classification, two steps should be followed. First, a signal should be selected that potentially carries information for differentiating between various dental materials. Then, a classification method should be

chosen to discriminate between these materials based on the extracted features from the signal (Figure 1.5).

Vibration and sound signals are two sources of information that can be used for classification. Air–turbine handpieces are very high speed cutting devices (40k–200k rpm), and thus they generate high frequency vibrations that can carry information of the cutting material. Studying vibration in dentistry is a wide research field, and regardless of the details all the investigations can be categorized in two main topics:

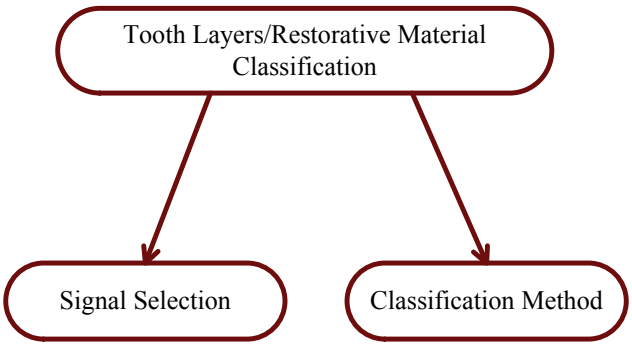

Figure 1.5 Two steps of the classification between tooth layers and restorative materials

(i) vibration analysis of dentistry's instruments such as ultrasonic scalers, [60], endosonic files, [61], ultrasonic retrograde systems, [62], electric toothbrushes, [63], dental laboratory vibrator, [64], and dental handpieces [65],

(ii) vibration analysis of teeth [66], dental implants, [67], and dental bonding agents, [68].

Castellini, et al., [69], analysed teeth vibration (0–100 kHz) as a non–invasive measurement procedure for the diagnosis of structural defects on human teeth. They applied progressive damages on a tooth, and claimed such an approach could eliminate the contribution of the tooth structure variability. They indicated that dental defects could increase resonance frequencies and create some anti–resonances. In another study, Lea, et al., [70], investigated the effects of water flow rate and power settings on the vibration patterns (0–100 kHz) of a dental ultrasonic scaler. They indicated that when

water flow was increased, vibration amplitude was decreased for low/medium power settings, whereas it remained constant for high power settings.

Carvalho, et al., [71], evaluated the dynamic stiffness of connective soft tissues around a dental implant using vibration signals (10–410 Hz). They suggested such results could be employed for designing an improved implant system where a flexible and damped element would reduce the currently rigid connections. In another study, Poole, et al., [65], investigated if vibrations (0.5–20 kHz) of dental handpieces could cause the hand–arm vibration syndrome, or enamel cracking. They tested five air–turbine and two electrical handpieces, and did not find any evidence of vibration syndrome or teeth cracking.

On the other hand, the difference among the mechanical properties of tooth layers and restorative materials (Table 1.1) implies that their cutting sounds should carry unique features that might be useful to accurately discriminate these materials. Moreover, cutting sounds are a valuable source of information that is readily and easily available during the cutting procedure. Thus far, no prior works have been found on discrimination of tooth layers and restorative materials based on the cutting sounds. Perhaps the closest study to this thesis was conducted by Kocher, et al., [10]. They used an ultrasonic dental scaler, and measured its oscillations (0–100 kHz) in contact with a tooth. The extracted features were Fourier coefficients; and a fuzzy nearest neighbor method was employed to recognize enamel, cementum, and calculus tissues. The results were highly successful and indicated the feasibility of their approach. However, no information was found in their report on recognizing the noncontact class (i.e. when the tip of the scaler did not have contact with the tooth).

The cutting sounds have been intensively studied in the field of tool–wear monitoring for decades, [72]. Sound waves generated during the cutting are important, and there have been many studies that indicated a correlation between these sounds and the tool wear. Trabelsi, et al., [73], investigated the sound radiation (0–10 kHz) in metal cutting. They used Fourier transform coefficients as the features, and employed the linear discriminate classifier to discriminate between sharp, worn, and broken tools based on their cutting sounds. The classification accuracies were 80%–100% for the sharp tool, 75%–88% for the worn tool, and 80%–100% for the broken tool.

Salgado, et al., [74], used motor current (0–300 Hz) and sound (0–25 kHz) during a cutting process to estimate the feed force and tool flank wear respectively. They employed singular spectrum analysis (SSA) to extract information correlated with tool wear from the sound signal, and support vector machines were used for estimation. They validated the proposed method for the real–time implementation, and indicated its reliability and effectiveness. In a similar study, Ota, et al., [75], extracted autocorrelation and reflection coefficients from cutting sounds (0–5 kHz) of machine tools, and used them to train an artificial neural network (ANN) for estimating the motor speed and chuck pressure.

Rodolfo, et al. [76], investigated tool–wear monitoring in a high–speed machining process (0–200 kHz), based on analysis of different signals in time and frequency domains. They concluded that the spectrum of cutting sounds was very sensitive to changes in tool condition. The location of the sensor varied some peaks; and a worn tool increased the amplitudes and created new harmonics from 100 kHz up to 160 kHz.

Rather than tool–wear, sound signals have been used in other monitoring investigations. Abu–El–Quran, et al., [77], proposed a robust security monitoring system that could classify different sounds (0–8 kHz) within a room. They used a hierarchical scheme to first classify between speech and non–speech signals, and then in the case of a non–speech signal, it was classified to a particular audio type. They employed mel–filtered cepstral coefficients (MFCCs), delta mel–filtered cepstral coefficients (ΔMFCC), and pitch ratio as the features, and utilized a time delay neural network for classification.

Yadav, et al., [78], used audio signals (0–12 kHz) for condition monitoring of internal combustion engine. They used fast Fourier transform (FFT) coefficients as the features, and utilized a classifying scheme based on the cross– and autocorrelation coefficient values. In another work, Wan, et al., [79], developed an automatic pipeline monitoring system using sound information (0.1–12 kHz) of road cutters. They utilized MFCC for the features, and employed a threshold classifier. Amft, et al., [80], presented an automatic dietary monitoring to predict food weight based on acoustic recognition of chewing (0–22 kHz). In their study, features included log–band spectral energy, cepstral coefficients, and linear predictive coefficients. They trained a nearest centroid classifier based on a Fisher's linear discriminant feature transformation. Shin, et al., [81],

developed an automatic system for real–time monitoring of health conditions using cough sounds (0.35–4 kHz). A hybrid model was proposed that included an artificial neural network (ANN) and a hidden Markov model (HMM). The ANN model used energy cepstral coefficients as the features.

Doukas, et al., [82], presented a fall detection platform that combined audio information (0–11 kHz) with motion and visual data. They used STFT as the features extracted from sound signals; and employed different classifiers such as SVM, nearest neighbor, ADAboost, etc. In another study, Istrate, et al., [83], investigated the detection and classification of alarming sounds (0–22 kHz) in a noisy environment for medical tele–monitoring. They used discrete wavelet transform coefficients as the features, and employed the Gaussian mixture model for classification.

The second step in classifying between tooth layers and restorative materials is choosing a classification method (Figure 1.5). Support vector machine (SVM), [84], is one of the most powerful algorithms for classification. SVM is a classifier that focuses on maximizing the separation between classes, and has been employed in various applications.

Choi, et al., [85], used SVM technique to classify the cardiac sounds (0–700 Hz) into normal and six abnormal cases. They extracted the features from power spectral density curve. Wang, et al., [86], employed SVM to classify environmental sounds (0–4 kHz) for home automation. They used mel–frequency cepstral coefficients (MFCC) as the features; and indicated that applying independent component analysis (ICA) to MFCC can improve the performance. In a similar study, Wang, et al., [87], also combined SVM with k–nearest neighbour method to classify twelve various home environmental sounds (0–8 kHz). They used spectrum centroid, spectrum spread, and spectrum flatness as the features, and indicated the accuracy of their classifier was superior to other methods such as hidden Markov models.

Ganapathiraju, et al., [88], proposed a method for recognizing speech based on support vector machines. They used SVM within the framework of hidden Markov model (HMM), and employed cepstral and energy coefficients as the features. Lin, et al., [89], developed a method for automatic emotion recognition in speech (0–8 kHz). They chose

Mel frequency cepstrum coefficients as the features, and utilized SVM to classify different emotional states such as anger, happiness, and sadness.

1.4. Speed Control of Air–Turbine Handpieces

As Figure 1.4 shows, the second objective of DAS is controlling the speed of air–turbine handpieces. In order to reach this objective, two steps should be considered, speed measurement and speed control (Figure 1.6). Dyson, et al., [90], studied different speed measurement methods, and compared their advantages and disadvantages. They eventually, suggested optical and magnetic approaches for air–turbine handpieces. In optical measurement, the dental bur was modified so that it was alternately reflective/non–reflective to light. The variation in the reflected light was counted by a transducer to obtain the speed. In the magnetic measurement, a similar approach was employed, except that a magnet was attached to the bur, and the transducer responded to variations in the magnetic field.

The speed control can enhance the efficiency of ATDH, and prevent removal of healthy tooth layers in restorative procedures. In order to control the speed of air–turbine handpieces, a control variable is needed so that the speed is manipulated through it. Dyson, et al., [4], indicated that that free–running speed (i.e. not load is applied to the handpiece) was dependent on the model of the handpiece, the type of employed gas, properties of the turbine, and the applied pressure:

$$N = \frac{c}{2\pi r}\sqrt{\frac{1-(1+\alpha P)^{\frac{-(\gamma-1)}{\gamma}}}{\gamma-1}} \qquad 1.1$$

where, N, c, and r, indicates the speed, the speed of sound, and the turbine radius respectively. In addition, γ, and P are gas specific heat ratio, and input pressure. α is a parameter that depends on the model of the handpiece. Among these variables; the applied pressure is controllable, and the speed control can be conducted through it.

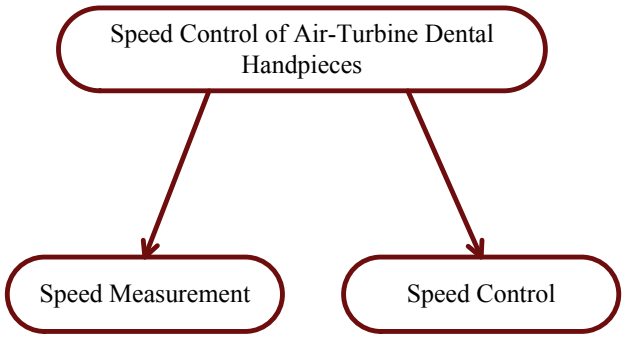

Figure 1.6 Two steps of the speed control of air–turbine dental handpieces

To control the pressure, using an on/off solenoid valve which is commanded by pulse width modulation (PWM) signals is a promising approach. In this technique, PWM signals with a proper rate switch the solenoid valve on and off so that the pressure in the valve outlet is regulated to a mean value. Increasing/decreasing the duty–cycle (D) of PWM signals will increase/decrease the outlet pressure and consequently the handpiece speed. This pressure control technique is fast and easy to implement. In addition, solenoid valves are durable and energy/cost efficient compared to other types of control valves, [91]. This technique has been used in various pneumatic applications. Royston, et al., [92], applied pulse–width modulation technique to a rotary valve to control the position of a pneumatic actuator. Noritsugu, [93], used PWM signals for an electro–pneumatic servomechanism to control the position of a pneumatic cylinder. Shen, et al., [94], combined PWM technique with a nonlinear model–based control strategy for trajectory tracking of pneumatic servo actuators. Varseveld, [91], proposed a novel PWM algorithm for on/off solenoid valves that allowed fast, accurate, and inexpensive position control for pneumatic actuators.

To provide a closed–loop speed control for air–turbine handpieces, the proportional integral (PI) controller can be used. PI control is a simple, inexpensive, and efficient method, that has been employed in many applications such as postural control, [95], heart rate control, [96], and limb rehabilitation, [97].

1.5. Organization of the Dissertation

This dissertation is comprised of four chapters which are organized as follow.

Chapter 1 was dedicated to the background and objectives of the present work. This chapter provided the necessary information on tooth, air–turbine/electrical handpieces and their comparison, dental restoration, mechanical properties of restorative materials and tooth layers, replacement of restoration, etc. In this chapter the pertinent literature was reviewed comprehensively and was presented through different sections. Different studies on air–turbine handpieces were categorized as comparison, side effects, machinability, and measurement/characterization.

Chapter 2 studies classification of restorative materials and tooth structures, which is one objective of the described dental assisting system (Figure 1.4). Considering two widely used restorative materials in dental operations (amalgam and composite), two cases of classification are investigated. The first case includes tooth, composite, and noncontact classes (TCN); whereas the second case is comprised of tooth, amalgam, and noncontact classes (TAN). Among different algorithms, the support vector machine (SVM) is chosen and its performance on the classification problem is evaluated from different aspects such as number of features, feature scaling methods, and the utilized kernels. The effect of temporal voting, hierarchical and one–against–one classification schemes, on the total accuracy is also studied in this chapter.

Chapter 3 provides a speed measurement and control technique for ATDH which is another objective of the dental assisting system (Figure 1.4). An indirect speed measurement method is introduced based on the vibration/sound of air–turbine handpieces. This measurement technique is explained theoretically based on the rotating unbalance concept and the vibration of a fixed–free beam. This indirect method is validated experimentally through a number of different tests, and can address the practical shortcomings of conventional speed measurement methods. To control the speed, an on/off solenoid valve is employed which is commanded by pulse width modulated (PWM) signals. This versatile approach enables ATDH's speed to be controlled by varying the duty–cycle of PWM signals. In order to conduct simulation analysis, a mathematical model of ATDH is obtained which includes a nonlinear static

part followed by a linear transfer function (Hammerstein model). Finally, a proportional–integral controller is designed and tested. It is demonstrated that the controller is capable of maintaining the speed in the loaded conditions. The performance and feasibility of this controller is confirmed by simulations and experiments.

In the end, Chapter 4 presents the conclusions and recommendation to facilitate further investigations and future works on the proposed dental assisting system.

2. Classification of Restorative Materials and Tooth Layers

2.1. Introduction

As it was explained in Chapter 1, replacing old restorations is very frequent in dentistry; however this operation causes tooth losses. Therefore, it would be highly advantageous if restorative materials can be classified from healthy tooth layers in the cutting procedures of such replacements. This classification was one objective of the proposed dental assisting system depicted in Figure 1.4.

Considering two widely used restorative materials i.e., amalgam and composite, and the fact that a tooth is not filled with both materials simultaneously, we are facing two cases of classification:

Case 1: classification between tooth, composite, and noncontact classes (TCN),

Case 2: classification between tooth, amalgam, and noncontact classes (TAN),

It should be noted that noncontact was considered as a “class”, because the classifier should be able to identify the free running handpiece, and differentiate it from the contact classes (tooth or composite/amalgam).

To study the above classification cases, this chapter is structured as follow; first the proposed methodology is introduced in sections 2.2 and 2.3. Then, the results are presented in section 2.4. Finally, this chapter provides the summary and conclusions in section 2.5.

2.2. . Methodology

To investigate TCN and TAN classification cases, a methodology is proposed which is depicted in Figure 2.1

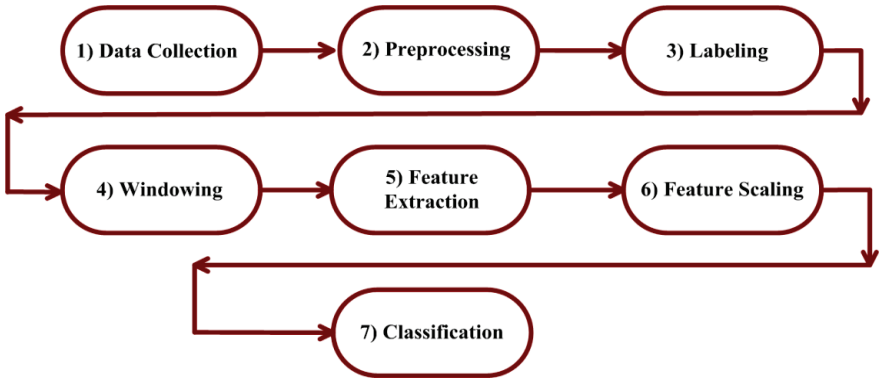

Figure 2.1 The proposed methodology for TCN and TAN classification cases

In the proposed methodology, seven different stages were considered as follows.

2.2.1. Data Collection

In this stage, the cutting sound signal was selected and recorded, because it is one of the rich sources that carries the information of the cutting material, and is readily and easily available during the cutting procedure. Another motivation for preferring sound signals to other signals, such as vibrations, was its potential for noncontact measurements. Moreover, sound signals have been used in similar problems in other areas such as engine fault diagnosis, [78], security monitoring, [77], and incorporating audio information into the scene recognition process, [98].

For data collection, we conducted several tests in a dental clinic with similar conditions to the cutting procedure performed by dentists. Research Ethics Approval was obtained from the office of research ethics at Simon Fraser University (File No. 2012s0157).

Discerning the restorative material and dental layers is difficult for a filled tooth in the mouth (in–vivo tests), which made it almost impossible to record the cutting sound of each material separately. Therefore, in this study, in–vitro tests were performed on cubic

samples $(1 \times 1 \times 1\ \mathrm{cm})$ of amalgam and composite, as well as one intact extracted human third molar.

The samples were fixed in a metal chuck (clamp). A "W & H Toplight 898le" ATDH and a "330 Diamond" bur were used for cutting, which are among common choices for dentists in restorative procedures. A high–frequency microphone (GRAS 40be) was employed (Figure 2.2) to record the cutting sounds. The sampling frequency was chosen 48 kHz; high enough to capture the maximum speed of the handpiece (~ 5 k rps: revolutions per second) based on Nyquist–Shannon sampling theorem, [99]. A high–speed data acquisition card (LDS Dactron Photon II, 75 kHz); and a signal processing software for frequency analysis (RT Pro Photon) were employed to sample and collect the data on a personal computer.

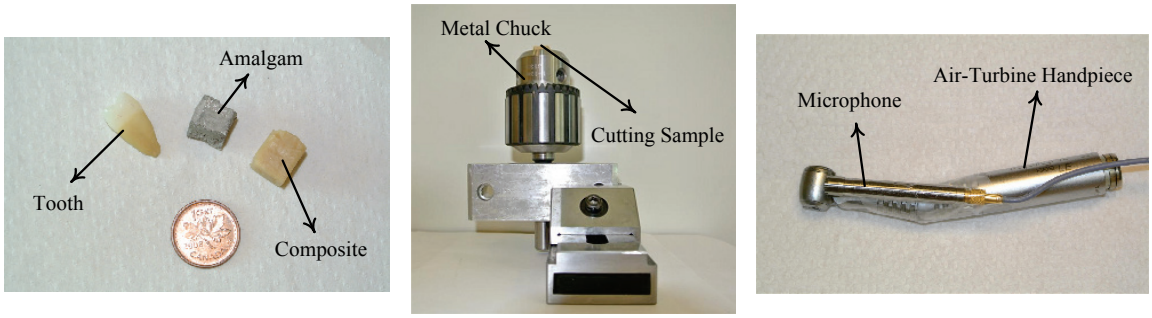

(a) (b) (c)

Figure 2.2 ***a) Composite, amalgam and tooth samples; b) The metal chuck (clamp) for holding the cutting samples; c) The microphone and air–turbine handpiece***

In obtaining the tooth data, the cutting sounds of enamel and dentin were recorded separately. In addition, in a real restorative process, the cuttings can be performed with/without using water. Therefore, in our experiments, we obtained the sound signals in both "dry" and "wet" cutting conditions. All cuttings were conducted three times in a parallel plane to the sample's surface by an experienced dentist.

The cutting procedure was comprised of three steps. First, the handpiece ran freely for $2-3\ \mathrm{s}$ (NonCon 1) and then the cutting was undertaken for $2-3\ \mathrm{s}$ (Con). In the last step (NonCon 2), the handpiece ran freely again for $1-2\ \mathrm{s}$ (Figure 2.3). In this

cutting procedure, the transition of a noncontact sound to a contact sound and vice versa were considered.

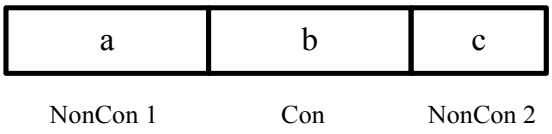

Figure 2.3 The format of each test; NonCon: Noncontact; Con: Contact

2.2.2. Preprocessing and Labeling

In these stages, the recorded data were filtered using a high–pass filter at 4 kHz to remove the effect of noises and disturbances (i.e. the compressor sound) at lower frequencies. In each test, the cutting part (Figure 2.3) was identified manually based on an increase to the signal power and a decrease to handpiece's speed[1]. These cutting data then labeled appropriately as tooth, composite, or amalgam. The free–running data of all tests were labeled as noncontact. It should be mentioned that in the labeling process, dry and wet cutting signals were considered together for each material to include pertinent information. Figure 2.4 shows a sample of a recorded sound signal. The cutting period is highlighted by the rectangle, and the rest of data are noncontact. The handpiece was off at low–power parts at the beginning and end of the signal, and so these parts were not considered for the analysis.

2.2.3. Windowing, Feature Extraction, and Feature Scaling

After preprocessing and labeling, the next stages of the proposed methodology are windowing, feature extraction, and feature scaling (Figure 2.1). The absolute value of short–time Fourier transform (STFT) coefficients were selected as the features. Hamming windowing with 50% of overlapping was used, because it is a common choice in audio signal processing, [100]. The window length should be chosen small, because we are interested in identifying the classes in a small period to be able to prevent the removal of healthy tooth structures. For this study, 2100 data samples were selected in

[1] More details are provided in Appendix A

each window, and since the sampling frequency was 48 kHz, the window–length was 2100/48000 ~ 44 ms.

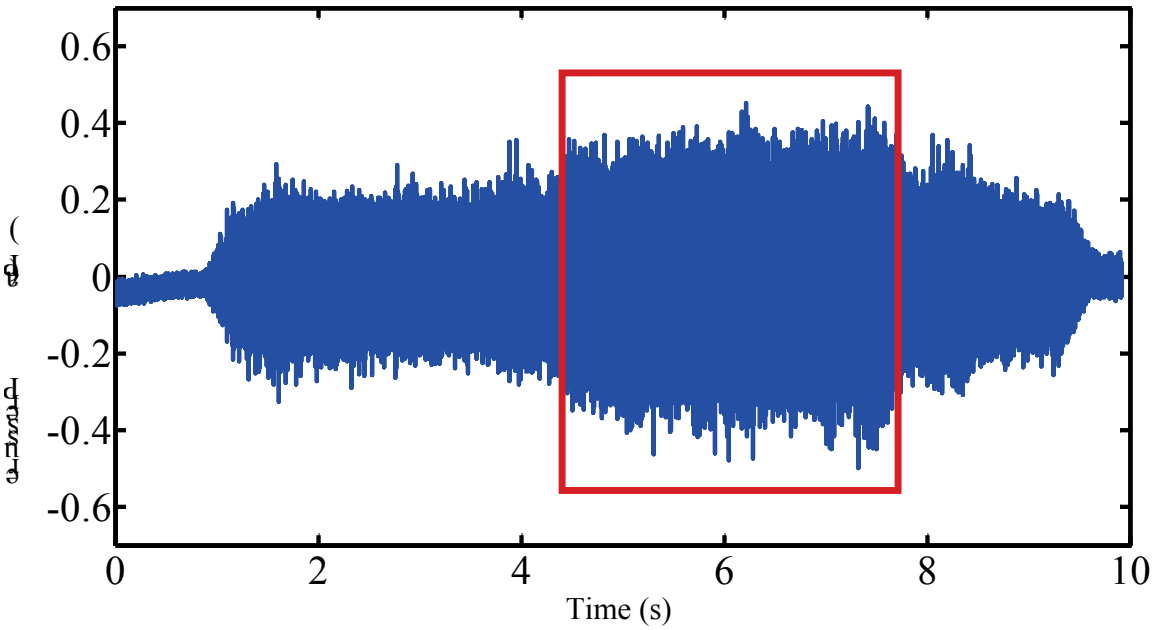

Figure 2.4 A sample of a recorded sound signal. The cutting period is highlighted by the rectangle, and the rest of data are noncontact

For each window, 2048 Fourier transform coefficients were obtained using the fast Fourier transform (FFT) algorithm in MATLAB platform[2]. Since each feature vector had 2048 elements that was a high dimension, the computation cost could have been increased. To reduce the dimension of each feature vector, an arithmetic averaging technique was used. In this technique, 2048 STFT coefficients were divided to p equal–sized groups ($\frac{2048}{\mathrm{p}}$ coefficients in each group). The data of each group were averaged arithmetically to obtain p features (Figure 2.5). The effect of p on the classification accuracy will be studied in section 2.4.1.

Feature scaling is usually utilized to avoid attributes in greater numeric ranges dominate those in smaller numeric ranges. In addition, it can prevent numerical difficulties during the calculation, [101]. For this research, two feature scaling methods

[2] To speed up the FFT computation in MATLAB, the number of coefficients should be chosen a power–of–2, [116].

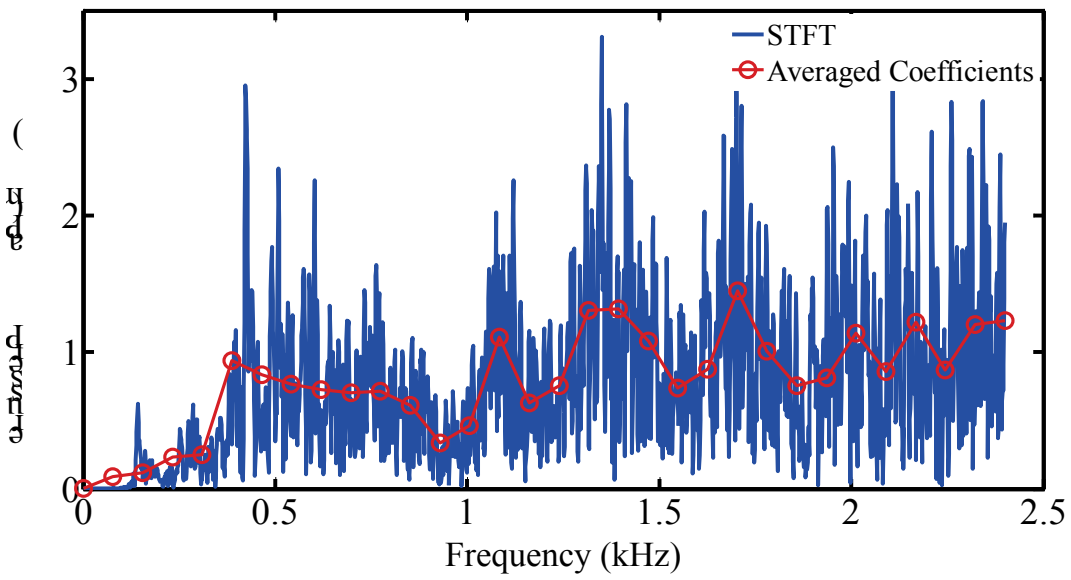

Figure 2.5 A sample STFT spectrum and the averaged coefficients for p=32

were investigated: linear scaling, and normal scaling. In the linear scaling, all the vector elements were projected linearly to the interval *[0,1]*; and in the normal scaling, the vector elements were normalized to have a zero mean and unit variance. The effect of these scaling methods on the classification accuracy will be discussed in section 2.4.2.

2.2.4. Classification

In this stage, support vector machine (SVM), which is one of the most powerful classification algorithms was chosen. In the next section, SVM will be introduced and explained briefly. A detailed description of this method can be found in references, [84], and [102]. In Appendix F, the classification accuracy of SVM will be compared with the artificial neural network (ANN), [84], which is another method of classification.

2.3. Support Vector Machines

Support vector machine (SVM) is a popular method for classification that has been employed in various applications such as environmental sound classification, [86], cardiac sound classification, [85], and speech recognition, [89].

SVM is a classifier that discriminates data points of different categories (classes), [103]. Each data point belongs to only one class, and is represented by an n–dimensional vector ($X_i \in R^n,\ i = 1, \dots, m$). A "linear" classifier discriminates the data points with a hyper–plane. Figure 2.6a shows two classes of data and different separating hyper–planes (in a two dimensional space, these hyper–planes are lines). Considering lines L_1, L_2, and L_3, different classifiers can be assumed that divide the two classes of data. The “margin” of a classifier is defined as the minimum distance between all data points and the hyper–plane. For example, the margin of L_1 is depicted in Figure 2.6b

SVM is a classifier that tries to find a hyper–plane that maximizes the margin. As Figure 2.6c indicates, L_2 is the line with the maximum margin.

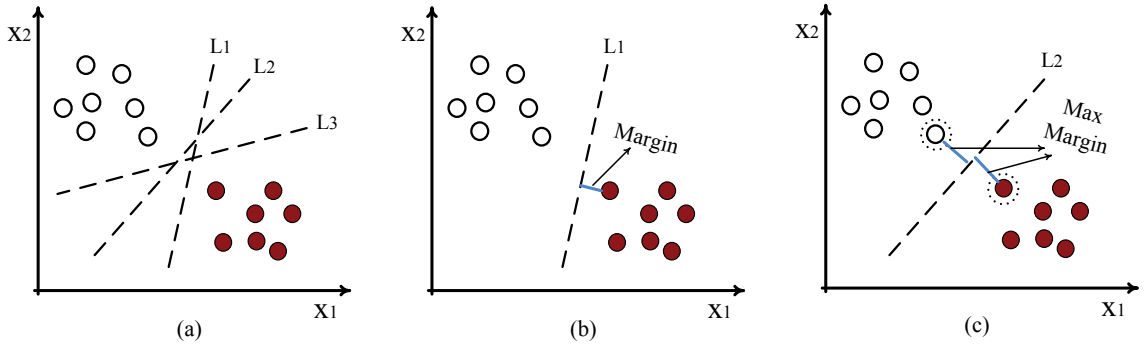

Figure 2.6 ***Support vector machine classifier, (a) different lines can divide the two classes of data; (b) the margin of L_1; (c) the maximum margin is obtained for L_2. The support vectors are indicated by dashed–circles.***

Each data point X_i is assigned a class–label y_i. For a two–class problem (Figure 2.6), the labels are considered either 1 or –1 ($y_i \in \{1, -1\}$). The hyper–plane takes the format of,

$$f(X) = w^T X + b \qquad 2.1$$

where, w and b are called the weight vector and the bias (w^Tdenotes the transpose of w). Finding the values of w and b is called training process, in which SVM uses a selective set of data points that are denoted as training data. After the training, another

set of data points can be used to evaluate the performance of SVM (testing data). In this study, it is assumed that training and testing data are separate from each other.

In order to correctly classify the training data, the hyper–plane f (Eq. 2.1) should be positive for positive data ($y_i = 1$), and negative for negative data ($y_i = -1$),

$$\begin{aligned} &\text{if} \quad y_i = 1, \qquad w^T X_i + b > 0 \\ &\text{if} \quad y_i = -1, \qquad w^T X_i + b < 0 \end{aligned} \tag{2.2}$$

Eq. 2.2 can be restated as,

$$y_i\left(w^T X_i + b\right) > 0 \tag{2.3}$$

If there exists such a hyper–plane f that correctly classifies all data points, then these data are called “linearly separable”.

Rather than correct classification, f should maximize the margin. As it was mentioned above, the margin is the minimum distance between the data points and the hyper–plane. The distance of a data point X_i to the hyper–plane f (Eq. 2.1) is,

$$\frac{\left|w^T X_i + b\right|}{\|w\|} \tag{2.4}$$

In Eq. 2.4, if weight and bias vectors are multiplied by a gain β ($w \rightarrow \beta w,\ b \rightarrow \beta b$), the distance will not change. Therefore, w and b can be rescaled so that,

$$y_i\left(w^T X_i + b\right) \geq 1 \tag{2.5}$$

According to Eq. 2.3, and the fact that y_i is either 1 or –1, the numerator of Eq. 4.4 can be replaced by $y_i\left(w^T X_i + b\right)$ as,

$$\frac{y_i(w^T X_i + b)}{\|w\|} \tag{2.6}$$

Considering Eq. 2.5 and Eq. 2.6, the margin (the minimum distance) is

$$\text{margin} = \frac{1}{\|w\|} \tag{2.7}$$

The closest data points to the hyper–plane f that satisfy $y_i(w^T X_i + b) = 1$ are called “support vectors”. The support vectors are indicated by dashed–circles in Figure 2.6c. As it was defined, SVM is a classifier that maximizes the margin. Maximizing Eq. 2.7 is equivalent to minimizing the following equation,

$$\frac{1}{2}\|w\|^2 \tag{2.8}$$

The factor $\frac{1}{2}$ is used for mathematical convenience, [103]. Based on Eq. 2.5 and Eq. 2.8, SVM is a constrained optimization problem as,

$$\min_w \frac{1}{2}\|w\|^2 \tag{2.9}$$

$$\text{subject to} \qquad y_i(w^T X_i + b) \geq 1 \tag{2.10}$$

The above constrained optimization problem can be solved using Lagrange multipliers, [103].

2.3.1. Non–Linearly Separable Data

As it was explained with Eq. 2.3, if a hyper–plane f exists such that it correctly classifies all data points, the data are called linearly separable. The optimization problem

in Eq. 2.9 and Eq. 2.10 does not have a solution if data points are not linearly separable. To deal with such data points, the modified SVM allows some misclassified data points, while it is maximizing the margin. This modification uses a slack variable $q_i \geq 0$, and the modified optimization problem can be stated as,

$$\min_{w,q} \quad \frac{1}{2}\|w\|^2 + C\sum_i q_i \tag{2.11}$$

$$\text{subject to} \qquad y_i\left(w^T X_i + b\right) \geq 1 - q_i \qquad q_i \geq 0 \tag{2.12}$$

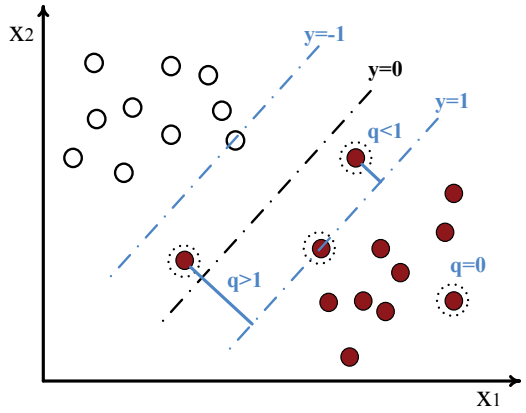

Figure 2.7 Introducing the slack variable q for non–linearly separable data

According to Eq. 2.12, and Figure 2.7, $q_i = 0$, corresponds to Eq. 2.10, and so X_i is either on the margin or correctly classified. For $0 < q_i < 1$, X_i is inside the margin and is correctly classified. For $1 < q_i$, X_i is misclassified. Based on Eq. 2.11, the amount of misclassification is minimized (the second term), while the margin is maximized (the first term). C is a hyper–parameter that compromises between the margin size and the amount of misclassification. Similar to Eq. 2.9 and Eq. 2.10, the modified optimization problem described by Eq. 2.11 and Eq. 2.12 can also be solved using Lagrange multipliers, [103].

2.3.2. Kernel Method

Sometimes data points that are not separable in their original space X are transformed to a new space $\phi(X)$ that usually has a higher dimension. In the new space $\phi(X)$, the transformed data points are separable. To reduce the computation cost of a higher dimension space, a technique called kernel method can be employed. The idea of this method is that for some new spaces $\phi(X)$, the dot product between the transformed data points $(\phi(X_i).\phi(X_j))$ are computed efficiently. It can be shown that the solution of Eq. 2.11 and Eq. 2.12 can be re–written so that it has only dot products of data points $(X_i.X_j)$, [84]. Therefore, when data points are transformed to a new space $\phi(X)$, the new solution only depends on the kernel function $\mathrm{Ker}(X_i, X_j) = \phi(X_i).\phi(X_j)$, and the kernel method is applicable.

Two commonly used kernels for SVM are radial–basis–function (RBF) kernel, and linear kernel which are described in Eq. 2.13 and Eq. 2.14 respectively, [84],

$$K(X_i, X_j) = \exp(-\gamma \|X_i - X_j\|^2) \qquad 2.13$$

$$\gamma > 0$$

$$K(X_i, X_j) = X_i.X_j \qquad 2.14$$

According to Eq. 2.14, in the linear kernel, the original space X and the new space $\phi(X)$ are identical. In Eq. 2.13, γ is a "hyper–parameter" (similar to C in Eq. 2.11). To find the optimal values of these hyper–parameters, usually a "grid search" approach is employed, in which the values of the hyper–parameters are changed; and the optimal values are found based on cross validation, [101]. In a ν–fold cross validation, the training data points are divided to ν equal–sized subsets. Then, $\nu - 1$ subsets are used for training, and the one remained subset is utilized for testing. The entire procedure is performed ν times, and the total classification error is obtained, [104]. Those values of C and γ will be selected that result the least error. In this study, the hyper–parameters were varied from $2^{-15}, 2^{-13}, \ldots$ to $2^{1}, 2^{3}$; and a 5–fold cross validation was employed.

2.3.3. Multi–Class SVM

SVM is basically designed for binary classifications. However, our problem in this study is a three–class classification. Hsu and Lin, [105], compared different methods for multi-class SVM, and concluded that a "one–against–one" (OAO) scheme was more suitable considering practical aspects. In this scheme, $\beta(\beta-1)/2$ binary classifiers are trained (β is the number of classes), and the class that receives the maximum "votes" is assigned to a test data.

2.4. Results

According to the described methodology (Figure 2.1), the recorded data were preprocessed, labeled, and used for feature extraction and scaling. The feature vectors extracted from two of the three repeated experiments were used for training SVM[3], and those of the third one were employed for testing. Table 2.1 indicates different groups of training and testing sets, and Table 2.2 shows the total number of samples for each group. The results of two classification cases (TCN and TAN) are studied separately during this chapter. The software LIBSVM, [106], was used for application of SVM. The classifier performance was evaluated from different aspects that had effects on the computational complexity and classification accuracy: number of features (p), scaling method, and kernel type.

In order to use SVM in real–time applications, less computational complexity is desired for testing (prediction), because the training can be performed offline.

Table 2.1 Different Groups for Training and Testing

Group Name	Training Set	Testing Set
G1	1 and 2	3
G2	1 and 3	2
G3	2 and 3	1

[3] The selection of the training data for support vector machine approach is discussed in Appendix B.

Table 2.2 Total Number of Training/Testing Samples for Each Group

	Total Number of Training/Testing Samples			
Groups [i]	**TCN (Training)** [ii]	**TCN (Testing)**	**TAN (Training)** [ii]	**TAN (Testing)**
G1	T (1175) [iii]	T (579)	T (1175)	T (579)
	C (621)	C (225)	A (577)	A (368)
	N (2102)	N (1021)	N (1914)	N (922)
G2	T (1146)	T (608)	T (1146)	T (608)
	C (508)	C (338)	C (661)	A (284)
	N (2076)	N (1047)	N (1925)	N (911)
G3	T (1187)	T (567)	T (1187)	T (567)
	C (563)	C (283)	C (652)	A (293)
	N (2068)	N (1055)	N (1833)	N (1003)

[i]: Different types of training/testing groups are defined in Table 2.1

[ii]: The classes are: T = Tooth, C = Composite, A = Amalgam, N = Noncontact

[iii]: The number of training/testing samples is shown in the parenthesis

In case of linear kernel, the prediction complexity is $O(p)$; where p is the number of features (The obtained w and b can be stored, and then the prediction is simply done using Eq. 2.1). For RBF kernel, the prediction computation is more complex, and is $O(n_{SV}p)$, [84], where n_{sv} indicates the number of support vectors. As it was mentioned in section 2.2.3, feature scaling can improve the classification accuracy by preventing attributes in greater numeric ranges dominate those in smaller ranges.

In this section, to train and test a SVM classifier for TCN, 64 features, linear feature scaling, and RBF kernel (Eq. 2.13), was used. For TAN case, 32 features, normal feature scaling, and linear kernel (Eq. 2.14), was employed. The reasons for such selections will be provided in sections 2.4.1 (Number of Features), 2.4.2 (Feature Scaling), and 2.4.3 (SVM Kernel). As it was described in section 2.3, to find the hyper–parameter values, a 5–fold cross validation was employed; and the results are displayed in Table 2.3. It should be mentioned that the cross–validation was performed on each group of Table 2.1 separately.

Table 2.3 ***The Hyper–Parameters' Values from 5–Fold Cross Validation (<u>TCN case</u>: 64 features, RBF kernel, linear scale; <u>TAN case</u>: 32 features, linear kernel, normal scale)***

Cases [i]	C_{G1} [ii]	γ_{G1}	CV_{G1} [iii]	C_{G2}	γ_{G2}	CV_{G2}	C_{G3}	γ_{G3}	CV_{G3}
TCN	8	0.5	99	32768	1	98	32768	1	99
TAN	32768	–	99	1	–	98	1	–	98

[i]: T = Tooth, C = Composite, A = Amalgam, N = Noncontact

[ii]: G1, G2, and G3 correspond to data sets specified in Table 2.1

[iii]: CV = Cross Validation accuracy (percentage) for each group

All the values of the Table 2.3 resulted in 98–100% cross validation accuracy, and therefore it was not needed to look for other values of C and γ. In this table, no values were obtained for γ in TAN case, because a linear kernel was employed. The hyper–parameters of Table 2.3 were used to train the SVM classifiers for TCN and TAN cases (one–against–one scheme was used, as it was explained in section 2.3.3). Table 2.4 and Table 2.5 indicate the accuracy of these classifiers on the testing data of each group.

Table 2.4 ***The Classification Accuracy of TCN Case (64 features, RBF kernel, linear scale)***

	Groups [ii]		
Classes [i]	**G1**	**G2**	**G3**
T	93 (579) [iii]	74 (608)	98 (567)
C	88 (225)	91 (338)	80 (283)
N	84 (1021)	97 (1047)	89 (1055)

[i]:T = Tooth, C = Composite, N = Noncontact

[ii]: Groups are based on Table 2.1

[iii]: The accuracy is represented by percentage. The number of testing samples is shown in the parenthesis

According to Table 2.4, the worst accuracy for TCN case was 74% which was obtained in classifying of 608 test–samples of tooth data (G2). The best accuracy for this case was for tooth too (G3) with 98% correct classification out of 567 test samples. For TAN case, as Table 2.5 indicates, the worst accuracy was for amalgam (G1) with 83% correct classification out of 368 test samples. The best accuracy for this case was for

both tooth (G3) and amalgam (G3) with 97% correct classification out of 567 and 293 test samples respectively.

Table 2.5 The Classification Accuracy of TAN Case (32 features, linear kernel, normal scale)

	Groups [ii]		
Classes [i]	**G1**	**G2**	**G3**
T	96 (579) [iii]	92 (608)	97 (567)
A	83 (368)	92 (284)	97 (293)
N	85 (922)	95 (911)	92 (1003)

[i]: T = Tooth, A = Amalgam, N = Noncontact

[ii]: Groups are based on Table 2.1

[iii]: The accuracy is represented by percentage. The number of testing samples is shown in the parenthesis

Considering all testing/training groups, the accuracy range and average for both cases are presented in Table 2.6. The range was the minimum to the maximum accuracy for each class. The average was obtained using the arithmetic mean of all the accuracies of a class.

In obtaining the above accuracies, there were different sources of error. The errors could be generally caused by the performance of classifier and/or the nature of cutting sounds. As Eq. 2.11 indicates, the classifier was allowed for some misclassification in the training stage, which might cause error in the testing stage. It was also possible that the training data were not “rich” enough to cover the space of some misclassified data. Numerical and computational limits of using SVM algorithm were another potential source for misclassification.

On the other hand, variations of cutting sounds from one experiment to another could be large for some data samples, which resulted in misclassification. These variations could be caused by some uncontrolled parameters such as cutting force, feed rate, temperature, etc. Moreover, labeling of data was not perfect, and in the transition between noncontact to contact data and vice versa, there could be some mislabelled data (Figure 2.4). Rather than mislabelled data, the classification error occurred more frequently in the transition region, perhaps because the features of this region were similar to those of both contact and noncontact regions. For example, in the

classification of one set of noncontact data (114 total samples), among the first 45 data samples, which were close to the contact data, only 1 sample was correctly classified. In another set of noncontact data (100 total samples), the last 11 samples that were just before the contact region were misclassified.

Table 2.6 The Classification Accuracy Range and Average (TCN case: 64 features, RBF kernel, linear scale; TAN case: 32 features, linear kernel, normal scale)

Accuracy	Case 1			Case 2		
	T	C	N	T	A	N
Range [ii]	74–98 [iii]	80–91	84–97	92–97	83–97	85–95
Average [ii]	88 [iii]	87	90	95	90	91

[i]: T = Tooth, C = Composite A = Amalgam, N = Noncontact

[ii]: Accuracy range and average were obtained based on Table 2.4 and Table 2.5 for TCN and TAN cases respectively

[iii]: The accuracy range and average are represented by percentage.

One way to analyse the classification results is using the confusion matrix, which is depicted for TCN (group G1) and TAN (group G1) in Figure 2.8 and Figure 2.9 respectively. In these matrices, the diagonal numbers (green) show the correct classifications, and the off–diagonal values (red) indicate the number of miss–classifications. Class 1 and 3 are tooth and noncontact, and class 2 is either composite (Figure 2.8), or amalgam (Figure 2.9). “Target” indicates the true class of each sample, whereas “output” shows the predicted class.

Analysing the columns of confusion matrices reveal the classification accuracies that were obtained for group G1 in Table 2.4 (TCN) and Table 2.5 (TAN). For example, the first column of Figure 2.8 indicates that among 579 tooth samples, 536 samples were correctly classified, 18 samples incorrectly classified as composite, and 25 samples misclassified as noncontact. Analysing the rows of confusion matrices show the accuracy of assigned labels by the classifier. For instance, the second row of Figure 2.9 shows that when the classifier assigned label “amalgam”, 96.8% of time it was a correct assignment.

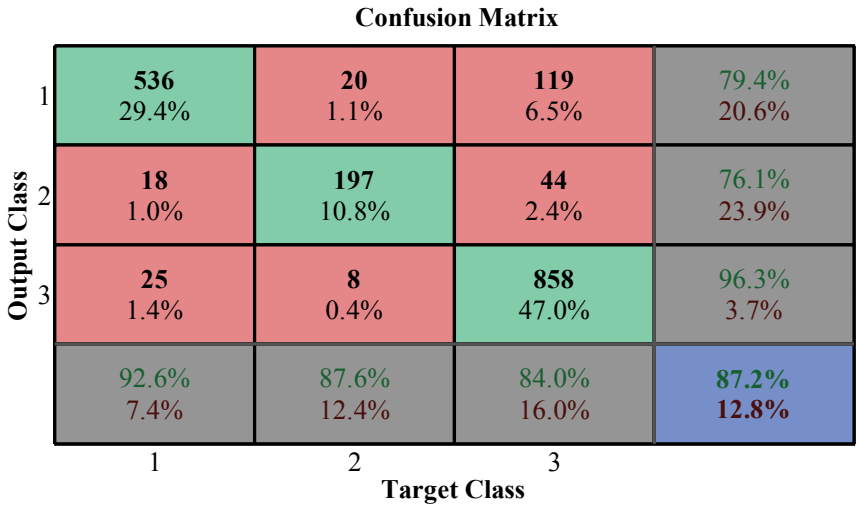

Figure 2.8 ***The confusion matrix for classification of TCN case (group G1), class 1 = tooth, class 2 = composite, class = noncontact***

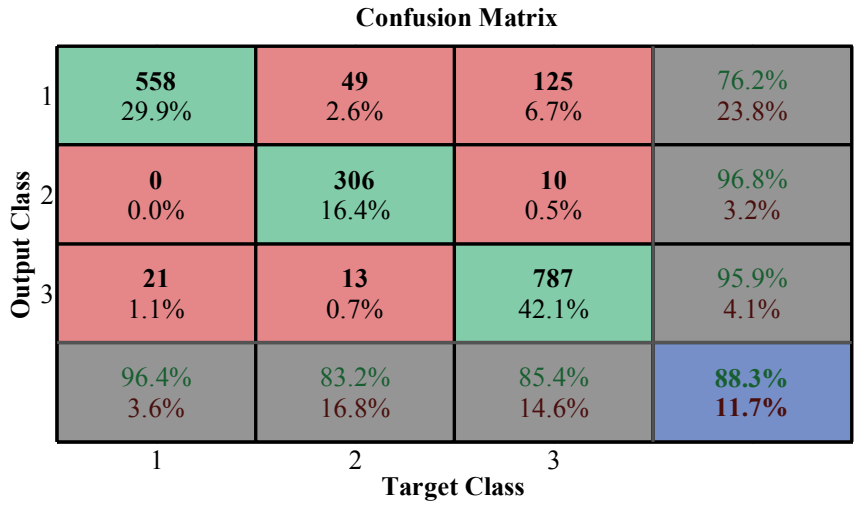

Figure 2.9 ***The confusion matrix for classification of TAN case (group G1), class 1 = tooth, class 2 = amalgam, class 3 = noncontact***

Following our discussions on the transition region, it can also be observed from above figures that most of the errors occurred in classifying between contact (tooth, composite, amalgam) and noncontact data. These errors mostly happened in the transition from the contact to noncontact data and vice versa, because of mislabelling, and similarity of contact and noncontact data.

Another source of error between contact and noncontact data could be stemmed from the nature of cutting procedures that utilized dental burs. The surface of a dental bur is not smooth, and contains blades for cutting the material. During the rotation of bur, and in the passing of one blade to another, there might be some noncontact moments, which generated noncontact sound that eventually caused classification inaccuracies between contact and noncontact classes.

2.4.1. Number of Features

The results of Table 2.4 (TCN case) and Table 2.5 (TAN case) were obtained for 64 and 32 features respectively. In this section, the effect of different number of features in the classification accuracy of both cases is studied. As explained in section 2.2.3, the absolute value of the first 2048 short–time Fourier transform (STFT) coefficients were selected and were divided to p equal–sized groups ($\frac{2048}{\mathrm{p}}$ coefficients in each group; $\mathrm{p} = 2, 4, 8, 16, \dots, 256, 512$). The data of each group were averaged arithmetically to obtain p features for both cases. In TCN case, RBF kernel (Eq. 2.13), and linear scaling was used; whereas in TAN case, linear kernel (Eq. 2.14), and normal scaling was employed. The reasons for such selections will be provided in sections 2.4.2 (Feature Scaling), and 2.4.3 (SVM Kernel). The optimal value of hyper–parameters as well as their corresponding cross validation accuracy for different number of features in each training/testing group is provided in Appendix C.

The obtained hyper–parameters were used to train the classifiers for TCN and TAN cases with different number of features, and the details can be found in Appendix C. Considering all the training/testing groups, the accuracy of TCN and TAN classifiers were computed for each number of features, and are plotted in logarithmic scale (powers of 2) in Figure 2.10 and Figure 2.11 respectively. The total accuracies in these figures were obtained considering the accuracies of all classes in all testing/training groups together. In Figure 2.10, the maximum total accuracy for TCN was 89% which was obtained for 64 features. Considering TAN in Figure 2.11, the maximum total accuracy was 92% that was occurred in 32, 64, and 128 features. Reminding the prediction complexity of linear kernel, $\mathrm{O}(\mathrm{p})$, less number of features (p) is desirable. Therefore for TAN, $\mathrm{p} = 32$ was chosen.

The accuracies of noncontact class in Figure 2.10, and tooth class in Figure 2.11 were almost constant, and did not vary significantly with respect to p. It seemed that the trained classifiers were biased toward these classes for lower number of features, and then increasing p could enhance the classification accuracies of other classes (tooth and composite in TCN, amalgam and noncontact in TAN) toward reaching the maximum total accuracy. Lower p's divided the spectral range to only few subintervals, and therefore the frequency resolution was very small, which greatly degraded the classifier performance. In lower number of features, the classifiers acted more like differentiating between two classes (contact and noncontact) rather than discriminating between three classes. For example in Figure 2.10, the classifier was biased toward noncontact class, and in Figure 2.11, it was biased toward contact classes (particularly tooth).

As these figures indicate, the total classification accuracies first enhanced by increasing the number of features, and then reduced for higher values of p. In the literature, this behaviour is referred as "peaking phenomenon", [107], which states that for a fixed sample size (that holds true in this study), the classification accuracy increases and then decreases as the number of features grows (a peak occurs). Generally, more features could increase the separability among classes; however, because of the limited size of data, the added features eventually acted similar to noises, and reduced the accuracies, [107].

2.4.2. Feature Scaling

In obtaining the results of Table 2.4 (TCN case) linear scaling was used; whereas for TAN case in Table 2.5, the normal scaling was employed. In this section, the effect of linear, normal, and no feature scaling on the classification accuracy of both cases are studied. In TCN case, 64 features, and RBF kernel (Eq. 2.13) was used, whereas for TAN case, 32 features, and linear kernel (Eq. 2.14) was utlizied. The reasons for such kernel selections will be provided section 2.4.3 (SVM Kernel).

The optimal value of hyper–parameters as well as their corresponding cross validation accuracy for linear, normal, and no feature scaling is provided in Appendix D.

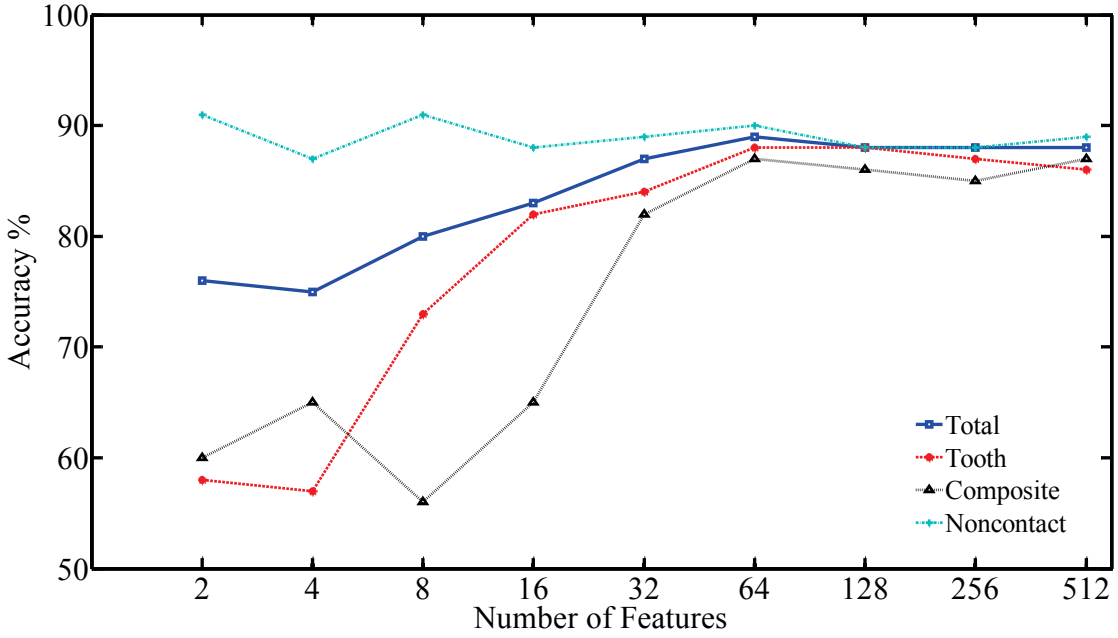

Figure 2.10 ***The effect of number of features on the accuracy of the TCN classifier considering all the training/testing groups (RBF kernel, linear scale). The features axis has logarithmic scale (powers of 2).***

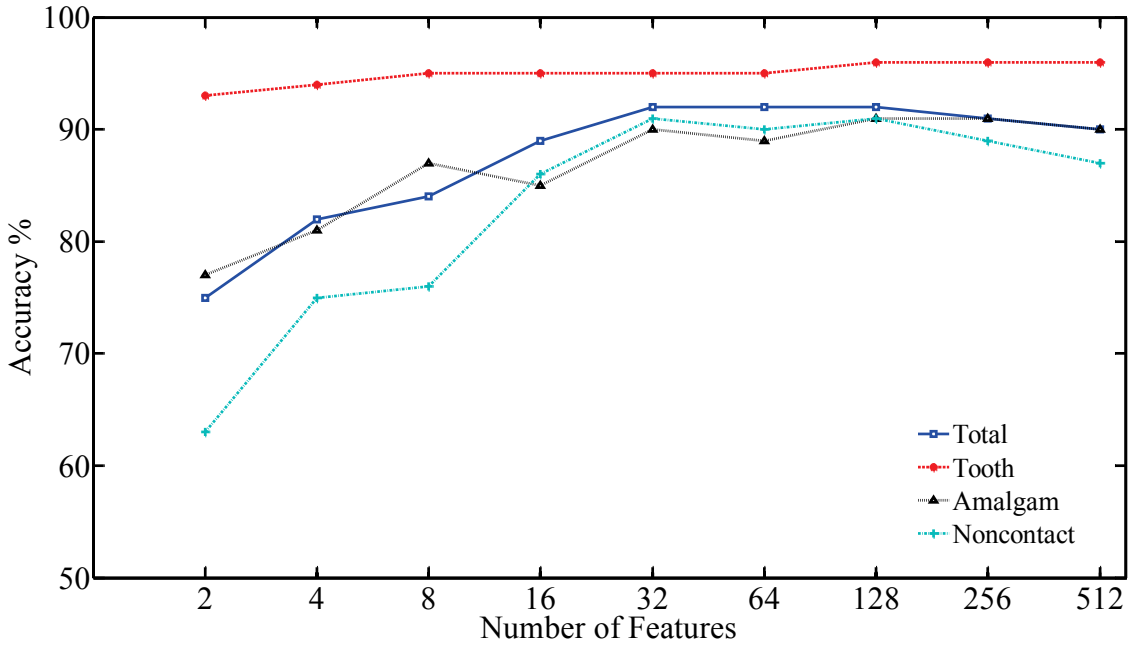

c

Figure 2.11 ***The effect of number of features on the accuracy of the TAN classifier considering all the training/testing groups (linear kernel, normal scale). The features axis has logarithmic scale (powers of 2).***

The obtained hyper–parameters then were used to train the SVM classifiers for TCN and TAN cases with different feature scaling methods. Table 2.7 (TCN case) and Table 2.8 (TAN case) indicate the accuracy of these classifiers on the testing data. It should be mentioned the same method of feature scaling was used for training and testing data.

Table 2.7 The Effect of Different Feature Scaling Methods in Classification Accuracy of TCN Case (64 features, RBF kernel)

		Feature Scaling Methods [iii]		
Groups [i]	**Classes** [ii]	**No Scaling**	**Linear**	**Normal**
G1	T (579) [iv]	74 [v]	93	93
	C (225)	79	88	78
	N (1021)	88	84	81
G2	T (608)	70	74	69
	C (338)	91	91	97
	N (1047)	98	97	98
G3	T (567)	84	98	97
	C (283)	64	80	76
	N (1055)	91	89	91

[i]: Different types of training/testing groups are defined in Table 2.1

[ii]: The classes are: T = Tooth, C = Composite, N = Noncontact

[iii]: Linear scaling: scaled to the interval [0,1]. Normal scaling: scaled to have zero mean and unit variance

[iv]: The number of test samples for each group/class is given in the parenthesis

[v]: The accuracy percentage of each group/class with the corresponding scaling method

Each row of Table 2.7 and Table 2.8 indicates the classification accuracy of a group/class with respect to its feature scaling method. For example in Table 2.8, noncontact class of G3 had 81%, 91%, and 92% accuracy for no scaling, linear scaling, and normal scaling respectively. Generally, feature scaling could increase the classification accuracy comparing to no scaling. It seems that similar to the previous section (Number of Features), when no scaling was applied, the classifiers were biased toward differentiating between two classes (contact and noncontact) rather than three classes.

Table 2.8 The Effect of Different Feature Scaling Methods in Classification Accuracy of TAN Case (32 features, linear kernel)

		Feature Scaling Methods [iii]		
Groups [i]	**Classes** [ii]	**No Scaling**	**Linear**	**Normal**
G1	T (579) [iv]	94	95	96
	A (368)	65	80	83
	N (922)	67	87	85
G2	T (608)	89	91	92
	A (284)	100	91	92
	N (911)	68	94	95
G3	T (567)	96	97	97
	A (293)	97	97	97
	N (1003)	81	91	92

[i]: Different types of training/testing groups are defined in Table 2.1

[ii]: The classes are: T = Tooth, A = Amalgam, N = Noncontact

[iii]: Linear scaling: scaled to the interval [0,1]. Normal scaling: scaled to have zero mean and unit variance

[iv]: The number of test samples for each group/class is given in the parenthesis

[v]: The accuracy percentage of each group/class with the corresponding scaling method

Although the difference between accuracies of no scaling in contact (tooth, composite/amalgam) and noncontact classes was not as significant as the difference among lower p's, it is still observable in above tables. As it was stated in section 2.2.2, all contact data mostly had higher signal powers (amplitudes) than noncontact data. Therefore, while no scaling was used, the classifiers could not efficiently discriminate between contact classes (tooth and composite in TCN; tooth and amalgam in TAN), which made them to act mostly as binary classifiers (between contact and noncontact classes). Employing scaling methods could enhance the classifiers performance for both cases, and the accuracies of all classes increased.

Considering all testing/training groups, the accuracy range and average of both cases for different feature scaling methods are presented in Table 2.9 and Table 2.10. The classification accuracy range was obtained from the minimum to the maximum accuracy for each class. The classification accuracy average was computed by the arithmetic mean of all the accuracies of a class.

Table 2.9 The Classification Accuracy Range and Average for Different Feature Scaling Methods in TCN Case (64 features, RBF kernel)

	Feature Scaling Methods [i]					
Classes [ii]	**No Scaling (Range)**	**No Scaling (Average)**	**Linear (Range)**	**Linear (Average)**	**Normal (Range)**	**Normal (Average)**
T	70–84 [iii]	76	74–98	88	69–97	86
C	64–91	79	80–91	87	76–97	85
N	88–98	92	84–97	90	81–98	90

[i]: Linear scaling: scaled to the interval [0,1]. Normal scaling: scaled to have zero mean and unit variance

[ii]: T = Tooth, C = Composite, N = Noncontact

[iii]: The accuracy range and average are represented by percentage

Table 2.10 The Classification Accuracy Range and Average for Different Feature Scaling Methods in TAN Case (32 features, linear kernel)

	Feature Scaling Methods [i]					
Classes [ii]	**No Scaling (Range)**	**No Scaling (Average)**	**Linear (Range)**	**Linear (Average)**	**Normal (Range)**	**Normal (Average)**
T	89–96 [iii]	93	91–97	94	92–97	95
A	65–100	85	80–97	89	83–97	90
N	67–81	72	87–94	91	85–95	91

[i]: Linear scaling: scaled to the interval [0,1]. Normal scaling: scaled to have zero mean and unit variance

[ii]: T = Tooth, A = Amalgam, N = Noncontact

[iii]: The accuracy range and average are represented by percentage

As Table 2.9 indicates, for TCN case, linear scaling had a more reliable response in the sense that it had the highest minimum range among all of the classes (except the noncontact class). In addition for TAN (Table 2.10), most often normal scaling had the highest minimum/maximum ranges among all of the classes (except the minimum range of the noncontact class). In TCN case, the total accuracy for different feature scaling methods was as 85%, 89%, and 88% for no scaling, linear scaling, and normal scaling respectively. The total accuracy for TAN case was 81%, 91%, and 92% for no scaling, linear scaling, and normal scaling respectively. According to these results, linear and normal scaling methods were selected for TCN and TAN cases respectively.

2.4.3. SVM Kernel

The previous results of Table 2.4 (TCN case) and Table 2.5 (TAN case) were obtained for RBF and linear kernels respectively. In this section, the effect of RBF (Eq. 2.13) and linear (Eq. 2.14) kernels on the classification accuracy of each case is studied. Similar to section 2.4, in TCN case, 64 features, and linear scaling was used; whereas in TAN case, 32 features, and normal scaling was employed.

The optimal value of hyper–parameters as well as their corresponding cross validation accuracy for RBF and linear SVM kernels is presented in Appendix E. The obtained hyper–parameters then were used to train the SVM classifiers for TCN and TAN using both RBF and linear kernels. Table 2.11 (TCN case) and Table 2.12 (TAN case) indicate the accuracy of these classifiers on the testing data.

As Table 2.11 shows, linear kernel for TCN case had a better result for noncontact classes. For example in the group G3, the classification accuracy of noncontact class was increased from 89% to 92% by changing the RBF kernel to the linear one. In other classes, except for composite of group G2, using RBF kernel resulted better classification accuracies. Considering the results of Table 2.12, it can be observed that in most of the classes/groups, using linear kernel for TAN case had a better accuracy comparing to the RBF kernel. The only two exceptions were amalgam class of group G3 and noncontact class of group G1.

As it was stated before, the computational complexity of using SVM with linear and RBF kernels is $O(p)$ and $O(n_{SV}p)$ respectively, where p is the number of features, and n_{sv} indicates the number of support vectors. In addition, as it was shown in section 2.4.1, the maximum accuracy for TCN and TAN cases was achieved at $p = 64$, and $p = 32$. Therefore, it can be concluded that the computational cost of using TCN case was more than TAN. Considering all testing/training groups, the accuracy range and average of both cases using different kernels are presented in Table 2.13 and Table 2.14.

As Table 2.13 indicates for TCN case, RBF kernel had a better accuracy range and average for tooth class comparing to linear kernel. For composite class, RBF had a

higher minimum range. In the noncontact class, although linear kernel had a more accurate range and average; its difference with RBF kernel was not significant.

Table 2.11 The Effect of Different SVM Kernels in Classification Accuracy of TCN Case (64 features, linear scale)

		SVM Kernels [iii]	
Groups [i]	**Classes** [ii]	**RBF**	**Linear**
G1	T (579) [iv]	93 [v]	83
	C (225)	88	87
	N (1021)	84	85
G2	T (608)	74	67
	C (338)	91	96
	N (1047)	97	98
G3	T (567)	98	93
	C (283)	80	69
	N (1055)	89	92

[i]: Different types of training/testing groups are defined in Table 2.1

[ii]: The classes are: T = Tooth, C = Composite, N = Noncontact

[iii]: RBF: Radial Basis Function (Eq. 2.13); Linear Kernel (Eq. 2.14)

[iv]: The number of test samples for each group/class is given in the parenthesis

[v]: The accuracy percentage of each group/class with the corresponding SVM kernel

The total accuracy of TCN case was 89%, 87% for RBF and linear kernels respectively. Considering these facts, it can be concluded that choosing the RBF kernel for TCN case would obtain more accurate results.

As Table 2.14 indicates for TAN case, the linear kernel had a better accuracy range and average for noncontact class comparing to RBF kernel. For amalgam and tooth classes, linear kernel had a higher minimum range. The total accuracy of TAN case was 86%, 92% for RBF and linear kernels respectively. According to these facts, it can be concluded that choosing the linear kernel for TAN case would obtain more accurate results.

Table 2.12 The Effect of Different SVM Kernels in Classification Accuracy of TAN Case (32 features, normal scale)

		SVM Kernels [iii]	
Groups [i]	**Classes** [ii]	**RBF**	**Linear**
G1	T (579) [iv]	96 [v]	96
	A (368)	74	83
	N (922)	87	85
G2	T (608)	91	92
	A (284)	81	92
	N (911)	87	95
G3	T (567)	97	97
	A (293)	98	97
	N (1003)	76	92

[i]: Different types of training/testing groups are defined in Table 2.1

[ii]: The classes are: T = Tooth, C = Composite, N = Noncontact

[iii]: RBF: Radial Basis Function (Eq. 2.13); Linear Kernel (Eq. 2.14)

[iv]: The number of test samples for each group/class is given in the parenthesis

[v]: The accuracy percentage of each group/class with the corresponding SVM kernel

2.4.4. Temporal Voting

Temporal voting is a promising approach to enhance the classification accuracy. As it was mentioned previously in section 2.2.3, the recorded sounds were windowed (framed) with 50% overlapping (Hamming windowing). The appropriate features were extracted from each window, and were considered as one sample data. In this approach, the used time interval is equal to the window–length (WL) as Figure 2.12a shows.

In the temporal voting approach, the time interval is chosen so that it covers more than one window. As Figure 2.12b indicates, the time interval is corresponding to five windows (considering 50% of overlapping). In such an approach, the class of each sample in the selected time interval is first found separately, i.e. the class of data associated with W1, W2, ..., W5. Then, the class that has the maximum votes would be assigned to the sample associated with W1 (Figure 2.12b). For example, if W1 and W3

are tooth class and W2, W4, and W5 are noncontact class; W1 will be assigned a noncontact class.

Table 2.13 The Classification Accuracy Range and Average for Different SVM Kernels in TCN Case (64 features, linear scale)

	SVM Kernels [i]			
Classes [ii]	**RBF (Range)**	**RBF (Average)**	**Linear (Range)**	**Linear (Average)**
T	74–98 [iii]	88	67–93	81
C	80–91	87	69–96	85
N	84–97	90	85–98	92

[i]: RBF: Radial Basis Function (Eq. 2.13); Linear Kernel (Eq. 2.14)

[ii]: T = Tooth, C = Composite, N = Noncontact

[iii] The accuracy range and average are represented by percentage

Table 2.14 The Classification Accuracy Range and Average for Different SVM Kernels in TAN Case (32 features, normal scale)

	SVM Kernels [i]			
Classes [ii]	**RBF (Range)**	**RBF (Average)**	**Linear (Range)**	**Linear (Average)**
T	91 –97 [iii]	95 [iii]	92–97	95
A	74–98	84	83–97	90
N	76–87	83	85–95	91

[i]: RBF: Radial Basis Function (Eq. 2.13); Linear Kernel (Eq. 2.14)

[ii]: T = Tooth, A = Amalgam, N = Noncontact

[iii] The accuracy range and average are represented by percentage

If the selected number of windows in the temporal voting approach is n_w (with 50% overlapping) and the length of each window is WL, the used time interval is

$$\frac{(n_w + 1)}{2} \text{WL} \qquad 2.15$$

In this section, the hyper–parameters of Table 2.3 was used to train TCN and TAN classifiers for different training/testing groups (Table 2.1). For TCN case, 64 features were selected, linear feature scaling was used, and RBF kernel was chosen.

For TAN case, 32 features were selected, normal feature scaling was employed, and linear kernel was used. Table 2.15 and Table 2.16 compare the effect of the temporal voting with different number of windows on the classification accuracies of the trained TCN and TAN classifiers.

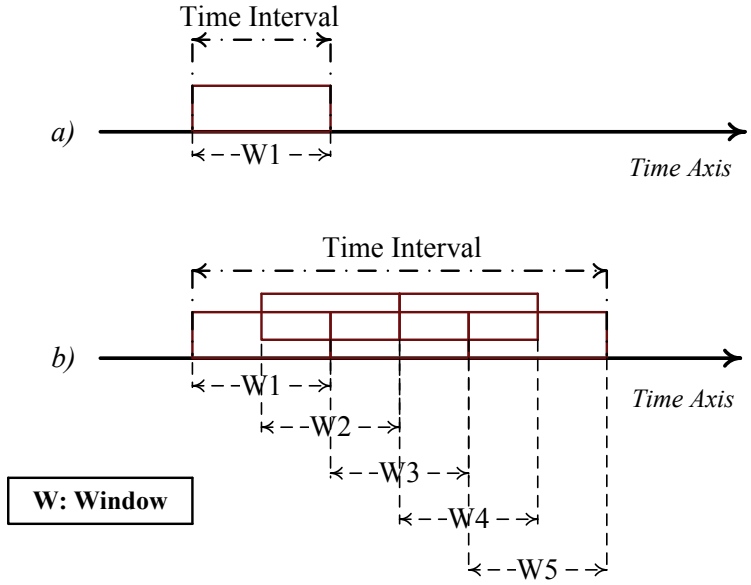

Figure 2.12 The Schematic of Temporal Voting Approach

Based on the results of Table 2.15 and Table 2.16, increasing the number of windows could enhance the classification accuracy. For example in Table 2.15, the classification accuracy of tooth in group G2 was increased from 74% to 81% by choosing 15 windows. Using the temporal voting approach also increased the used time interval; as for the example, it was changed from 44 ms (1 window) to 350 ms (15 windows). Generally, there is a compromise between the classification accuracy, and the used time interval, because a higher accuracy in a shorter time is desirable. The used time interval of temporal voting approach can be compared to human reaction–time. Thus far, no investigations were found in the literature on reaction–time of dentists in restoration procedures for preventing removal of healthy tooth layers. However, the averaged human recognition reaction–time was reported to be around 384 ms, [108]. In recognition reaction–time experiments, there were various stimuli, and the participants should have responded only to some of them (not all), which was the most similar reaction–time to our study.

Table 2.15 The Effect of the Temporal Voting with Different Number of Windows in The Classification Accuracy of TCN Case (64 features, RBF kernel, linear scale)

		Number of Windows (n_w)										
Groups [i]	**Classes** [ii]	**1**	**2**	**5**	**10**	**15**	**20**	**25**	**30**	**35**	**40**	**44**
	T (579) [iv]	93 [iii]	94	95	96	97	98	99	100	100	100	100
G1	C (225)	88	88	88	92	92	94	95	96	100	100	100
	N (1021)	84	86	86	88	89	90	90	91	92	93	93
	T (608)	74	74	78	78	81	82	84	84	86	86	86
G2	C (338)	91	94	93	99	100	100	100	100	100	100	100
	N (1047)	97	98	98	98	98	98	98	98	98	98	98
	T (567)	98	99	99	100	100	100	100	100	100	100	100
G3	C (283)	80	80	80	84	85	89	90	90	90	90	90
	N (1055)	89	90	90	91	92	94	95	95	95	95	95

[i]: Different types of training/testing groups are defined in Table 2.1

[ii]: The classes are: T = Tooth, C = Composite, N = Noncontact

[iii]: The accuracy percentage of each group/class and number of windows

[iv]: The number of test samples for each group/class is given in the parenthesis

The least time interval, corresponded to one window (~44 ms), was approximately 9 times smaller than the averaged human recognition reaction–time. To have a time interval less than 384 ms, the number of windows should be less than 17 according to Eq. 2.15. However, dental restoration procedures are complicated operations and discerning the boundary of dental materials is very challengeable for dentists, because of limited functionality of human senses. Therefore, the recognition reaction–time for restorative operations seems to be more than the reported value.

Table 2.17 compares the accuracy range and average for $n_w = 15$ (corresponding to 350 ms time interval) with $n_w = 1$ (corresponding to 44 ms).

The results of Table 2.17 indicate the effect of using the temporal voting approach in improving the accuracy ranges and averages of both cases. The total accuracy of TCN was increased from 89% for $n_w = 1$ to 93% for $n_w = 15$. The total accuracy of TAN was also increased from 92% to 94% for $n_w = 1$ and $n_w = 15$ respectively.

Table 2.16 The Effect of the Temporal Voting with Different Number of Windows in The Classification Accuracy of TAN Case (32 features, linear kernel, normal scale)

		Number of Windows ($\mathbf{n_w}$)										
Groups [i]	**Classes** [ii]	**1**	**2**	**5**	**10**	**15**	**20**	**25**	**30**	**35**	**40**	**44**
	T (579) [iv]	96 [iii]	97	98	98	99	100	100	100	100	100	100
G1	A (368)	83	82	80	81	79	80	80	80	81	82	83
	N (922)	85	86	84	86	86	86	86	83	86	86	85
	T (608)	92	93	94	94	95	96	96	97	97	97	98
G2	A (284)	92	93	94	94	96	97	97	97	97	97	97
	N (911)	95	96	96	97	97	97	97	97	97	97	97
	T (567)	97	98	99	99	100	100	100	100	100	100	100
G3	A (293)	97	98	99	100	100	100	100	100	100	100	100
	N (1003)	92	93	92	94	95	95	95	95	95	96	96

[i]: Different types of training/testing groups are defined in Table 2.1

[ii]: The classes are: T = Tooth, A = Amalgam, N = Noncontact

[iii]: The accuracy percentage of each group/class and number of windows

[iv]: The number of test samples for each group/class is given in the parenthesis

Table 2.17 The Classification Accuracy Range and Average for Different Number of Windows in Using the Temporal Voting Approach for Both Cases (<u>TCN case</u>: 64 features, RBF kernel, linear scale; <u>TAN case</u>: 32 features, linear kernel, normal scale)

Classes [i]	$\mathbf{n_w = 1}$ **(Range)** [ii]	$\mathbf{n_w = 1}$ **(Average)**	$\mathbf{n_w = 15}$ **(Range)**	$\mathbf{n_w = 15}$ **(Average)**
T	74–98 [iii]	88 [iii]	81–100	92
C	80–91	87	92–100	93
N	84–97	90	89–98	93
T	92–97	95	95–100	98
A	83–97	90	79–100	91
N	85–95	91	86–97	93

[i]: The classes are: T = Tooth, C = Composite, A = Amalgam, N = Noncontact

[ii]: $\mathrm{n_w}$ = Number of windows in the temporal voting approach. $\mathrm{n_w} = 1$ means not using the temporal voting approach

[iii]: The percentage of accuracy range and average for each class/group/number of windows in the temporal voting approach

2.4.5. Classification Scheme

As it was mentioned in section 2.3.3, the one–against–one (OAO) scheme was used for multi–class SVM. An alternative approach is considering a hierarchical classification scheme, which is depicted in Figure 2.13. In this scheme, a hierarchical structure with two levels is considered. In the first level, the classifier decides if the data belong to the contact or noncontact classes. The second level is used for contact data, and based on the classification case, it determines between tooth/composite (case 1 in Figure 2.13), or tooth/amalgam (case 2 in Figure 2.13).

In order to employ the hierarchical scheme for TCN case, two bi–class models for contact/noncontact (Con/N) and tooth/composite (T/C) were obtained. To train these models, 64 averaged FFT coefficients were selected as features and each feature vector was linearly scaled. An RBF kernel was chosen and the optimal values for hyper–parameters were found by a 5–fold cross validation. Table 2.18 shows the optimal values of the hyper–parameters.

The cross–validation accuracies of Table 2.18 were between 99%–100%, and therefore the obtained hyper–parameters were chosen for training the bi–class models. Table 2.19 shows the classification accuracies of the developed models for different training/testing groups. The developed models of Table 2.19 were employed in the hierarchical scheme (Figure 2.13), and Table 2.20 shows the classification accuracy of this scheme for TCN case and compares the results with the one–against–one (OAO) scheme.

As Table 2.20 shows, the hierarchical scheme improved the classification accuracy of the tooth class for groups G1 and G2. The accuracy in classification of composite of G2 as well as noncontact classes of G2 and G3 were also increased for the hierarchical scheme. Considering all the training/testing groups, Table 2.21 represents the classification accuracy range and average of each class for hierarchical and OAO schemes (TCN case).

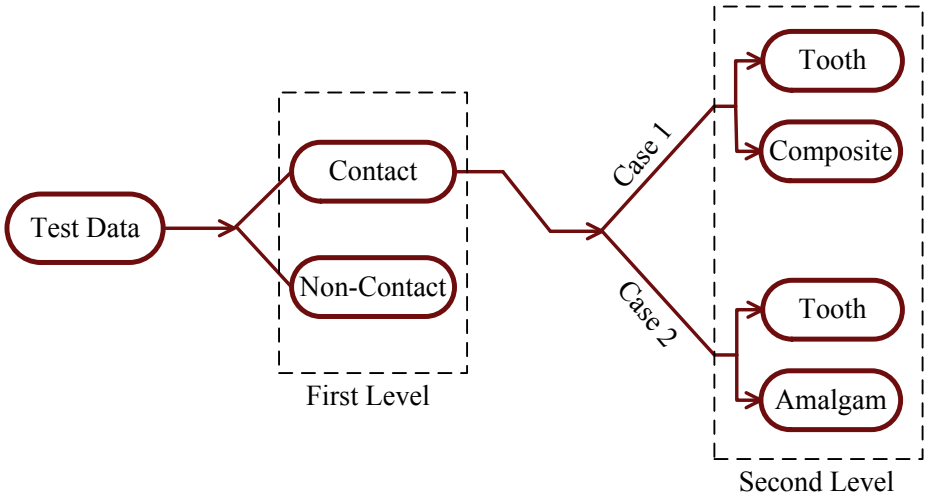

Figure 2.13 The hierarchical classification scheme

Table 2.18 The Hyper–Parameters' Values from 5–Fold Cross Validation for the Hierarchical Classification Scheme in TCN Case (64 features, RBF kernel, linear scale)

Bi–Class Models [i]	C_{G1} [ii]	γ_{G1}	CV_{G1} [iii]	C_{G2}	γ_{G2}	CV_{G2}	C_{G3}	γ_{G3}	CV_{G3}
Con/N	32768	2	99	8	2	99	32768	2	99
T/C	32768	1	100	32768	0.5	100	2	0.5	100

[i]: Con = Contact, N = Noncontact, T = Tooth, C = Composite

[ii]: G1, G2, and G3 corresponds to data sets specified in Table 2.1

[iii]: CV = Cross Validation accuracy (percentage) for each group

As Table 2.21 indicates, OAO scheme had a better minimum accuracy range and average over the hierarchical approach for composite and noncontact classes. In addition, the total accuracy for the hierarchical and OAO schemes was 88%, and 89% respectively.

Similar to TCN case, two bi–class models for contact/noncontact (Con/N) and tooth/amalgam (T/A) were obtained for TAN case. To train these models, 32 averaged FFT coefficients were selected as the features, and each feature vector was normally scaled to have zero mean and unit variance. A linear kernel was chosen, and the optimal values for hyper–parameters were found by a 5–fold cross validation. Table 2.22 shows the optimal values of the hyper–parameters; and Table 2.23 indicates the classification accuracies of the developed models for different training/testing groups.

Table 2.19 The Classification Accuracy of Bi–Class Models of the Hierarchical Scheme for TCN Case (64 features, RBF kernel, linear scale)

Bi–Class Models [i]	Classes [i]	Groups [ii] G1	G2	G3
Con/N	Con	98 (804) [iii]	92 (946)	96 (850)
	N	76 (1021)	98 (1047)	91 (1055)
T/C	T	98 (579)	87 (608)	98 (567)
	C	81 (225)	97 (338)	87 (283)

[i]: Con = Contact, N = Noncontact, T = Tooth, C = Composite

[ii]: Groups are based on Table 2.1

[iii]: The accuracy is represented by percentage. The number of testing samples is shown in the parenthesis.

Table 2.20 The Comparison between One–Against–One and Hierarchical Classification Schemes for TCN Case (64 features, RBF kernel, linear scale)

Classification Scheme [i]	Classes [ii]	Groups [iii] G1	G2	G3
Hierarchical	T	97 (579) [iv]	75 (608)	97 (567)
	C	77 (225)	96 (338)	80 (283)
	N	76 (1021)	98 (1047)	91 (1055)
One–Against–One	T	93 (579)	74 (608)	98 (567)
	C	88 (225)	91 (338)	80 (283)
	N	84 (1021)	97 (1047)	89 (1055)

[i]: Hierarchical scheme is depicted Figure 2.13

[ii]: The classes are: T = Tooth, C = Composite, N = Noncontact

[iii]: Different types of training/testing groups are defined in Table 2.1

[iv]: The classification accuracy percentage of each class/group/classification scheme. The number of testing samples is shown in the parenthesis.

The developed models of Table 2.23 were employed in the hierarchical scheme (Figure 2.13), and Table 2.24 shows the classification accuracy of this scheme for TAN case and compares the results with one–against–one (OAO) scheme.

Table 2.21 The Classification Accuracy Range and Average of Hierarchical and One–Against–One (OAO) Schemes for TCN Case (64 features, RBF kernel, linear scale)

	Classification Schemes [i]			
Classes [ii]	**Hierarchical (Range)**	**Hierarchical (Average)**	**OAO (Range)**	**OAO (Average)**
T	75–97 [ii]	89 [ii]	74–98	88
C	77–96	86	80–91	87
N	76–98	88	84–97	90

[i]: Hierarchical scheme is depicted Figure 2.13. OAO: One Against One

[ii]: T = Tooth, C = Composite, N = Noncontact

[iii]: The percentage of accuracy range and average for each case/class/classification scheme

Table 2.22 The Hyper–Parameters' Values from 5–Fold Cross Validation for the Hierarchical Classification Scheme in TAN Case (32 features, linear kernel, normal scale)

Bi–Class Models [i]	C_{G1} [ii]	CV_{G1} [iii]	C_{G2}	CV_{G2}	C_{G3}	CV_{G3}
Con/N	0.25	96	0.5	95	1	94
T/A	32768	100	32768	100	32768	100

[i]: Con = Contact, N = Noncontact, T = Tooth, A = Amalgam

[ii]: G1, G2, and G3 corresponds to data sets specified in Table 2.1

[iii]: CV = Cross Validation accuracy (percentage) for each group

According to Table 2.24, tooth class of group G2, amalgam class of group G1, and noncontact class of groups G1 and G3, had a better accuracy in the hierarchical scheme. For other classes/groups, OAO scheme had better performance. The maximum difference between the accuracies of both schemes was for tooth of G1, in which the OAO classification was 17% (96%–79%) more accurate than the hierarchical scheme. Table 2.25 represents the classification accuracy range and average of each class for hierarchical and OAO schemes (TAN case).

As Table 2.25 indicates, except for the noncontact class, OAO classification had more accurate average and range comparing to the hierarchical scheme. The total accuracy for the OAO classification was 92%, whereas for the hierarchical scheme was 91%.

At the end, it should also be mentioned that the computational complexity of hierarchical scheme is less than OAO, because it included two binary classifiers ("contact vs. noncontact", and "tooth vs. composite (amalgam)"), whereas OAO comprised three binary classifiers ("tooth vs. noncontact", "composite (amalgam) vs. noncontact", and "tooth vs. composite (amalgam)".

Table 2.23 The Classification Accuracy of Bi–Class Models of the Hierarchical Scheme for TAN Case (32 features, linear kernel, normal scale)

		Groups [ii]		
Bi–Class Models [i]	**Classes [i]**	**G1**	**G2**	**G3**
Con/N	Con	86 (947) [iii]	90 (892)	95 (860)
	N	93 (922)	89 (911)	97 (1003)
T/A	T	100 (368)	97 (608)	99 (567)
	A	88 (579)	100 (284)	100 (293)

[i]: Con = Contact, N = Noncontact, T = Tooth, A = Amalgam

[ii]: Groups are based on Table 2.1

[iii]: The accuracy is represented by percentage. The number of testing samples is shown in the parenthesis.

Table 2.24 The Comparison between One–Against–One and Hierarchical Classification Schemes for TAN Case (32 features, linear kernel, normal scale)

		Groups [ii]		
Training	**Classes [i]**	**G1**	**G2**	**G3**
Hierarchical	T	79 (579) [iii]	94 (608)	96 (567)
	A	85 (368)	80 (284)	94 (293)
	N	93 (922)	89 (911)	97 (1003)
One–Against–One	T	96 (579)	92 (608)	97 (567)
	A	83 (368)	92 (284)	97 (293)
	N	85 (922)	95 (911)	92 (1003)

[i]: The classes are: T = Tooth, A = Amalgam, N = Noncontact

[ii]: Different types of training/testing groups are defined in Table 2.1

[iii]: The accuracy percentage of each training/class/group. The number of testing samples is shown in the parenthesis.

In addition, considering the fact that the total classification accuracy of OAO scheme for both cases was only 1% more, the hierarchical scheme can be chosen whenever less computational complexity is desirable.

Table 2.25 The Classification Accuracy Range and Average of One–Against–One and Hierarchical Schemes for TAN Case (32 features, linear kernel, normal scale)

	Classification Schemes [i]			
Classes [ii]	**Hierarchical (Range)**	**Hierarchical (Average)**	**OAO (Range)**	**OAO(Average)**
T	79–96 [iii]	90 [iii]	92–97	95
A	80–94	86	83–97	90
N	89 –97	93	85–95	91

[i]: Hierarchical scheme is depicted Figure 2.13. OAO: One Against One

[ii]: T = Tooth, A = Amalgam, N = Noncontact

[iii]: The percentage of accuracy range and average for each case/class/classification scheme

2.4.6. Variability of Tooth

The previous results were obtained using the data that were collected by performing cutting on one tooth (tooth 1). These data then were divided to different training and testing groups as Table 2.1 indicates. In order to investigate, the effect of tooth variability on the classification accuracy, another experiment was conducted similar to the previous one, but on another intact extracted human third molar (tooth 2). All the collected data from tooth 1 were used for training, and the data from tooth 2 was used for testing. Similar to previous results, for TCN case, 64 features, linear scaling, and RBF kernel were used, whereas for TAN, 32 features, normal scaling, and linear kernel were employed. The hyper–parameters were found using 5–fold cross validation, and are presented in Table 2.26.

The obtained hyper–parameters then were used to train the TCN and TAN classifiers. The performances of the trained classifiers were tested on data collected from tooth 2, as Table 2.27 shows.

Since the tests were performed only on tooth 2, the classes were tooth and noncontact (based the test format depicted in Figure 2.3). The variation between

different teeth caused a reduction in the classification accuracies; however, they were still in an acceptable range (the minimum was 70% among 1476 test samples). Considering all data, the total accuracies of testing on tooth 2 were 72% and 79% for TCN and TAN cases respectively.

Table 2.26 The Hyper–Parameters' Values from 5–Fold Cross Validation Using All Data Collected from Tooth 1 (TCN case: 64 features, RBF kernel, linear scale; TAN case: 32 features, linear kernel, normal scale)

Cases [i]	C	γ	CV [ii]
TCN	16	1	98
TAN	0.25	–	92

[i]: T = Tooth, C = Composite, A = Amalgam, N = Noncontact

[ii]: CV = Cross Validation accuracy (percentage) for each group

Table 2.27 The Classification Accuracies of Testing on Tooth 2 (TCN case: 64 features, RBF kernel, linear scale; TAN case: 32 features, linear kernel, normal scale)

	Cases	
Classes [i]	TCN [i]	TAN [i]
T	70 (1476) [ii]	79 (1476)
N	74 (1432)	80 (1432)

[i]: T = Tooth, C = Composite, A = Amalgam, N = Noncontact

[ii]: The accuracy is represented by percentage. The number of testing samples is shown in the parenthesis

2.5. Summary and Conclusions

In this chapter, according to two widely used restorative materials i.e., amalgam and composite, and the fact that a tooth is not filled with both materials simultaneously, two classification cases were studied. In the first case, tooth, composite, and noncontact classes were considered (TCN), whereas in the second case, tooth, amalgam, and noncontact classes were chosen (TAN).

A methodology was proposed for studying the classification cases which had seven stages as data collection, preprocessing, labeling, windowing, feature extraction,

feature scaling, and classification. For TCN, it was indicated that 64 features, linear scaling, and RBF kernel had a better performance. In this case, the following accuracy ranges were obtained: tooth (74%–98%), composite (80%–91%), and noncontact (84%–97%). For TAN, it was shown that 32 features, normal scaling, and linear kernel obtained more accurate results. In this case, the accuracy ranges were 92%–97% for tooth, 83%–97% for amalgam, and 85%– 95% for noncontact class.

These results indicated that for TCN and TAN cases, different combinations from number of features, method of scaling, and type of kernel obtained the maximum accuracies. The proposed method was also applicable for real–time implementations, because the window–length was less than 44 ms, which caused the decision to be made on a small fraction of time. In addition, the computational complexity of using SVM was appropriate, in particular for the linear kernel.

After investigating the effect of the above mentioned factors, the concept of temporal voting was introduced and it was indicated that the overall performance of both cases was improved. For example, when $\mathrm{n_w} = 15$ (number of windows), the results in TCN case were: tooth (81%–100%), composite (92%–100%), and noncontact class (89%–98%). In TAN case, the results were 95%–100% for tooth, 79%–100% for amalgam, and 86%–97% for noncontact class. The used time interval for 15 windows was less than human recognition response-time; however, more studies should be conducted to obtain the dentists' response-time in recognition of tooth layers from restorative materials.

The effect of hierarchical scheme was also studied, and its results were compared to those of the one–against–one (OAO) scheme. It was concluded that OAO approach had a better performance than hierarchical scheme for both cases. However, the difference between the total accuracies of these schemes in both cases was only 1%, and the computational complexity of hierarchical scheme was less than OAO. Therefore, for future implementations, the hierarchical scheme may be preferred because of its less computational cost, and small accuracy difference to OAO scheme.

The reasons for misclassifications were different, however one important source of error was identifying the data in the transition from noncontact to contact region and

vice versa (Figure 2.3). In chapter 3, we will see that the frequency of handpiece sound indicates the speed. In the exact moment of contacting, the handpiece speed reduced, however the reduction was not significant in the first time-windows after the contact (transition region). The same explanations hold true for the exact moment of noncontact (after the contact), in which the speed-increase was not significant in the transition region.

As it was explained, the handpiece speed was used for labeling (directly) and classification (indirectly through the averaged FFT coefficients). Therefore, labeling and classification of the transition data were challenging, because their spectral properties were similar to both contact and noncontact data. In order to reduce the effect of such an error for future investigations, perhaps designing an objective mechanism that sends a signal in the exact time of contact/noncontact (Figure 2.3) can increase labeling accuracy. Also, the effect of other features in discriminating between contact and noncontact data in the transition region should be studied.

The classification accuracies were also studied with respect to number of features (p), and scaling methods. Employing either low number of features or no scaling methods changed the performance of trained SVM models to behave more as binary classifiers between contact and noncontact data rather than discriminating between three classes. It seemed poor spectral resolution at lower p's and deficient signal–power resolution for no scaling approach decreased the classification accuracies.

So far, there have not been any studies indicating how much accuracy is desirable in identifying tooth layers from restorative materials. However, the obtained results seemed acceptable for a first–time study (89% for TCN, and 91% for TAN). In section 2.4.6, the effect of tooth variability was studied on the classification accuracy. Although, the results were promising, they were acquired using a small number of test samples (two teeth). In addition, the effect of various factors on the discrimination performance was unknown; in particular in real–time circumstances. These factors include, but are not limited to, type of air–turbine handpiece, type of cutting bur, type of tooth as well as its gender and age. It is highly recommended for any future studies continuing this research, to investigate the effect of these factors on the classification performance.

3. Speed Measurement and Control

3.1. Introduction

This chapter discusses about speed measurement and control of air–turbine dental handpieces (ATDH). Speed control is one objective of the proposed dental assisting system (DAS) (Figure 1.4); because it adds autonomy to DAS to take appropriate actions. In addition, speed control can improve the efficiency of air–turbine handpieces, particularly when they are compared with electrical handpieces.

In this chapter, first a practical and effective speed measurement method is introduced, and validated theoretically and experimentally. In the next step, an on/off solenoid valve is employed which is commanded by the pulse width modulation (PWM) technique to manipulate the handpiece speed. A model from the duty–cycle of PWM signal to the measured speed is developed that enables us to perform simulation analysis. Finally, a closed loop proportional–integral (PI) controller is designed and its performance in maintaining the handpiece speed is experimentally verified.

3.2. Speed Measurement

In order to provide a feedback control for air–turbine dental handpieces, the first step is the speed measurement. Although this measurement might be trivial for most control applications, it is a challenging task for ATDH. During dental operations, a dentist uses the handpiece with various positions and orientations. The speed measurement method should be designed so that, neither it gets affected by these variations nor it restricts the manoeuvrability of the handpiece.

To satisfy the above goals, an indirect method of speed measurement is proposed which is based on the handpiece vibration measurement, and analyzing that in the frequency domain. In this approach, the frequency of the vibration indicates the

handpiece speed. This methodology can be explained theoretically based on the rotating unbalance concept and the vibration of a fixed–free beam.

3.2.1. Rotating Unbalance and Fixed–Free Beam

The asymmetry mass distribution in a rotating system causes unbalance, [109]. This will happen in almost all rotational systems due to the imperfections in the manufacturing of the components. The unbalance in a rotary system such as air–turbine with the speed ω revolutions per second (rps) causes vibrations at the same frequency ω (Hz) in the whole body (Figure 3.1a).

Typically, the unbalance is represented by a mass m_0 which rotates with the speed of ω around the rotational axis (Figure 3.1b). A system of springs and dampers also represents the stiffness and damping of the bearings which support the rotating shaft. These springs and dampers connect the air–turbine to the handpiece body. Figure 3.1c shows a simplified model of Figure 3.1b in which the turbine's vibration is in only one orientation. In this orientation, if the relative displacement between the turbine and the body is z, the displacement of mass m_0 after time t will be

$$d_{m_0}(t) = z(t) + e\sin(\omega t) \tag{3.1}$$

The forces that body apply to the combined masses (m_0 and M_t) are $-K_T\, z(t)$ and $-C_T \frac{d}{dt} z(t)$; where K_T and C_T are the total spring constant and the total damping coefficient in the z orientation. Using Newton's second law, the motion equation is

$$-K_T\, z(t) - C_T \frac{d}{dt} z(t) = (M_t - m_0) \frac{d^2}{dt^2} z(t) + m_0 \frac{d^2}{dt^2} [z(t) + e\sin(\omega t)] \tag{3.2}$$

Rearranging the above equation results in

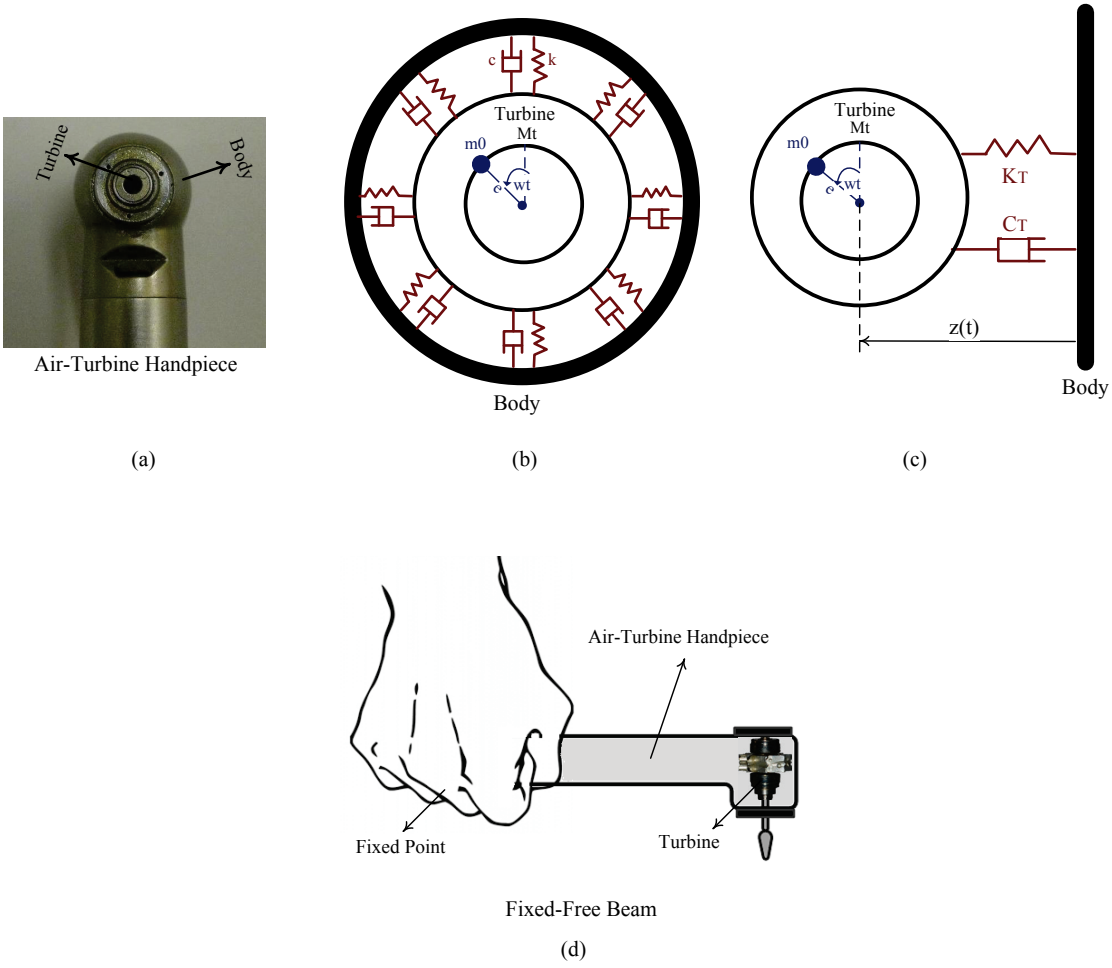

Figure 3.1 ***(a): The body and turbine of an air–turbine handpiece, (b) A mass–spring–damper model of a rotating turbine that has unbalance, (c): A simplified model of plot (b) in which the vibration is assumed to be in one orientation, (d): The handpiece body from the hand gripping point to the head can be modeled as a fixed–free beam.***

$$M_t \frac{d^2}{dt^2} z(t) + C_T \frac{d}{dt} z(t) + K_T z(t) = m_0 \omega^2 e \sin(\omega t) \qquad 3.3$$

The steady–state solution to the above equation can be expressed as

$$z(t) = A \sin(\omega t - \theta) \qquad 3.4$$

So that,

$$A = \frac{m_0 e}{M_t} \frac{r^2}{\sqrt{(1-r^2)^2 + (2\zeta r)^2}} \tag{3.5}$$

$$\theta = \tan^{-1} \frac{2\zeta r}{1-r^2} \tag{3.6}$$

$$\bar{\omega}_n = \sqrt{\frac{K_T}{M_t}}, \quad \zeta = \frac{C_T}{2\sqrt{K_T M_t}}, \quad r = \frac{\omega}{\bar{\omega}_n} \tag{3.7}$$

Considering the above solution, the force that is applied to the body in the orientation z is

$$F_z = K_T\, z(t) + C_T \frac{d}{dt} z(t) \tag{3.8}$$

As Eq. 3.4 illustrates, $z(t)$ is sinusoidal with frequency ω which induces the same frequency to F_z. The handpiece body from the hand gripping point to the head can be modeled as a fixed–free beam as Figure 3.1d displays. The vibration of such a beam is, [109]

$$w(x,t) = \sum_{n=1}^{\infty} W_n(x)\, q_n(t) \tag{3.9}$$

where x and t denote for position and time. $W_n(x)$, and $q_n(t)$, are the nth vibration mode–shape (spatial term), and the corresponding generalized coordinate of that mode (temporal term). $W_n(x)$ can be found through solving the following differential equation,

$$E\,I\,\frac{d^4}{dx^4}W_n(x) - \omega_n^2\,\rho\,A\,W_n(x) = 0; \qquad n = 1, 2, \cdots \tag{3.10}$$

where A, ρ, ω_n, E, and I are cross–sectional area of the beam, mass density, beam's nth natural frequency, Young's modulus, and beam cross–section moment of inertia respectively. Using these formulations, the forced–vibration equation for the body is, [109]

$$E\,I\sum_{n=1}^{\infty}\frac{d^4}{dx^4}W_n(x)\,q_n(t) + \rho\,A\sum_{n=1}^{\infty}W_n(x)\,\frac{d^2}{dt^2}q_n(t) = F_z \tag{3.11}$$

The solution of $q_n(t)$ can be expressed as

$$q_n(t) = A_n\cos\omega_n t + B_n\sin\omega_n t + \frac{1}{\rho\,A\,b\,\omega_n}\int_0^t Q_n(\tau)\sin\omega_n(t-\tau)\,d\tau \tag{3.12}$$

where

$$Q_n(t) = \int_0^l F_z\,W_n(x)dx \tag{3.13}$$

$$b = \int_0^l W_n^2(x)dx \tag{3.14}$$

In the above equations, l indicates the handpiece length from the gripping point to the head. Given the solution of q_n, the total vibration can be determined from Eq. 3.9. The first two terms on the right hand side of Eq. 3.12 denote the transient vibration, and the third term represents the steady–state vibration that is resulting from the forcing function F_z. As Eq. 3.8 indicates, the frequency of the force is ω, which is the same as the handpiece speed considering Eq. 3.1. In the steady–state, the body vibrates with the

force frequency ω and therefore, the speed of the handpiece can be measured indirectly by obtaining the frequency of its vibration.

According to Eq. 3.9, different points on the handpiece can experience different vibration intensities depending on their position; however the frequency of the vibration is the same for all of them. Similar explanations can be given for various orientations of the handpiece (relative to the gripping point) which does not change the vibration frequency. As a result, as long as the sensor that captures the vibration is sufficiently sensitive, there is no real advantage in picking a position/orientation for sensor attachments. In addition, the gripping point of the hand does not affect the measurements, because the vibration frequency is independent of the handpiece length (Eq. 3.13). Given these degrees of freedom, the indirect method makes the measurements convenient, and guarantees the manoeuvrability of the handpiece.

3.2.2. Experimental Validation

The indirect speed measurement method was explained theoretically based on the rotating unbalance and the fixed–free beam concepts. To validate this method experimentally, different tests were carried out. A test setup was provided (Figure 3.2) in which the vibration signal and the speed of the air–turbine handpiece (NSK, Mach–Lite XT M) were measured by a “Dytran 3035BG” accelerometer and an ‘E30A–Pittman–500–cpr’ encoder respectively. A high speed data acquisition card (LDS Dactron Photon II, 75 KHz), and a signal processing software (RT–Pro Photon) were used for obtaining the frequency spectrum. Table 3.1 summarizes the results, and Figure 3.3 demonstrates a sample spectrum diagram.

The results of Table 3.1 indicate the measurements of both methods were very close to each other which validated the capability of the indirect method in capturing the handpiece speed. In this experiment, using the encoder for direct measurements involved couplings between the dental bur (the cutter) and the encoder shaft which induced inertia and reduced the speed range considerably.

To indicate the performance of the indirect method in a higher speed range, another experiment was conducted on an electrical handpiece. The electrical handpiece

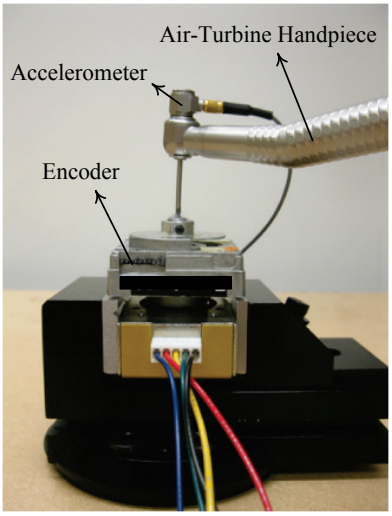

Figure 3.2 The experimental setup for the indirect speed measurement

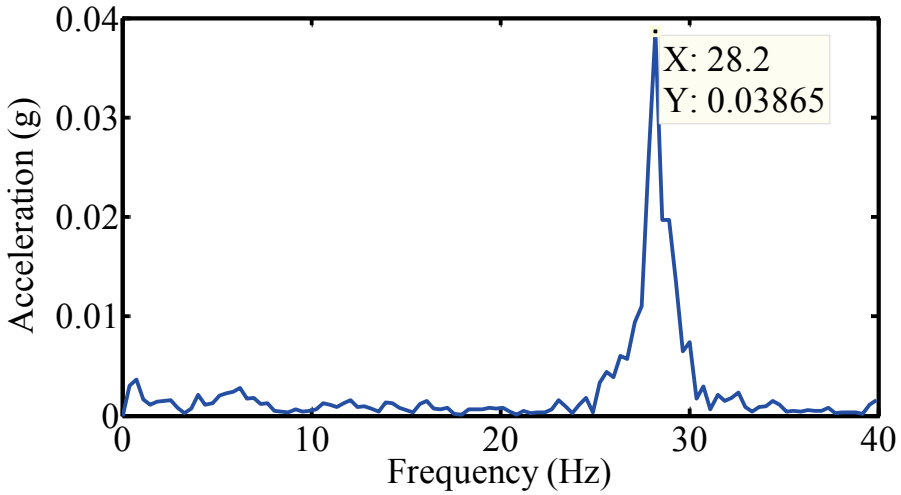

Figure 3.3 A typical vibration spectrum for the air–turbine handpiece obtained

was equipped with a speed measurement unit, and its speed range was higher than the coupled air–turbine handpiece. The rotation in electrical handpieces is similar to ATDH, except that they are driven by electricity. Therefore, the same explanations and formulations can be proposed for electrical handpieces based on the rotating unbalance/fixed–free beam, which made indirect measurements possible. Table 3.2 presents a comparison between the direct and indirect speed measurement methods for an “NSK TI25L” electrical handpiece.

Table 3.1 Speed Measurement Method Comparison for the Air–Turbine Handpiece

Number	Indirect Method [i] (rps [ii])	Direct Method [iii] (rps)
1	28.2	27.2
2	39.2	40.1
3	38.8	38.4
4	33.6	33.7

[i]: Indirect speed measurement is the proposed method based on the vibration analysis

[ii]: Direct speed measurement was done by an encoder

[iii]: rps = Revolutions per second

Table 3.2 Speed Measurement Method Comparison for the Electrical Handpiece

Number	Indirect Method [i] (rps [ii])	Direct Method [iii] (rps)
1	168	166.67
2	250	250
3	333	333.33

[i]: Indirect speed measurement is the proposed method based on the vibration analysis

[ii]: Direct speed measurement was done by the speed measurement unit of the electrical handpiece

[iii]: rps = Revolutions per second

The result of Table 3.2 illustrates a close agreement between both methods of speed measurements, and confirms the capability of the indirect method in higher speed ranges.

One of the benefits of using the indirect method was its independency from the sensor position or handpiece orientation. In order to validate this property practically, an experiment was conducted. During this test, it was also investigated if the handpiece sound could be used in the indirect speed measurement. The nature and characteristic of sound and vibration are similar to each other, and most of the time these signals can be used interchangeably. Moreover, the real advantage of the sound signal was that it could be captured by microphones without any attachment to the handpiece, which made the speed measurement contactless.

Figure 3.4 displays the test setup in which, one 3D accelerometer (Dytran 3133A1) and one 1D accelerometer (Dytran 3035BG) were placed on the head and the body of the handpiece respectively. The vibration and the sound of the handpiece were captured using these accelerometers and a “GRAS 40be” microphone. The results are presented in Figure 3.5 and Figure 3.6.

Figure 3.5 compares the vibration spectrum of the handpiece for various orientations (x, y, and z in Cartesian coordinates). In this figure, the peak frequency was the same for all orientations, which confirmed the independency of the indirect speed measurement from the handpiece orientation. The same explanation held true for the top and middle plots of Figure 3.6 that display the vibration spectrum of the handpiece for different measurement positions (head and body). These plots indicate that the indirect measurement was not dependent on the measurement position. In addition as the bottom plot of Figure 3.6 shows, the peak frequency in the sound spectrum was the same as the vibration. This equality validates the capability of sound signals for indirect measurements.

3.3. Speed Control

The speed control was conducted through the input pressure to the handpiece. A pulse width modulation (PWM) technique, similar to the one used for electrical devices was adopted to manipulate the pressure. In this technique, PWM signals with a proper rate switched the solenoid valve on and off so that the pressure in the valve outlet was regulated to a mean value. Increasing/decreasing the duty–cycle (D) of PWM signals could increase/decrease the outlet pressure and consequently the handpiece speed. This pressure control technique was fast and easy to implement.

In addition, solenoid valves are durable and energy/cost efficient compared to other types of control valves, [91].

During loaded conditions, the handpiece speed reduced, and a closed–loop control was needed to compensate this reduction to maintain the speed at a constant level. A closed–loop proportional integral (PI) control is a simple, inexpensive, and efficient method for this purpose that can be described in discrete time as

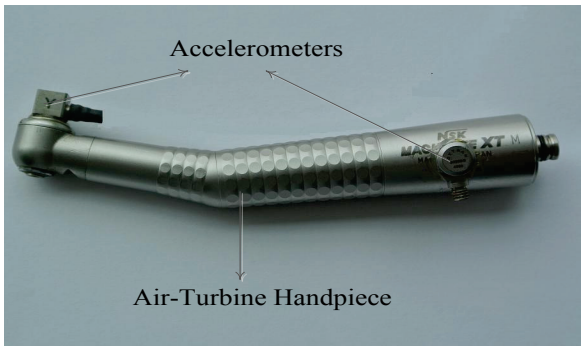

Figure 3.4 ***One 3D and one 1D accelerometers placed on the head and body of the air–turbine handpiece***

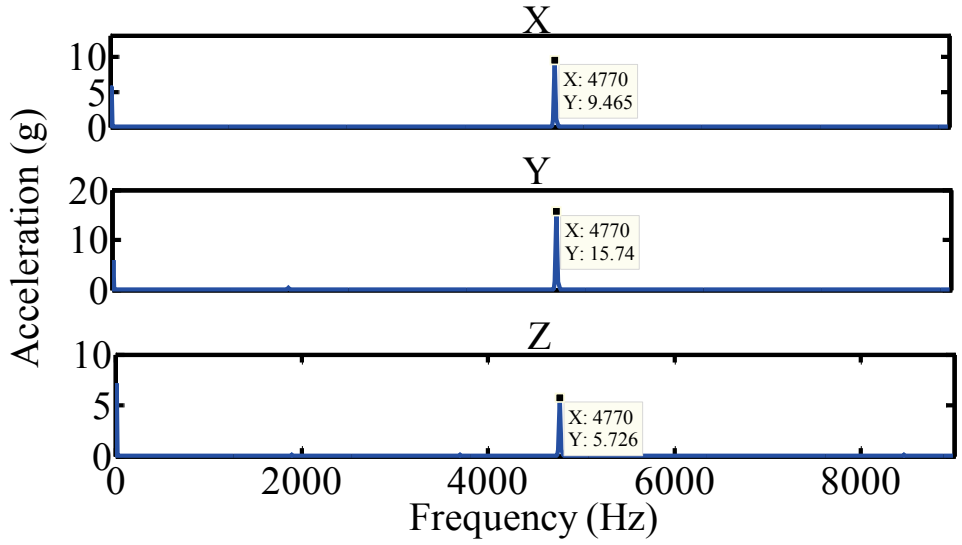

Figure 3.5 ***Studying the effect of orientations (x, y, and z in Cartesian coordinates) in capturing the vibration peak of the air–turbine handpiece***

$$u(n) = K_p\,\bar{e}(n) + K_i \sum_{j=0}^{n} \bar{e}(j) \qquad 3.15$$

where K_p, K_i, $\bar{e}$, u , and n are proportional gain, integral gain, error signal, control signal, and time sample respectively. The input to the controller was the error signal $\bar{e}$ which was obtained by subtracting the measured speed from the reference speed. The

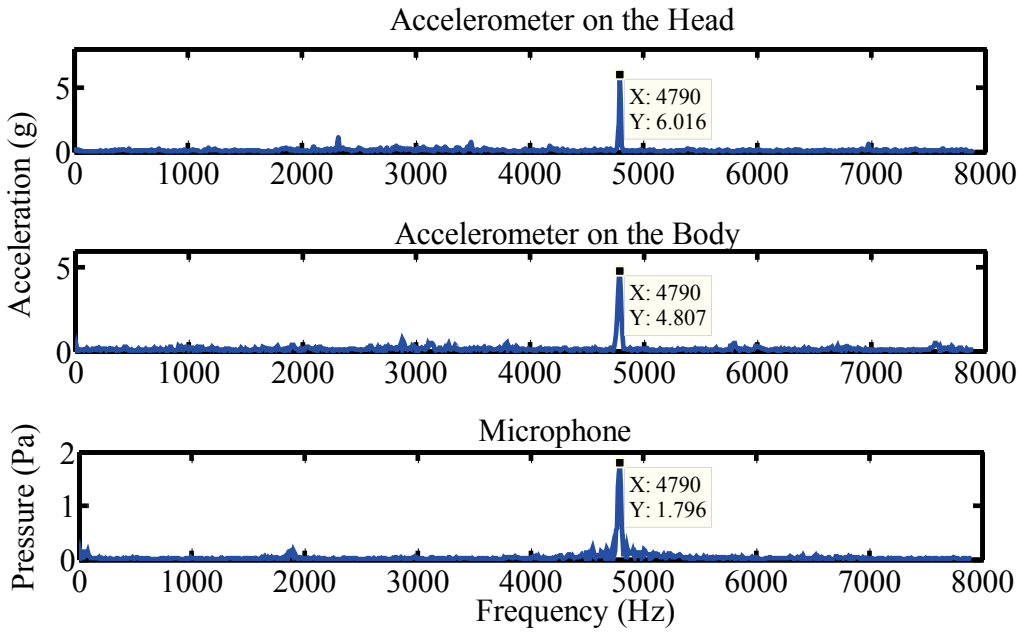

Figure 3.6 Studying the effect of positions (head, body, and non–contact measurement) in capturing the sound/vibration peak of the air–turbine handpiece

output of the controller was the control signal u that ass considered to be the duty–cycle D in our study. Experimental Validation

An experimental test setup (Figure 3.7) was designed to investigate the performance of the proposed method for manipulating the handpiece speed. Figure 3.8 demonstrates the schematic of this setup, in which a fast response on/off solenoid valve (Parker, 100psi, 12V) was selected and used in the ATDH flow path. The pressure was fixed at 60 psi at the inlet of the valve. The vibration/sound of the handpiece was obtained using the appropriate sensor, i.e. accelerometer/microphone. The sensor signal then was employed for determining the handpiece speed using the indirect measurement method. PWM signals were generated in LabView platform, and were amplified by a controllable power–supply (PS2x300W) to activate the solenoid valve. A "NI 6211" data acquisition card was utilized for interfacing between the personal computer and the sensor or valve.

In this setup, changing the duty–cycle of PWM signals could vary the mean–value of the pressure in the valve outlet, which set the handpiece revolutions at a

different speed. Figure 3.9 demonstrates the handpiece speed for three different duty–cycles (D=45%, 60%, 100%). As it is observable, changing the duty–cycle of PWM signals varied the steady–state speed of the handpiece.

3.3.1. Model Development

The previous results demonstrated a relationship between the speed and the duty–cycle. Developing a mathematical model that could describe this relationship was significantly important for a better understanding of the system behavior, and performing simulation analysis. A simple model was preferred to facilitate the analysis, but at the same time it should have sufficient accuracy to capture main dynamics of the system. To develop such a model, the data were collected in open–loop experiments, and the modeled system was assumed to be from the applied duty–cycle (D) to the measured speed (Figure 3.8).

The shape of the response in Figure 3.9 suggested that the nature of the system could be represented by a process model which is defined as a linear and low–order transfer–function, [110]. A process model can be described by a static gain ($\mathrm{K_s}$), a time delay ($\mathrm{T_d}$), and one or more poles ($\mathrm{P_1}, \mathrm{P_2}, \ldots$). Different orders of the process model were utilized for our system to determine the best one. In obtaining these models, the step response to the full duty–cycle (D =100%) was considered; and the ratio of the mean absolute error (MAE) to the steady–state value (SSV) in the interval of 0–5 s was used for comparison.

The least–squares method, [111], was employed for estimating the parameters, and the results are summarized in Table 3.3.

The values for the static gain and the time delay were $\mathrm{K_s} = 48$, and $\mathrm{T_d} = 0.2$ respectively. In addition as Table 3.3 shows, the first–order model had the best accuracy among others. This fact could also be confirmed from the dominant pole of higher–order models (–3.5 in the second–order, and –3.64 in the third–order) that was very close to the pole of the first–order model (–3.8).

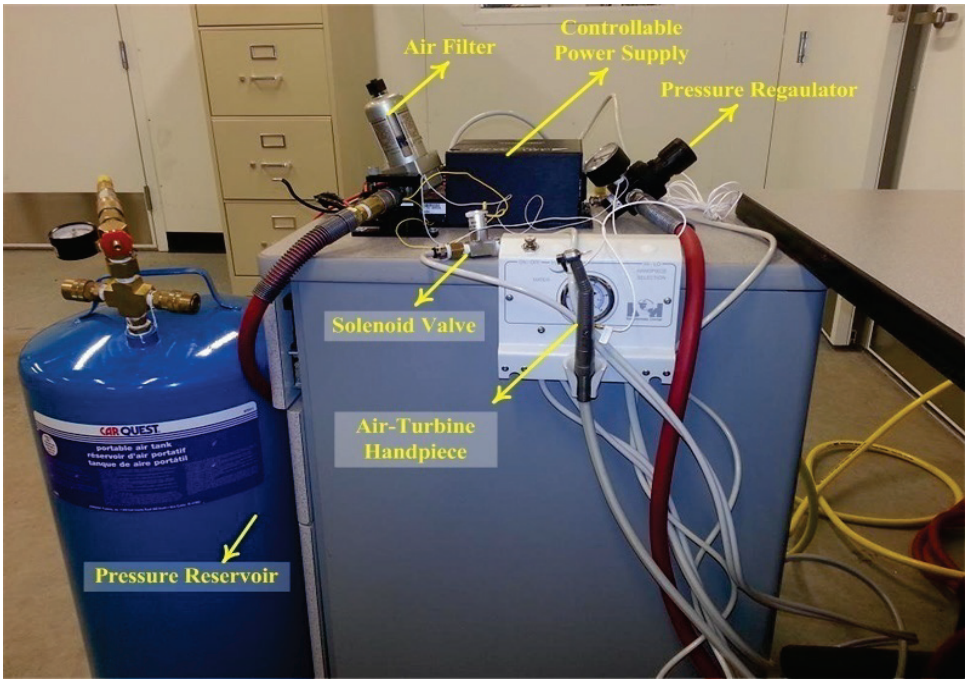

Figure 3.7 The experimental setup for manipulating the handpiece speed

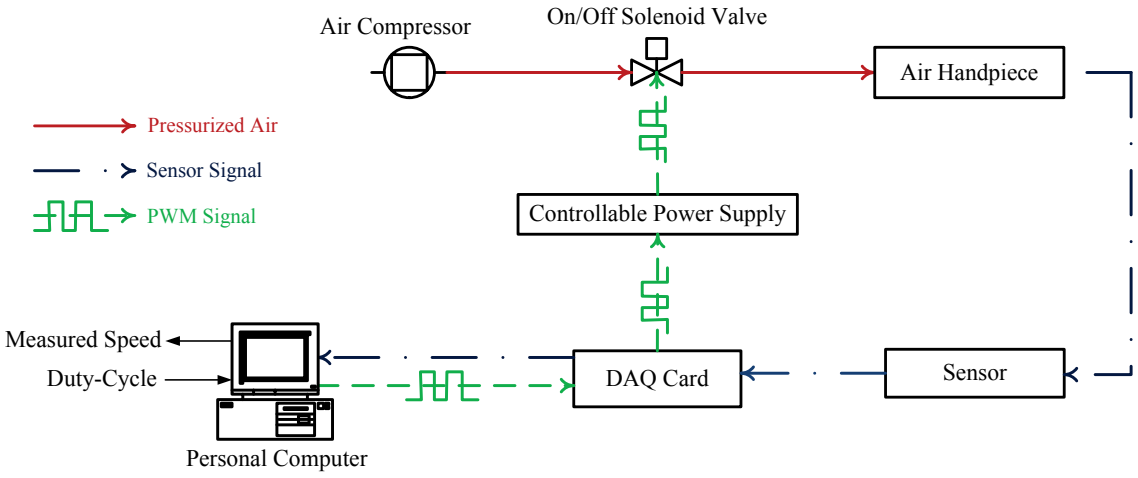

Figure 3.8 The schematic diagram of the proposed method for manipulating the handpiece speed.

This proximity indicated that higher–order models could be reduced to the first–order, and so the transfer function from the applied duty–cycle to the measured speed could be represented by

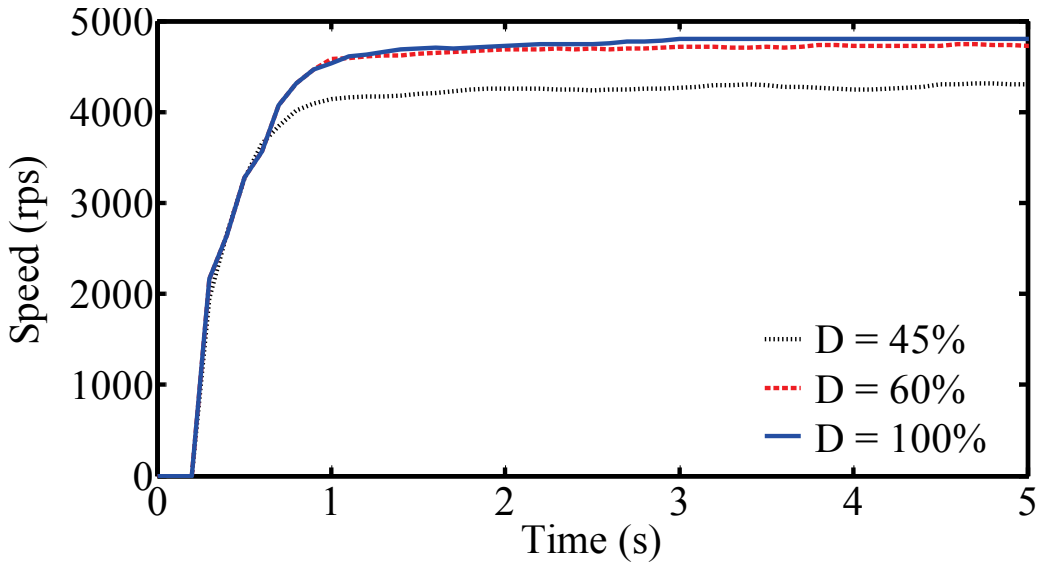

Figure 3.9 ***A comparison between different duty–cycles and their corresponding measured speeds***

Table 3.3 ***A Comparison between Different Orders of the Process Model***

Model Order	P_1 [i]	P_2 [i]	P_3 [i]	MAE/SSV % [ii]
First	–3.8	—	—	0.90
Second	–3.5	–70.61	—	1.24
Third	–3.64	–16	–131.2	2.1092

[i]: Poles; The static gain, and the time delay were obtained $K_s = 48$, and $T_d = 0.2$ respectively.

[ii]: The percentage ratio of the maximum absolute error (MAE) to the steady–state value (SSV)

$$G(s) = \frac{48e^{-0.2s}}{(s + 3.8)} \qquad 3.16$$

where s showed the Laplace domain.

To evaluate the performance of the above model, its response to the full duty–cycle was simulated and compared to the experimental data as Figure 3.10 displays.

The results depicted in this Figure 3.10 indicated a close agreement between simulation and measurement, and confirmed the accuracy of the developed model G.

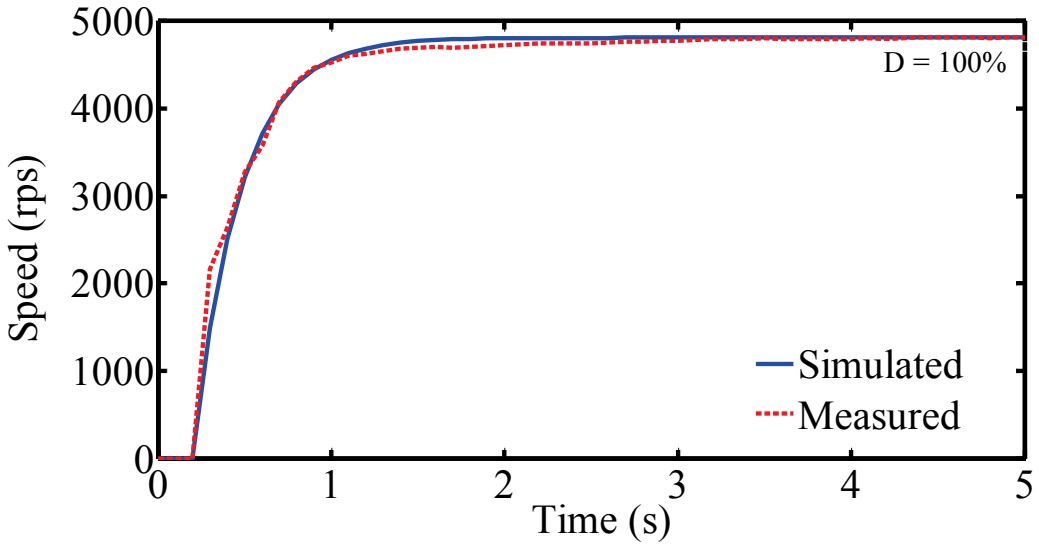

Figure 3.10 ***A comparison between the measured and simulated speeds for the full duty–cycle. The simulated results obtained from the model G described by Eq. 3.16***

The model described by Eq. 3.16 is obtained for the full duty–cycle, and could not represent the behavior of the system for other duty–cycles. To overcome this challenge, the model G should have been modified so that it reflected the system's nonlinearities. The system's major nonlinearity was in the steady–state responses as Figure 3.9 shows. A static relation between the applied duty–cycle and the static gain could model such nonlinearity. To do this, a Hammerstein model, [112], was considered in which a nonlinear static function was placed before the linear transfer function G. Such a nonlinear function mapped each duty–cycle to a static gain $\mathrm{K_{nl}}$. Given this nonlinear modeling, the total transfer function from the applied duty–cycle to the measured speed was

$$\mathrm{G_T(s,D)} = \mathrm{K_{nl}(D)}\,\frac{48\mathrm{e}^{-0.2s}}{(\mathrm{s}+3.8)} \qquad 3.17$$

It is obvious that for D =100%, the value of $\mathrm{K_{nl}}$ was 1. For other duty–cycles, $\mathrm{K_{nl}}$ was assumed to have a piecewise linear structure as shown in Figure 3.11. In this figure, the marked points indicate duty–cycles 45%, 60%, 100%, and their corresponding values. In Figure 3.12, the response of $\mathrm{G_T}$ to duty–cycles of 45%, and 60% were

compared to their corresponding experimental results which validated the accuracy and efficiency of the developed model G_T.

3.3.2. Closed–Loop PI Controller

As it is mentioned earlier, the handpiece speed would decrease during loaded conditions, and a closed–loop proportional integral (PI) controller was proposed for maintaining the speed. The model obtained in the previous section provided a useful platform for simulation analysis and designing the controller. Given this model, the PI controller was employed and the response of the system was simulated in the presence of loads. Figure 3.13 displays the result and compares it with the case that no controller was used. As we can see, the controller attenuated the loads and maintained the speed effectively.

In order to practically evaluate the performance of the PI controller, an experimental test was conducted similar to the above simulation. The values of the proportional and integral gains were primarily determined by simulations and then were fine–tuned experimentally as Figure 3.14 shows. The top plot in Figure 3.14 indicates the response of the system for $K_P = 170$ and $K_I = 2$. This combination caused an overshoot and a slow settling–time. As the middle plot of Figure 3.14 shows, decreasing these gains reduced the settling–time; but the overshoot remained relatively high.

Eventually, tuning the proportional and integral gains to $K_P = 10$ and $K_I = 0.5$, resulted in a damped response without any overshoots and an acceptable settling–time (the bottom plot of Figure 3.14).

Given these tuned gains, the performance of the PI controller was tested practically in the presence of loads. As Figure 3.15 displays, the designed controller could successfully attenuate the imposed loads, and maintain the speed.

3.4. Summary and Conclusions

This chapter introduced an effective and practical speed measurement and control technique for air–turbine dental handpieces (ATDH).

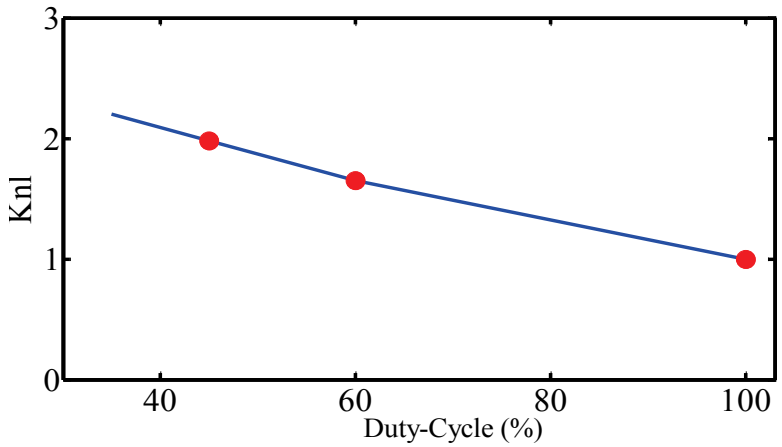

Figure 3.11 ***The static gain K_{nl} in Eq. 3.17 is assumed to be piecewise linear with respect to the duty–cycle. The marked data points indicate duty–cycles 45%, 60%, and their corresponding values***

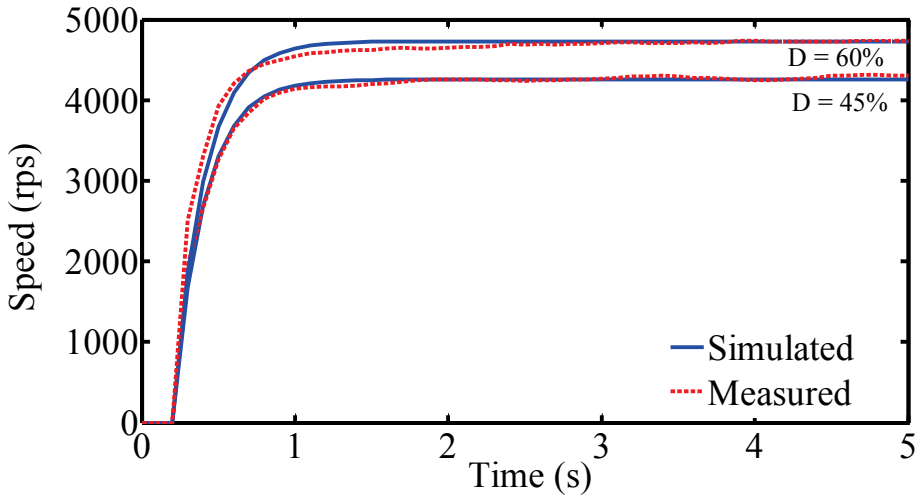

Figure 3.12 ***A comparison between the measured and simulated speeds for duty–cycles 45%, 60%. The simulated results obtained from the model G_T described by*** *Eq. 3.17*

Various speed measurement methods for ATDH have been studied by Dyson and Darvell, [90], in which optical and magnetic techniques were highly recommended. These methods required confining the ATDH in the workspace of the measurement setup, because the position and orientation of the handpiece should have been maintained stationary with respect to the light/magnetic source and sensor. These methodologies imposed bur modifications and restricted ATDH's movement, which substantially reduced the maneuverability needed for dental operations.

On the other hand, direct methods of speed measurement such as utilizing commercially available rotary encoders were not suitable either, because they involved couplings between the handpiece bur and the sensor shaft. As it was indicated, these couplings would impose inertia to the bur and reduced the speed considerably. In addition, these handpieces were high–speed devices, and costly encoders were needed for precise and reliable measurements.

It should also be noted that measuring of ATDH's speed through the supplied air variables such as pressure or flow was not a proper approach. These variables could only estimate the free–running speed, because in loaded conditions the speed would decrease for the same supplied pressure/flow, and therefore another measurement strategy should have been employed.

As an alternative approach, an indirect method of speed measurement was introduced based on the vibration/sound of air–turbine handpieces. This measurement technique was explained theoretically and validated experimentally through a number of different tests. It was shown that this method did not depend on either sensor position or handpiece orientation. Thus, it allowed the measurements to be obtained without confining the handpiece to a setup workspace and/or restricting the maneuver. More importantly, the capability of the indirect technique in using sound signals was highly beneficial, since employing microphones could make the non–contact measurements possible.

Having a practical and efficient speed measurement method, the handpiece speed could be controlled by manipulating the applied pressure. This manipulation for commercially available ATDH is provided through a foot pedal operated by dentists. This approach is open–loop, subjective, and highly dependent on the individual abilities and experience of dentists. The present study introduced another method for controlling the speed, which was closed–loop, objective, and automatic.

In the proposed method, the speed manipulation was done by employing an on/off solenoid valve which was commanded by pulse width modulated (PWM) signals. In this chapter, it was shown that varying the duty–cycle of the PWM signals could change the speed of ATDH. The relationship between the applied duty–cycle and the

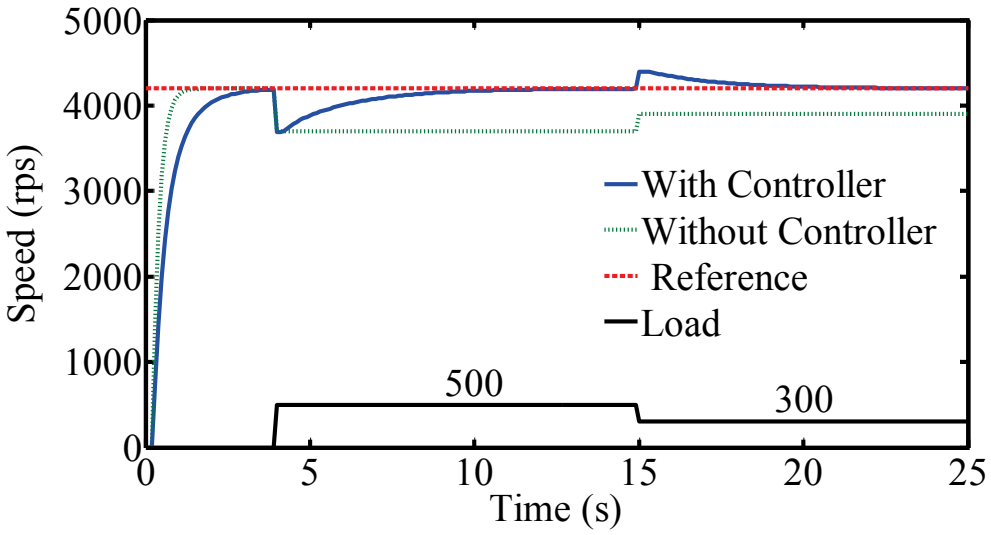

Figure 3.13 ***Simulation results indicate the ability of the designed controller for maintaining the speed in loaded conditions. The value of each load is written on top of it. The reference speed is 4200 rps***

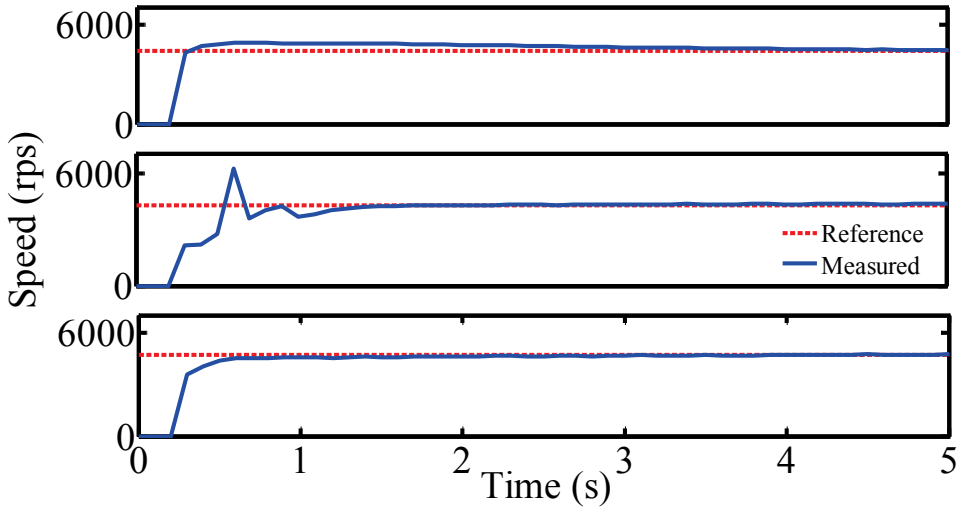

Figure 3.14 ***Three typical responses of the closed–loop system. The PI parameters are: top plot:*** $K_P = 170$, $K_I = 2$; ***middle plot:*** $K_P = 10$, $K_I = 0.75$; ***bottom plot:*** $K_P = 10$, $K_I = 0.5$

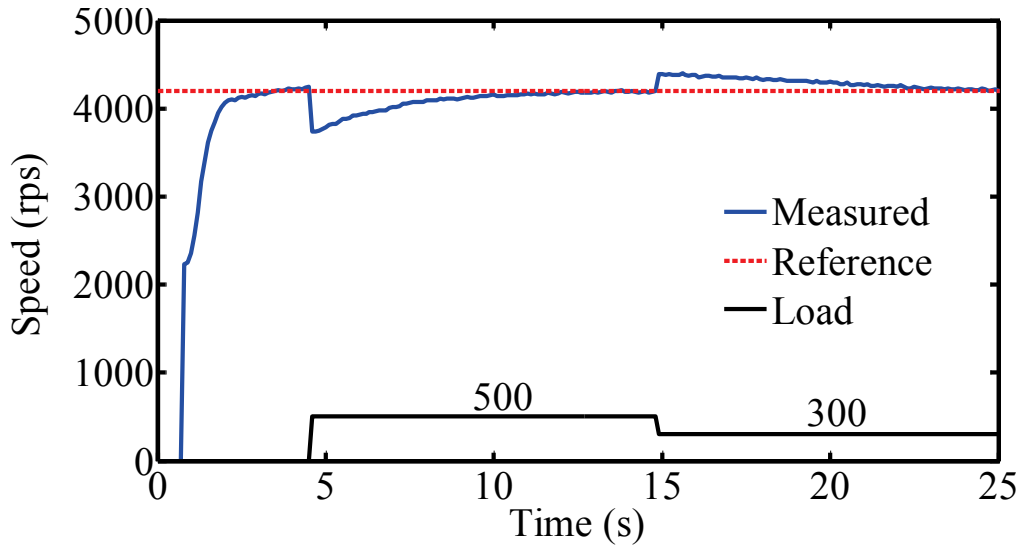

Figure 3.15 Experimental results indicate the ability of the designed controller for maintaining the speed in loaded conditions. The value of each load is written on top of it. The reference speed is 4200 rps

measured speed was described by a Hammerstein model that included a first–order transfer function with a time–delay, and a piecewise nonlinear static function.

In order to maintain the handpiece speed in loaded conditions, a closed–loop proportional integral (PI) controller was utilized. This controller successfully attenuated the imposed loads on the handpiece and the speed was maintained. The performance and practicality of the proposed speed controlling approach was verified by the simulation and experimental results.

4. Conclusions and Recommendations

In this dissertation, a dental assisting system (DAS) was proposed for procedures that are performed by air–turbine dental handpieces (ATDH). The objectives of DAS were classification between tooth layers and restorative materials, and controlling the speed of ATDH. This thesis was the first study that indicated the feasibility of classification between tooth layers and dental materials based on their cutting sounds. In addition, a closed–loop speed controller was proposed for air–turbine handpieces, and its feasibility was confirmed through simulations and experiments.

Ultimately, the final application of the proposed DAS will be preventing inadvertent removal of tooth layers during complex restorative procedures. This innovative method can assist dentists and dental students in discerning the boundary of a tooth and restorative materials objectively. In particular, this method has great teaching values in dental educational institutes where dental students develop their tactile and sensory experience practicing on models, extracted teeth and patients.

This study was at the proof–of–concept stage, which provides a solid ground for further investigations. The results were very promising, but they were obtained using a small number of cutting samples. Therefore, perhaps the most important plan for future studies is increasing the sample size, particularly tooth samples. Moreover, the effect of these factors on the generated cutting sound and classification accuracy should be studied: type of air–turbine handpiece, type of cutting bur, type of tooth as well as its gender and age, location of microphone, and different practitioners (i.e. tests are performed by various dentists).

Considering the proposed methodology, the labeling process was very time–consuming, and a computer–assisted method that can automatically label the collected data is highly suggested. In addition, the effect of windowing type (rectangular, hanning, etc), length of window, type of features (i.e. cepstrum coefficients, wavelet coefficients, etc), and type of classification approach should be investigated on the total accuracy.

The classification between tooth layers and restorative materials were conducted off–line; and therefore an experimental setup should be provided to verify it in real–time. To improve the response time of the speed controller, a solenoid valve with larger orifice in the inlet/outlet should be used. Other control strategies such as the model–predictive–control can also be studied.

The two objectives of DAS (i.e. classification and speed control) were performed separately. To evaluate the final performance of DAS, these two should be tested together to realize and reduce the time–lag between identifying a particular cutting zone, and taking a speed control action. In addition, after applying the speed control action, new patterns may occur in the cutting sound; and therefore their effects should be studied too.

References

[1] L. C. Junqueira and J. Carneiro, *Basic Histology: Text & Atlas, 10th Edition*. McGraw-Hill/Appleton & Lange, 2002.

[2] “Wikipedia.” [Online]. Available: http://en.wikipedia.org/wiki/Human_tooth.

[3] “Electric handpiece systems,” *Am. Dent. Assoc. Prof. Prod. Rev.*, vol. 2, no. 1, pp. 6–11, 2007.

[4] J. E. Dyson and B. W. Darvell, “Flow and free running speed characterization of dental air turbine handpieces,” *J. Dent.*, vol. 27, no. 7, pp. 465–477, Sep. 1999.

[5] S. L. Eikenberg, “Comparison of the cutting efficiencies of electric motor and air turbine dental handpieces,” *Gen. Dent.*, vol. 49, no. 2, pp. 199–204, 2001.

[6] C. Choi, C. F. Driscoll, and E. Romberg, “Comparison of cutting efficiencies between electric and air-turbine dental handpieces,” *J. Prosthet. Dent.*, vol. 103, no. 2, pp. 101–117, Feb. 2010.

[7] G. J. Christensen, “Are electric handpieces an improvement?,” *J. Am. Dent. Assoc.*, vol. 133, no. 10, pp. 1433–1434, Oct. 2002.

[8] B. J. Kenyon, I. Van Zyl, and K. G. Louie, “Comparison of cavity preparation quality using an electric motor handpiece and an air turbine dental handpiece,” *J. Am. Dent. Assoc.*, vol. 136, no. 8, pp. 1101–1105, Aug. 2005.

[9] R. G. Craig and J. M. Powers, *Restorative Dental Materials*, 11th ed. Mosby Inc., 2002.

[10] T. Kocher, J. Strackeljan, and D. Behr, “Feasibility of computer-assisted recognition of different dental hard tissues,” *J. Dent. Res.*, vol. 79, no. 3, pp. 829–834, Mar. 2000.

[11] I. A. Mjor and A. Jokstad, “Five-year study of class II restorations in permanent teeth using amalgam, glass polyalkenoate (ionomer) cement and resin-based composite materials,” *J. Dent.*, vol. 21, pp. 338–343, 1993.

[12] C. J. Collins, R. W. Bryant, and K. L. Hodge, “A clinical evaluation of posterior composite resin restorations: 8-year findings,” *J. Dent.*, vol. 26, pp. 311–317, 1998.

[13] J. A. Soncini, N. N. Maserejian, F. Trachtenberg, M. Tavares, and C. Hayes, “The longevity of amalgam versus compomer/composite restorations in posterior primary and permanent teeth,” *J. Am. Dent. Assoc.*, vol. 138, no. 6, pp. 763–772, 2007.

[14] C. W. Drake, “A comparison of restoration longevity in maxillary and mandibular teeth,” *J. Am. Dent. Assoc.*, vol. 116, no. 6, pp. 651–654, May 1988.

[15] G. H. Johnson, D. J. Bales, G. E. Gordon, and L. V Powell, “Clinical performance of posterior composite resin restorations,” *Quintessence Int. (Berl).*, vol. 23, no. 10, pp. 705–711, Oct. 1992.

[16] A. O. Adegbembo and P. A. Watson, “Removal, replacement and placement of amalgam restorations by Ontario dentists in 2002,” *J. Can. Dent. Assoc. (Tor).*, vol. 71, no. 8, pp. 565–565f, Sep. 2005.

[17] M. Bernardo, H. Luis, M. D. Martin, B. G. Leroux, T. Rue, J. Leitão, and T. A. DeRouen, “Survival and reasons for failure of amalgam versus composite posterior restorations placed in a randomized clinical trial,” *J. Am. Dent. Assoc.*, vol. 138, no. 6, pp. 775–783, Jun. 2007.

[18] J. C. Setcos, R. Khosravi, N. H. F. Wilson, C. Shen, M. Yang, and I. A. Mjör, “Repair or replacement of amalgam restorations: decisions at a USA and a UK dental school,” *Oper. Dent.*, vol. 29, no. 4, pp. 392–397, 2004.

[19] E. D. Roumanas, “The frequency of replacement of dental restorations may vary based on a number of variables, including type of material, size of the restoration, and caries risk of the patient,” *J. Evid. Based. Dent. Pract.*, vol. 10, no. 1, pp. 23–24, Mar. 2010.

[20] J. D. Bader and D. A. Shugars, “What do we know about how dentists make caries-related treatment decisions?,” *Community Dent. Oral Epidemiol.*, vol. 25, no. 1, pp. 97–103, Feb. 1997.

[21] V. V Gordan, C. W. Garvan, J. S. Richman, J. L. Fellows, D. B. Rindal, V. Qvist, M. W. Heft, O. D. Williams, and G. H. Gilbert, “How dentists diagnose and treat defective restorations: evidence from the dental practice-based research network,” *Oper. Dent.*, vol. 34, no. 6, pp. 664–673, 2009.

[22] V. V Gordan, “In vitro evaluation of margins of replaced resin-based composite restorations,” *J. Esthet. Dent.*, vol. 12, no. 4, pp. 209–215, Jan. 2000.

[23] V. V Gordan, “Clinical evaluation of replacement of class V resin based composite restorations,” *J. Dent.*, vol. 29, no. 7, pp. 485–488, Sep. 2001.

[24] V. V Gordan, E. Mondragon, and C. Shen, “Replacement of resin-based composite: evaluation of cavity design, cavity depth, and shade matching,” *Quintessence Int. (Berl).*, vol. 33, no. 4, pp. 273–278, Apr. 2002.

[25] F. Sardenberg, C. C. Bonifácio, M. M. Braga, J. C. P. Imparato, and F. M. Mendes, “Evaluation of the dental structure loss produced during maintenance and replacement of occlusal amalgam restorations,” *Braz. Oral Res.*, vol. 22, no. 3, pp. 242–246, 2008.

[26] J. E. Dyson and B. W. Darvell, “The development of the dental high-speed air turbine handpiece. Part 1,” *Aust. Dent. J.*, vol. 38, no. 1, pp. 49–58, Feb. 1993.

[27] T. F. Watson, D. Flanagan, and D. G. Stone, “High and low torque handpieces: cutting dynamics, enamel cracking and tooth temperature,” *Br. Dent. J.*, vol. 188, no. 12, pp. 680–686, Jun. 2000.

[28] K. Nishimura, M. Ikeda, T. Yoshikawa, M. Otsuki, and J. Tagami, “Effect of various grit burs on marginal integrity of resin composite restorations,” *J. Med. Dent. Sci.*, vol. 52, no. 1, pp. 9–15, Mar. 2005.

[29] C. Ercoli, M. Rotella, P. D. Funkenbusch, S. Russell, and C. Feng, “In vitro comparison of the cutting efficiency and temperature production of 10 different rotary cutting instruments. Part I: Turbine,” *J. Prosthet. Dent.*, vol. 101, no. 4, pp. 248–261, Apr. 2009.

[30] D. L. Leonard and D. G. Charlton, “Performance of high-speed dental handpieces subjected to simulated clinical use and sterilization,” *J. Am. Dent. Assoc.*, vol. 130, no. 9, pp. 1301–1311, Sep. 1999.

[31] L. Firoozmand, R. Faria, M. A. Araujo, R. di Nicoló, and M. F. Huthala, “Temperature rise in cavities prepared by high and low torque handpieces and Er:YAG laser,” *Br. Dent. J.*, vol. 205, no. 1, p. E1; discussion 28–29, Jul. 2008.

[32] J. E. Dyson and B. W. Darvell, “Aspects of the design of modern dental air turbine handpieces,” *Aust. Dent. J.*, vol. 38, no. 6, pp. 456–470, Dec. 1993.

[33] J. E. Dyson and B. W. Darvell, “A laboratory evaluation of two brands of disposable air turbine handpiece,” *Br. Dent. J.*, vol. 182, no. 1, pp. 15–21, Jan. 1997.

[34] K. Ishihama, H. Koizumi, T. Wada, S. Iida, S. Tanaka, T. Yamanishi, A. Enomoto, and M. Kogo, “Evidence of aerosolised floating blood mist during oral surgery,” *J. Hosp. Infect.*, vol. 71, no. 4, pp. 359–364, Apr. 2009.

[35] M. S. Toroğlu, M. C. Haytaç, and F. Köksal, “Evaluation of aerosol contamination during debonding procedures,” *Angle Orthod.*, vol. 71, no. 4, pp. 299–306, Aug. 2001.

[36] A. S. M. Pong, J. E. Dyson, and B. W. Darvell, “Discharge of lubricant from air turbine handpieces,” *Br. Dent. J.*, vol. 198, no. 10, pp. 637–640, May 2005.

[37] L. Checchi, L. Montebugnoli, and S. Samaritani, “Contamination of the turbine air chamber: a risk of cross infection,” *J. Clin. Periodontol.*, vol. 25, no. 8, pp. 607–611, Aug. 1998.

[38] D. L. Lewis and R. K. Boe, “Cross-infection risks associated with current procedures for using high-speed dental handpieces,” *J. Clin. Microbiol.*, vol. 30, no. 2, pp. 401–406, Feb. 1992.

[39] K. Masuda, M. Ohta, S. Ohsuka, M. Matsuyama, M. Ashoori, T. Usami, M. ITO, M. Ueda, and T. Kaneda, “Bacteriological evaluation of a new air turbine handpiece for preventing cross-contamination in dental procedures,” *Nagoya J. Med. Sci.*, vol. 57, no. 1–4, pp. 69–76, 1994.

[40] S. Ohsuka, M. Ohta, K. Masuda, T. Kaneda, and M. Ueda, “Microbiological evaluation of a newly designed dental air-turbine handpiece for anti-cross contaminations,” *Int. J. Prosthodont.*, vol. 7, no. 3, pp. 201–208, 1994.

[41] M. Matsuyama, T. Usami, K. Masuda, N. Niimi, M. Ohta, and M. Ueda, “Prevention of infection in dental procedures,” *J. Hosp. Infect.*, vol. 35, no. 1, pp. 17–25, Jan. 1997.

[42] L. Montebugnoli and G. Dolci, “Effectiveness of two devices designed to prevent fluid retraction in a high-speed handpiece,” *J. Prosthet. Dent.*, vol. 84, no. 2, pp. 225–228, Aug. 2000.

[43] U. Romeo, A. Galanakis, F. Lerario, G. M. Daniele, G. Tenore, and G. Palaia, “Subcutaneous emphysema during third molar surgery: a case report,” *Braz. Dent. J.*, vol. 22, no. 1, pp. 83–86, Jan. 2011.

[44] I. Watanabe, N. Baba, E. Watanabe, M. Atsuta, and T. Okabe, “Effect of heat treatments on machinability of gold alloy with age-hardenability at intraoral temperature,” *J. Dent.*, vol. 32, no. 1, pp. 9–15, Jan. 2004.

[45] H. Miyawaki, M. Taira, K. Wakasa, and M. Yamaki, “Dental high-speed cutting of four cast alloys,” *J. Oral Rehabil.*, vol. 20, no. 6, pp. 653–661, Nov. 1993.

[46] H. Miyawaki, M. Taira, and M. Yamaki, “Cutting effectiveness of diamond points on commercial core composite resins and cements,” *J. Oral Rehabil.*, vol. 23, no. 6, pp. 409–415, Jun. 1996.

[47] N. Tanaka, M. Taira, K. Wakasa, H. Shintani, and M. Yamaki, “Cutting effectiveness and wear of carbide burs on eight machinable ceramics and bovine dentin,” *Dent. Mater.*, vol. 7, no. 4, pp. 247–253, Oct. 1991.

[48] P. J. Brockhurst and R. Shams, “Dynamic measurement of the torque-speed characteristics of dental high speed air turbine handpieces,” *Aust. Dent. J.*, vol. 39, no. 1, pp. 33–38, Feb. 1994.

[49] J. E. Dyson and B. W. Darvell, “Torque, power and efficiency characterization of dental air turbine handpieces,” *J. Dent.*, vol. 27, no. 8, pp. 573–586, Nov. 1999.

[50] B. W. Darvell and J. E. Dyson, “A testing machine for dental air-turbine handpiece characteristics: free-running speed, stall torque, bearing resistance,” *Oper. Dent.*, vol. 30, no. 1, pp. 26–31, 2005.

[51] K. Elias, A. A. Amis, and D. J. Setchell, “The magnitude of cutting forces at high speed,” *J. Prosthet. Dent.*, vol. 89, no. 3, pp. 286–291, Mar. 2003.

[52] L. Yin, X. Song, S. Qu, T. Huang, P. Mei, Z. Yang, and J. Li, “Performance evaluation of a dental handpiece in simulation of clinical finishing using a novel 2DOF in vitro apparatus,” *J. Eng. Med.*, pp. 929–938, 2006.

[53] D. M. Monagahn, N. H. F. Wilson, and B. W. Darvell, “The performance of air-turbine handpieces in general dental practice,” *Oper. Dent.*, vol. 30, no. 1, pp. 16–25, 2005.

[54] D. S. Norkiewicz, M. A. Sundberg, R. F. Druckman, and L. G. Breault, “Maintenance and repair of high-speed dental handpieces,” *Gen. Dent.*, vol. 49, no. 6, pp. 636–641, 2001.

[55] T. Miyazaki, Y. Hotta, J. Kunii, S. Kuriyama, and Y. Tamaki, “A review of dental CAD/CAM: current status and future perspectives from 20 years of experience,” *Dent. Mater. J.*, vol. 28, no. 1, pp. 44–56, Jan. 2009.

[56] T. Kapos, L. M. Ashy, G. O. Gallucci, H.-P. Weber, and D. Wismeijer, “Computer-aided design and computer-assisted manufacturing in prosthetic implant dentistry,” *Int. J. Oral Maxillofac. Implants*, vol. 24, pp. 110–117, Jan. 2009.

[57] J. A. Buchanan, “Use of simulation technology in dental education,” *J. Dent. Educ.*, vol. 65, no. 11, pp. 1225–1231, Nov. 2001.

[58] T. S. Al-Jewair, A. F. Qutub, G. Malkhassian, and L. J. Dempster, “A systematic review of computer-assisted learning in endodontics education,” *J. Dent. Educ.*, vol. 74, no. 6, pp. 601–611, Jun. 2010.

[59] S. K. Lechner, G. A. Thomas, M. Bradshaw, and K. M. Lechner, “Planning oral rehabilitation: case-based computer assisted learning in clinical dentistry,” *Br. Dent. J.*, vol. 191, no. 3, pp. 152–156, Aug. 2001.

[60] S. C. Lea, B. Felver, G. Landini, and A. D. Walmsley, “Ultrasonic scaler oscillations and tooth-surface defects,” *J. Dent. Res.*, vol. 88, no. 3, pp. 229–234, Mar. 2009.

[61] S. C. Lea, A. D. Walmsley, P. J. Lumley, and G. Landini, “A new insight into the oscillation characteristics of endosonic files used in dentistry,” *Phys. Med. Biol.*, vol. 49, no. 10, pp. 2095–2102, May 2004.

[62] P. L. M. Tomson, S. C. Lea, P. J. Lumley, and A. D. Walmsley, “Performance of ultrasonic retrograde systems,” *J. Endod.*, vol. 33, no. 5, pp. 574–577, May 2007.

[63] M. Zampini, S. Guest, and C. Spence, “The role of auditory cues in modulating the perception of electric toothbrushes,” *J. Dent. Res.*, vol. 82, no. 11, pp. 929–932, Nov. 2003.

[64] J. R. Martin, D. Watt, and R. Yemm, “An analysis of the performance of a dual-frequency dental laboratory vibrator,” *J. Dent.*, vol. 8, no. 3, pp. 275–278, Sep. 1980.

[65] R. L. Poole, S. C. Lea, J. E. Dyson, A. C. C. Shortall, and A. D. Walmsley, “Vibration characteristics of dental high-speed turbines and speed-increasing handpieces,” *J. Dent.*, vol. 36, no. 7, pp. 488–493, Jul. 2008.

[66] H.-M. Huang, C.-Y. Tsai, H.-F. Lee, C.-T. Lin, W.-C. Yao, W.-T. Chiu, and S.-Y. Lee, “Damping effects on the response of maxillary incisor subjected to a traumatic impact force: a nonlinear finite element analysis,” *J. Dent.*, vol. 34, no. 4, pp. 261–268, Apr. 2006.

[67] H.-M. Huang, S.-Y. Lee, C.-Y. Yeh, and C.-T. Lin, “Resonance frequency assessment of dental implant stability with various bone qualities: a numerical approach,” *Clin. Oral Implants Res.*, vol. 13, no. 1, pp. 65–74, Feb. 2002.

[68] R. Whiting, A. Campbell, and H. Baksh, “In vitro evaluation of dental bonding agents using shear and vibrational methods,” *J. Dent.*, vol. 30, no. 1, pp. 21–27, Jan. 2002.

[69] P. Castellini, L. Scalise, and G. M. Revel, “Vibration measurements for diagnosis of structural defects on human teeth,” *Measurement*, vol. 27, no. 1, pp. 29–42, Jan. 2000.

[70] S. C. Lea, G. Landini, and A. D. Walmsley, “Vibration characteristics of ultrasonic scalers assessed with scanning laser vibrometry,” *J. Dent.*, vol. 30, no. 4, pp. 147–151, May 2002.

[71] L. Carvalho, R. A. S. Moreira, and J. A. Simões, “Application of a vibration measuring technique to evaluate the dynamic stiffness of porcine periodontal ligament,” *Technol. Heal. Care*, vol. 14, no. 4–5, pp. 457–65, Jan. 2006.

[72] J. Sun, M. Rahman, Y. . Wong, and G. . Hong, “Multiclassification of tool wear with support vector machine by manufacturing loss consideration,” *Int. J. Mach. Tools Manuf.*, vol. 44, no. 11, pp. 1179–1187, 2004.

[73] H. Trabelsi and E. K.-A. Jr, “Pattern-recognition analysis of sound radiation in metal cutting,” *Int. J. Adv. Manuf. Technol.*, vol. 6, no. 3, pp. 220–231, 1991.

[74] D. Salgado and F. Alonso, “An approach based on current and sound signals for in-process tool wear monitoring,” *Int. J. Mach. Tools Manuf.*, vol. 47, no. 14, pp. 2140–2152, 2007.

[75] Y. Ota and B. Wilamowski, “Identifying cutting sound characteristics in machine tool industry with a neural network,” in *IEEE International Joint Conference on Neural Networks*, 1998, vol. 3, pp. 2459–2464.

[76] R. E. Haber, J. E. Jiménez, C. R. Peres, and J. R. Alique, “An investigation of tool-wear monitoring in a high-speed machining process,” *Sensors Actuators A Phys.*, vol. 116, no. 3, pp. 539–545, 2004.

[77] A. R. Abu-El-Quran, R. A. Goubran, and A. D. C. Chan, “Security Monitoring Using Microphone Arrays and Audio Classification,” *IEEE Trans. Instrum. Meas.*, vol. 55, no. 4, pp. 1025–1032, Aug. 2006.

[78] S. K. Yadav, K. Tyagi, B. Shah, and P. K. Kalra, “Audio Signature-Based Condition Monitoring of Internal Combustion Engine Using FFT and Correlation Approach,” *IEEE Trans. Instrum. Meas.*, vol. 60, no. 4, pp. 1217–1226, Apr. 2011.

[79] C. Wan, A. Mita, and T. Kume, “An automatic pipeline monitoring system using sound information,” *Struct. Control Heal. Monit.*, vol. 17, no. 1, pp. 83–97, Feb. 2010.

[80] O. Amft, M. Kusserow, and G. Tröster, “Bite weight prediction from acoustic recognition of chewing,” *IEEE Trans. Biomed. Eng.*, vol. 56, no. 6, pp. 1663–1672, Jun. 2009.

[81] S.-H. Shin, T. Hashimoto, and S. Hatano, “Automatic detection system for cough sounds as a symptom of abnormal health condition,” *IEEE Trans. Inf. Technol. Biomed.*, vol. 13, no. 4, pp. 486–493, Jul. 2009.

[82] C. N. Doukas and I. Maglogiannis, “Emergency fall incidents detection in assisted living environments utilizing motion, sound, and visual perceptual components,” *IEEE Trans. Inf. Technol. Biomed.*, vol. 15, no. 2, pp. 277–289, Mar. 2011.

[83] D. Istrate, E. Castelli, M. Vacher, L. Besacier, and J.-F. Serignat, “Information extraction from sound for medical telemonitoring,” *IEEE Trans. Inf. Technol. Biomed.*, vol. 10, no. 2, pp. 264–274, Apr. 2006.

[84] C. M. Bishop, *Pattern Recognition and Machine Learning*. Springer, 2007.

[85] S. Choi and Z. Jiang, “Cardiac sound murmurs classification with autoregressive spectral analysis and multi-support vector machine technique,” *Comput. Biol. Med.*, vol. 40, no. 1, pp. 8–20, 2010.

[86] J. C. Wang, H. P. Lee, J. F. Wang, and C. B. Lin, “Robust environmental sound recognition for home automation,” *IEEE Trans. Autom. Sci. Eng.*, vol. 5, no. 1, pp. 25–31, Jan. 2008.

[87] J. C. Wang, J. F. Wang, K. W. He, and C. S. Hsu, “Environmental sound classification using hybrid SVM/KNN classifier and MPEG-7 audio low-level descriptor,” in *The IEEE International Joint Conference on Neural Network*, 2006, pp. 1731–1735.

[88] A. Ganapathiraju, J. Hamaker, and J. Picone, “Hybrid SVM/HMM architectures for speech recognition,” in *International Conference on Spoken Language Processing*, 2000, vol. 4, pp. 504–507.

[89] Yi-Lin Lin and Gang Wei, “Speech emotion recognition based on HMM and SVM,” in *International Conference on Machine Learning and Cybernetics*, 2005, vol. 8, pp. 4898–4901.

[90] J. E. Dyson and B. W. Darvell, “Dental air turbine handpiece performance testing,” *Aust. Dent. J.*, vol. 40, no. 5, pp. 330–338, Oct. 1995.

[91] R. B. van Varseveld and G. M. Bone, “Accurate position control of a pneumatic actuator using on/off solenoid valves,” *IEEE/ASME Trans. Mechatronics*, vol. 2, no. 3, pp. 195–204, 1997.

[92] T. Royston and R. Singh, “Development of a pulse-width modulated pneumatic rotary valve for actuator position control,” *J. Dyn. Syst. Meas. Control*, vol. 115, pp. 495–505, 1993.

[93] T. Noritsugu, “Development of PWM mode electro-pneumatic servomechanism, part II: Position control of a pneumatic cylinder,” *J. Fluid Control*, vol. 17, no. 2, pp. 7–28, 1987.

[94] X. Shen, J. Zhang, E. Barth, and M. Goldfarb, “Nonlinear model-based control of pulse width modulated pneumatic servo systems,” *J. Dyn. Syst. Meas. Control*, vol. 128, pp. 663–669, 2006.

[95] A. Mahboobin, P. Loughlin, C. Atkeson, and M. Redfern, “A mechanism for sensory re-weighting in postural control,” *Med. Biol. Eng. Comput.*, vol. 47, no. 9, pp. 921–929, Sep. 2009.

[96] M. Tosato, K. Yoshida, E. Toft, V. Nekrasas, and J. J. Struijk, “Closed-loop control of the heart rate by electrical stimulation of the vagus nerve,” *Med. Biol. Eng. Comput.*, vol. 44, no. 3, pp. 161–169, Mar. 2006.

[97] R. Morales, F. J. Badesa, N. García-Aracil, J. M. Sabater, and C. Pérez-Vidal, “Pneumatic robotic systems for upper limb rehabilitation,” *Med. Biol. Eng. Comput.*, vol. 49, no. 10, pp. 1145–1156, Oct. 2011.

[98] S. Chu, S. Narayanan, C. -c. Kuo, and M. Mataric, “Where am I? Scene Recognition for Mobile Robots using Audio Features,” in *2006 IEEE International Conference on Multimedia and Expo*, 2006, pp. 885–888.

[99] A. V. Oppenheim and R. W. Schafer, *Discrete-Time Signal Processing*, 3rd ed. Prentice Hall, 2009.

[100] J. O. Smith III, *Spectral Audio Signal Processing*. W3K Publishing, 2011.

[101] C. Hsu, C. Chang, and C. Lin, “A practical guide to support vector classification,” 2003.

[102] C. Burges, “A tutorial on support vector machines for pattern recognition,” *Data Min. Knowl. Discov.*, 1998.

[103] H. Yu and S. Kim, “SVM tutorial: Classification, regression, and ranking,” *Handb. Nat. Comput.*, 2009.

[104] T. Hastie, R. Tibshirani, and J. Friedman, *The Elements of Statistical Learning: Data Mining, Inference, and Prediction*, 2nd ed. Springer, 2009.

[105] C. W. Hsu and C. J. Lin, “A comparison of methods for multiclass support vector machines,” *IEEE Trans. Neural Networks*, vol. 13, no. 2, pp. 415–425, Jan. 2002.

[106] C. C. Chang and C. J. Lin, “LIBSVM: a library for support vector machines,” *Trans. Intell. Syst. Technol.*, vol. 2, no. 3, pp. 27:1–27:27, 2011.

[107] A. Navot, R. Gilad-Bachrach, Y. Navot, and N. Tishby, “Is Feature Selection Still Necessary?,” in *Subspace, Latent Structure and Feature Selection*, vol. 3940, C. Saunders, M. Grobelnik, S. Gunn, and J. Shawe-Taylor, Eds. Berlin, Heidelberg: Springer Berlin Heidelberg, 2006, pp. 127–138.

[108] R. J. Kosinski, “A Literature Review on Reaction Time,” 2010. [Online]. Available: http://biae.clemson.edu/bpc/bp/Lab/110/reaction.htm.

[109] S. S. Rao, *Mechanical Vibrations*, 5th ed. Prentice Hall, 2010.

[110] K. J. Astrom and T. Hagglund, *PID Controllers: Theory, Design, and Tuning*, 2nd ed. Instrument Society of America, 1995.

[111] L. Ljung, *System Identification: Theory for the User*. Prentice Hall, 1999.

[112] E. Bai and M. Fu, “A blind approach to Hammerstein model identification,” *IEEE Trans. Signal Process.*, vol. 50, no. 7, pp. 1610–1619, 2002.

[113] C. M. Bishop, *Neural Networks for Pattern Recognition*. Oxford University Press, 1994.

[114] K. R. Farrell, R. J. Mammone, and K. T. Assaleh, “Speaker recognition using neural networks and conventional classifiers,” *IEEE Trans. Speech Audio Process.*, vol. 2, no. 1, pp. 194–205, 1994.

[115] T. McConaghy, H. Leung, E. Bosse, and V. Varadan, “Classification of audio radar signals using radial basis function neural networks,” *IEEE Trans. Instrum. Meas.*, vol. 52, no. 6, pp. 1771–1779, Dec. 2003.

[116] “MATLAB Documentation - MathWorks.” [Online]. Available: http://www.mathworks.com/help/matlab/ref/nextpow2.html.

Appendices

Appendix A.

Data Labeling

In order to label the data, the time and frequency representations of the recorded signals were used. As Figure 2.3 indicates, the format of the tests included contact and noncontact parts. Generally, the contact part had a higher power than the noncontact one, and the handpiece speed was decreased during the contact. In chapter 3, it was shown that sound frequency indicates the handpiece speed (revolution per second: rps). Therefore, an increase to the signal power (time–domain representation) as well as a decrease to the signal frequency (frequency–domain representation) indicates the contact part. These two representations were used to label the data manually and according to the cutting material.

Figure A. 1a indicates the time–domain representation of a recorded signal. The low power parts at the beginning and end of this signal were useless and were discarded. The data inside the red box shows the contact data. As it is observable, the signal power was increased for the contact data. In addition as Figure A. 1b and Figure A. 1c show, the handpiece speed was decreased for the contact data. These observations were used to assign the contact data manually. The labeling of the contact data was done based on the cutting material (i.e. tooth, composite, or amalgam).

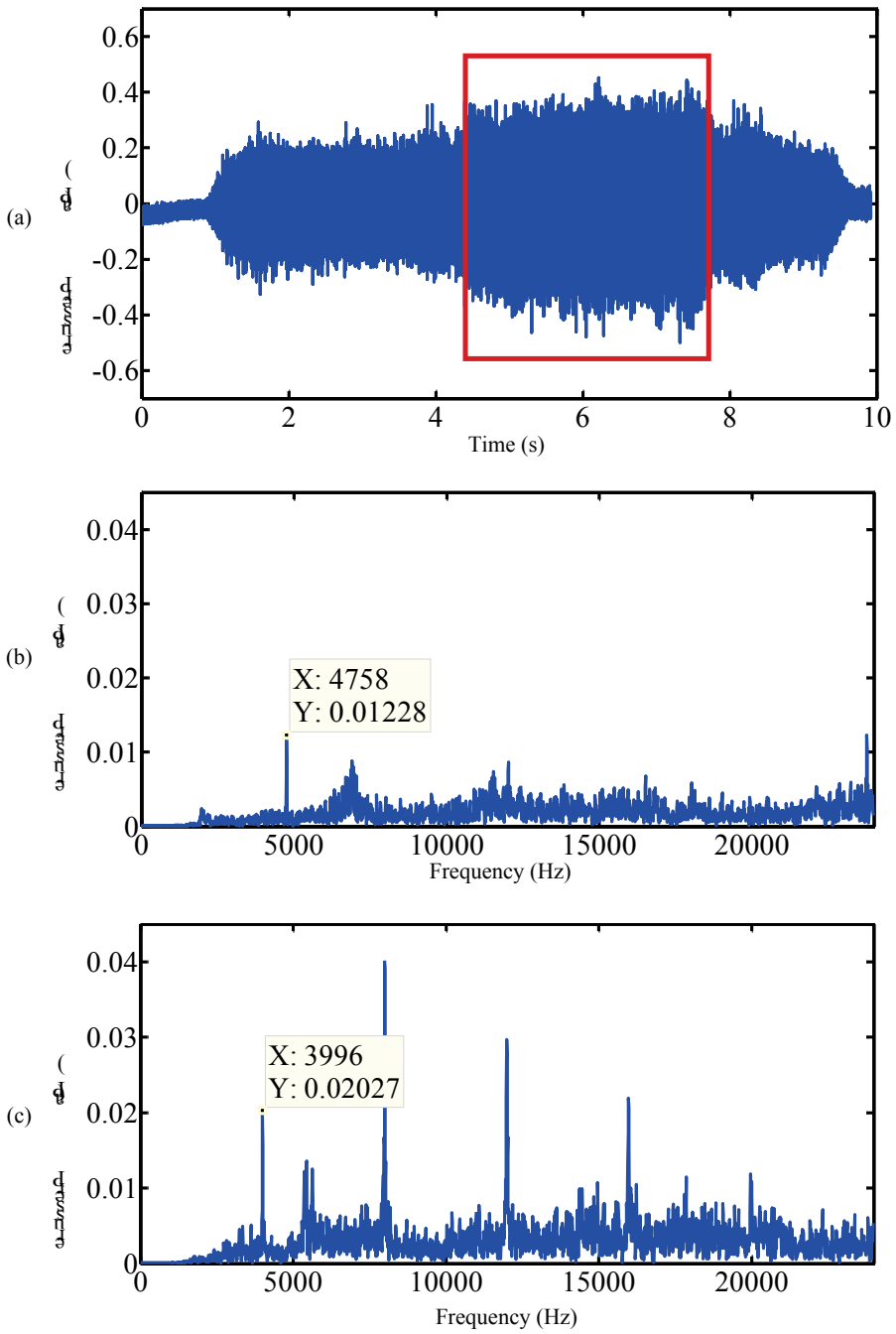

Figure A. 1 ***Manual data labeling; (a) The time–domain representation of a recorded signal. The selected data inside the red box indicate the contact data; (b) The frequency–domain representation of the noncontact data. The frequency of the indicated peak is the handpiece speed; (c) The frequency–domain representation of the contact data. The handpiece speed is decreased in comparison to the noncontact data of (b).***

Appendix B.

Selection of Training Data

In this appendix, the selection of training data for the support vector machine approach is discussed. Two selection schemes for training data were considered. In the first one, all of the training data were used; and in the second scheme, the number of training samples was equal for each class. n_{ad} and n_{ed} are the number of training samples for each class in the "all–data" and "equal–data" schemes respectively. Table B. 1 (TCN case) and Table B. 2 (TAN case) indicate the number of samples (n_{ad} and n_{ed}) for each group of data.

Table B. 1 The Samples' Number in Each Selection Scheme of the Training Data for TCN Case

		Selection Schemes of The Training Data [iii]	
Groups [i]	**Classes** [ii]	**All–Data (n_{ad})** [iv]	**Equal–Data (n_{ed})** [v]
G1	T	1175	620
	C	621	620
	N	2102	620
G2	T	1146	505
	C	508	505
	N	2076	505
G3	T	1187	560
	C	563	560
	N	2068	560

[i]: Different types of training/testing groups are defined in Table 2.1

[ii]: The classes are: T = Tooth, C = Composite, N = Noncontact

[iii]: Selection schemes of the training data are: "all–data" = all of the training data were used; "equal–data" = the number of training samples was equal for each class

[iv]: n_{ad}: the number of training samples for each class in the all–data scheme

[v]: n_{ed}: the number of training samples for each class in the equal–data scheme

Table B. 2 The Samples' Number in Each Selection Scheme of the Training Data for TAN Case

Groups [i]	Classes [ii]	Selection Schemes of The Training Data [iii]	
		All–Data ($\mathbf{n_{ad}}$) [iv]	Equal–Data ($\mathbf{n_{ed}}$) [v]
G1	T	1175	575
	A	577	575
	N	1914	575
G2	T	1146	660
	A	661	660
	N	1925	660
G3	T	1187	650
	A	652	650
	N	1833	650

[i]: Different types of training/testing groups are defined in Table 2.1

[ii]: The classes are: T = Tooth, A = Amalgam, N = Noncontact

[iii]: Selection schemes of the training data are: "all–data"= the number of samples all of the training data were used; "equal–data" = the number of training samples was equal for each class

[iv]: $\mathrm{n_{ad}}$: the number of training samples for each class in the all–data scheme

[v]: $\mathrm{n_{ed}}$: the number of training samples for each class in the equal–data scheme

In obtaining the equal–data scheme of Table B. 1 and Table B. 2, the minimum number of samples among all classes of each group was found. Then, the maximum multiple of 5 which was less than that minimum was considered as $\mathrm{n_{ed}}$. For example in group G2 of Table B. 2, between tooth, amalgam, and noncontact classes; the minimum number of samples belonged to amalgam (661). The maximum multiple of 5 which was less than 661 was 660, and therefore 660 was chosen as the number of each class in the equal–data selection scheme ($\mathrm{n_{ed}}$).

In choosing the $\mathrm{n_{ed}}$ samples out of $\mathrm{n_{ad}}$, an algorithm was used as follow,

- If the difference between $\mathrm{n_{ad}}$ and $\mathrm{n_{ed}}$ was greater than or equal to $\frac{\mathrm{n_{ad}}}{2}$, the training data were down–sampled by 2.
- If the difference between $\mathrm{n_{ad}}$ and $\mathrm{n_{ed}}$ was less than $\frac{\mathrm{n_{ad}}}{2}$ and greater than 4, the training data was divided to five equal parts, and the first sample of each part was excluded.

- If the difference between n_{ad} and n_{ed} was less 5, a number of samples equal to this difference was excluded from the end of training data.

The above algorithm was repeated until n_{ed} samples were obtained.

After selecting the training data, in the TCN case, 64 averaged short–time Fourier Transform (STFT) coefficients were selected as the features; each feature vector was linearly scaled; and the radial basis function (RBF) kernel was used. For the TAN case, 32 averaged STFT coefficients were the extracted features, each feature vector was normally scaled; and the linear kernel was utilized. The data were divided to the training/testing groups as Table 2.1 indicates. The value of hyper–parameters were obtained by a grid–search approach and based on 5–fold cross validation.

Table B. 3 (TCN) and Table B. 4 (TAN) indicate the optimal value of hyper–parameters as well as their corresponding cross validation accuracy for two selection schemes of the training data.

As the results of Table B. 3 indicate, in the TCN case, the cross validation accuracy of both selection schemes was similar to each other. However for TAN case (Table B. 4), the equal–data scheme had better cross validation accuracy than the all–data scheme.

The hyper–parameters of Table B. 3 and Table B. 4 were used to train the classifiers of both cases with different selection schemes of the training data. Table B. 5 (TCN case) and Table B. 6 (TAN case) indicate the accuracy of these classifiers on the testing data.

As the results of Table B. 5 indicate for TCN case, the classification accuracy of the equal–data scheme in the tooth class was more than the all–data scheme for groups G2 and G3. In the classification of the composite class, for all the groups the equal–data scheme was more accurate. Considering the noncontact class, only in group G1 the equal–data had a better performance.

For TAN case, as Table B. 6 shows, similar results were obtained. The equal–data scheme was more accurate than all–data scheme in classification of the tooth (groups G2 and G3), the amalgam (all groups), and the noncontact class (group G3).

Table B. 3 The Hyper–Parameters' Values from 5–Fold Cross Validation for Different Selection Schemes of the Training Data in TCN Case (64 features, RBF kernel, linear scale)

		Selection Schemes of The Training Data [i]	
Groups [ii]	**Hyper–Parameters** [iii]	**All–Data**	**Equal–Data**
G1	γ	1	0.5
	C	32	8
	CV	99	99
G2	γ	1	1
	C	16	32768
	CV	98	98
G3	γ	2	1
	C	32768	32768
	CV	99	99

[i]: Selection schemes of the training data are: "all–data" = all of the training data were used; "equal–data" = the number of training samples was equal for each class

[ii]: G1, G2, and G3 corresponds to data sets specified in Table 2.1

[iii]: C and γ are based on Eq. 2.11, and Eq. 2.13 respectively. CV = 5–fold cross validation accuracy percentage.

In this case, the amalgam classification accuracy of group G1 for the all–data scheme was almost zero (1%)! Even using the equal–data scheme could not enhance the accuracy enough (32%). Therefore for group G1 of TAN case, the number of training samples was manually chosen as for tooth 10 samples, amalgam 50 samples, and noncontact 10 samples. The amalgam classification accuracy for manual–data scheme was significantly improved with respect to the all–data and equal–data schemes.

Table B. 7 (TCN) and Table B. 8 (TAN) represent the classification accuracy range and average of each class for different selection schemes of the training data.

According to Table B. 7, the equal–data scheme had better minimum range accuracy for all classes. The accuracy average of composite class was significantly increased for the equal–data scheme (87%–70% = 17%). In other classes, the average accuracy for both selection schemes was the same. Considering all the groups and

classes, the total accuracy of TCN case was 87% and 89% for all–data and equal–data schemes respectively.

As the results of Table B. 8 indicate, a combination of equal/manual–data scheme (the manual scheme was only used for group G1) had better accuracy range and average for tooth and amalgam classes. The accuracy average of the amalgam class was considerably enhanced for the equal/manual–data scheme (90%–57% = 33%). The total accuracy of TAN case was 86% for the all–data scheme, while it was 92% for the equal/manual–data scheme.

Table B. 4 The Hyper–Parameters' Values from 5–Fold Cross Validation for Different Selection Schemes of the Training Data in TAN Case (32 features, linear kernel, normal scale)

		Selection Schemes of The Training Data [i]	
Groups [ii]	**Hyper–Parameters [iii]**	**All–Data**	**Equal–Data**
G1	C	32768	2
	CV	97	98
G2	C	16	1
	CV	96	98
G3	C	1	1
	CV	96	98

[i]: Selection schemes of the training data are: "all–data" = all of the training data were used; "equal–data" = the number of training samples was equal for each class

[ii]: G1, G2, and G3 corresponds to data sets specified in Table 2.1

[iii]: C and γ are based on Eq. 2.11, and Eq. 2.13 respectively. CV = 5–fold cross validation accuracy percentage

Table B. 5 The Effect of Selection Schemes of the Training Data in Classification Accuracy of TCN Case (64 features, RBF kernel, linear scale)

		Selection Schemes of The Training Data [iii]	
Groups [i]	**Classes** [ii]	**All–Data**	**Equal–Data**
G1	T (579) [iv]	96 [v]	93
	C (225)	64	88
	N (1021)	80	84
G2	T (608)	71	74
	C (338)	80	91
	N (1047)	98	97
G3	T (567)	97	98
	C (283)	63	80
	N (1055)	93	89

[i]: Different types of training/testing groups are defined in Table 2.1

[ii]: The classes are: T = Tooth, C = Composite, N = Noncontact

[iii]: Selection schemes of the training data are: “all–data” = all of the training data were used; “equal–data” = the number of training samples was equal for each class

[iv]: The number of test samples for each group/class is given in the parenthesis

[v]: The accuracy percentage of each group/class with the corresponding selection scheme

Table B. 6 The Effect of Selection Schemes of the Training Data in Classification Accuracy of TAN Case (32 features, linear kernel, normal scale)

		Selection Schemes of The Training Data [iii]		
Groups [i]	**Classes** [ii]	**All–Data**	**Equal–Data**	**Manual–Data**
G1	T (579) [iv]	93 [v]	90	96
	A (368)	1	32	83
	N (922)	89	87	85
G2	T (608)	91	92	–
	A (284)	90	92	–
	N (911)	97	95	–
G3	T (567)	96	97	–
	A (293)	95	97	–
	N (1003)	89	92	–

[i]: Different types of training/testing groups are defined in Table 2.1

[ii]: The classes are: T = Tooth, C = Composite, N = Noncontact

[iii]: Selection schemes of the training data are: “all–data” = all of the training data were used; “equal–data” = the number of training samples was equal for each class; “manual–data” = the number of training samples for group G1 was chosen manually as tooth (10 samples), amalgam (50 samples), and noncontact (10 samples)

[iv]: The number of test samples for each group/class is given in the parenthesis

[v]: The accuracy percentage of each group/class with the corresponding selection scheme

Table B. 7 The Classification Accuracy Range and Average for Different Selection Schemes of The Training Data for TCN Case (64 features, RBF kernel, linear scale)

	Selection Schemes of The Training Data [i]			
Classes [ii]	**All–Data (Range)**	**All–Data (Average)**	**Equal–Data (Range)**	**Equal–Data (Average)**
T	71–97	88	74–98	88
C	63–80	70	80–91	87
N	80–98	90	84–97	90

[i]: Selection schemes of the training data are: "all–data" = all of the training data were used; "equal–data" = the number of training samples was equal for each class

[ii]: T = Tooth, C = Composite, N = Noncontact

[iii]: The percentage of accuracy range and average for each case/class/classification scheme

Table B. 8 The Classification Accuracy Range and Average for Different Selection Schemes of The Training Data for TAN Case (32 features, linear kernel, normal scale)

	Selection Schemes of The Training Data [i]			
Classes [ii]	**All–Data (Range)**	**All–Data (Average)**	**Equal/Manual–Data (Range)**	**Equal/Manual–Data (Average)**
T	91–96	93	92–97	95
A	1–95	57	83–97	90
N	89–97	92	85– 95	91

[i]: Selection schemes of the training data are: "all–data" = all of the training data were used; "equal–data" = the number of training samples was equal for each class; "manual–data" = the number of training samples for group G1 was chosen manually as tooth (10 samples), amalgam (50 samples), and noncontact (10 samples)

[ii]: T = Tooth, A = Amalgam, N = Noncontact

[iii]: The percentage of accuracy range and average for each case/class/classification scheme

Appendix C.

Number of Features (Tables)

Table C. 1 The Hyper–Parameters' Values from 5–Fold Cross Validation for Different Number of Features in TCN case (RBF kernel, linear scale)

Groups [ii]	Hyper–Parameters [iii]	Number of Features [i]								
		2	**4**	**8**	**16**	**32**	**64**	**128**	**256**	**512**
G1	γ	2	4	8	4	2	0.5	0.5	0.25	0.125
	C	8192	128	8	4	4	8	32768	32768	32768
	CV	87	97	99	99	99	99	99	99	99
G2	γ	8	8	8	8	2	1	0.25	0.25	0.03125
	C	32768	512	4	8	16	32768	8	2	4
	CV	82	91	96	98	98	98	98	98	98
G3	γ	4	8	8	8	2	1	0.5	0.25	0.125
	C	32768	64	4	4	8	32768	32768	32768	4
	CV	82	90	97	99	99	99	99	98	98

[i]: The features are averaged short–time Fourier transform coefficients

[ii]: Different types of training/testing groups are defined in Table 2.1

[iii]: C and γ are based on Equations 2.11, and 2.13 respectively. CV = 5–fold cross validation accuracy percentage

Table C. 2 The Hyper–Parameters' Values from 5–Fold Cross Validation for Different Number of Features in TAN case (linear kernel, linear scale)

Groups [ii]	Hyper–Parameters [iii]	Number of Features [i] 2	4	8	16	32	64	128	256	512
G1	C	32768	32	32	32768	32768	32768	32768	32768	32768
	CV	94	94	97	99	99	99	99	97	94
G2	C	2	16	32	16	1	0.25	0.03125	0.03125	0.03125
	CV	80	90	94	96	98	98	98	98	98
G3	C	4	4096	32768	1	1	32768	32768	0.25	0.125
	CV	83	93	96	97	98	98	99	99	98

[i]: The features are averaged short–time Fourier transform coefficients

[ii]: Different types of training/testing groups are defined in Table 2.1

[iii]: C is based on Eq. 2.11. CV = 5–fold cross validation accuracy percentage

Table C. 3 The Effect of Different Number of Features in Classification Accuracy of TCN case (RBF kernel, linear scale)

		Number of Features [i]								
Groups [ii]	**Classes** [iii]	**2**	**4**	**8**	**16**	**32**	**64**	**128**	**256**	**512**
	T (579) [iv]	55 [v]	30	48	75	83	93	96	96	96
G1	C (225)	46	48	66	71	72	88	81	84	83
	N (1021)	87	85	89	88	88	84	76	75	77
	T (608)	58	70	81	75	75	74	73	74	70
G2	C (338)	59	69	76	89	93	91	95	93	94
	N (1047)	98	89	96	96	97	97	97	98	98
	T (567)	60	70	90	97	97	98	96	94	94
G3	C (283)	72	74	23	31	77	80	80	77	81
	N (1055)	89	87	89	80	84	89	91	91	91

[i]: The features are averaged short–time Fourier transform coefficients

[ii]: Different types of training/testing groups are defined in Table 2.1

[iii]: The classes are: T = Tooth, C = Composite, N = Noncontact

[iv]: The number of test samples for each group/class is given in the parenthesis

[v]: The accuracy percentage for each group/class/number of features

Table C. 4 The Effect of Different Number of Features in Classification Accuracy of TAN case (linear kernel, normal scale)

		Number of Features [i]								
Groups [ii]	**Classes** [iii]	**2**	**4**	**8**	**16**	**32**	**64**	**128**	**256**	**512**
	T (579) [iv]	98 [v]	97	97	97	96	95	97	98	98
G1	A (368)	42	78	93	83	83	79	83	85	84
	N (922)	66	72	71	79	85	90	86	82	79
	T (608)	84	87	90	91	92	93	92	92	92
G2	A (284)	100	100	98	87	92	92	94	95	94
	N (911)	62	71	73	91	95	94	97	96	95
	T (567)	96	97	97	97	97	98	98	98	98
G3	A (293)	100	66	70	85	97	99	97	96	94
	N (1003)	62	80	84	89	92	87	89	88	87

[i]: The features are averaged short–time Fourier transform coefficients

[ii]: Different types of training/testing groups are defined in Table 2.1

[iii]: The classes are: T = Tooth, A = Amalgam, N = Noncontact

[iv]: The number of test samples for each group/class is given in the parenthesis

[v]: The accuracy percentage for each group/class/number of features

Appendix D.

Feature Scaling (Tables)

Table D. 1 The Hyper–Parameters' Values from 5–Fold Cross Validation for Different Feature Scaling Methods in TCN Case (64 features, RBF kernel)

		Feature Scaling Methods [i]		
Groups [ii]	**Hyper–Parameters [iii]**	**No Scaling**	**Linear**	**Normal**
G1	γ	2	0.5	0.0078
	C	32768	8	16
	CV	98	99	99
G2	γ	2	1	2.4414e–004
	C	32768	32768,	128
	CV	98	98	98
G3	γ	4	1	0.0156
	C	16384	32768,	32768
	CV	96	99	98

[i]: Linear scaling: scaled to the interval [0,1]. Normal scaling: zero mean and unit variance

[ii]: Different types of training/testing groups are defined in Table 2.1

[iii]: C and γ are based on Equations 2.11, and 2.13 respectively. CV = 5–fold cross validation accuracy percentage

Table D. 2 The Hyper–Parameters' Values from 5–Fold Cross Validation for Different Feature Scaling Methods in TAN Case (32 features, linear kernel)

		Feature Scaling Methods [i]		
Groups [ii]	**Hyper–Parameters [iii]**	**No Scaling**	**Linear**	**Normal**
G1	C	32768	32	32768
	CV	91	100	99
G2	C	32768	64	1
	CV	93	98	98
G3	C	32768	32	1
	CV	94	98	98

[i]: Linear scaling: scaled to the interval [0,1]. Normal scaling: scaled to have zero mean and unit variance

[ii]: Different types of training/testing groups are defined in Table 2.1

[iii]: C is based on Eq. 2.11. CV = 5–fold cross validation accuracy percentage

Appendix E.

Support Vector Machine Kernel (Tables)

Table E. 1 The Hyper–Parameters' Values from 5–Fold Cross Validation for Different SVM Kernels in TCN Case (64 features, linear scale)

		SVM Kernels [i]	
Groups [ii]	**Hyper–Parameters [iii]**	**RBF**	**Linear**
G1	γ	0.5	–
	C	8	8
	CV	99	99
G2	γ	1	–
	C	32768	8
	CV	98	98
G3	γ	1	–
	C	32768	4
	CV	99	97

[i]: RBF: Radial Basis Function (Eq. 2.13); Linear Kernel (Eq. 2.14)

[ii]: G1, G2, and G3 corresponds to data sets specified in Table 2.1

[iii]: C and γ are based on Equations 2.11, and 2.13 respectively. CV = 5–fold cross validation accuracy percentage

Table E. 2 The Hyper–Parameters' Values from 5–Fold Cross Validation for Different SVM Kernels in TAN Case (64 features, normal scale)

		SVM Kernels [i]	
Groups [ii]	**Hyper–Parameters [iii]**	**RBF**	**Linear**
G1	γ	0.0078125	–
	C	32768	32768
	CV	100	99
G2	γ	0.125	–
	C	32	1
	CV	99	98
G3	γ	0.0625	–
	C	128	1
	CV	99	98

[i]: RBF: Radial Basis Function (Eq. 2.13); Linear Kernel (Eq. 2.14)

[ii]: G1, G2, and G3 corresponds to data sets specified in Table 2.1

[iii]: C and γ are based on Eq. 2.11, and Eq. 2.13 respectively. CV = 5–fold cross validation accuracy percentage

Appendix F.

Artificial Neural Network

Artificial neural network (ANN) is another machine learning algorithm that is a very powerful tool for learning complex relationships between inputs and outputs, [84], [113]. Moreover, ANN has been used for classification of audio signals such as speaker, [114] and radar signals, [115].

In this appendix, the artificial neural network is employed for our classification problem. Similar to the SVM approach, for TCN case, 64 averaged STFT coefficients were selected as the features, and each feature vector was linearly scaled. For TAN case, 32 averaged STFT coefficients were selected as the features, and each feature vector was normally scaled. The data for ANN were also divided to the same training/testing groups as Table 2.1. The structure of the ANN, including the hidden and output layers is depicted in Figure F. 1

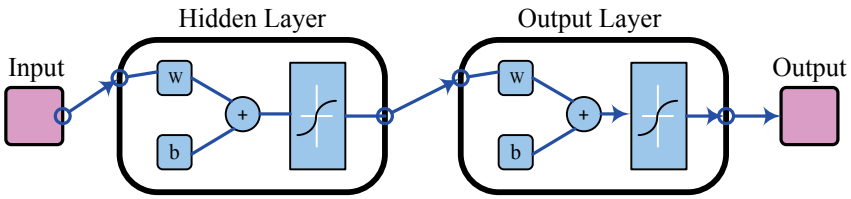

Figure F. 1 The schematic of artificial neural network

In Figure F. 1, the input is the feature vector, and W and b are the weight and bias respectively. The block after the summation block is the activation function that was selected as the "sigmoid" in this study. The sigmoid function (σ) is represented as, [84]

F.1

$$\sigma(\alpha) = \frac{1}{1 + \mathrm{e}^{-\alpha}}$$

where α is the argument of the sigmoid function. To perform the classification, the number of neurons in the output layer was chosen 3 for both TCN and TAN cases, because each case has 3 classes. The class labels in the output were formed as E_i's

$$E_i = \left[\overbrace{0 \dots 0}^{i-1}\ 1\ 0 \dots 0\right] \qquad i = 1, 2, 3 \qquad \text{F.2}$$

In this format, $E_1 = [1,0,0]$, $E_2 = [0,1,0]$, and $E_3 = [0,0,1]$ represents the labels for tooth, composite/amalgam, and non–contact classes respectively. During the training, W and b were found so that the mean–square–error between the network outputs and labels became minimum. For application of this method, neural network toolbox of MATLAB was employed, which utilized backpropagation, [84], for training, and randomly chose the initial values of weights (W) and biases (b). To train the artificial neural network, the same training data were employed that were previously used for the SVM approach. Up to 15% of the training samples were selected randomly for each of the validation and testing purposes. Training automatically stopped when an increase was occurred in the mean square error of the validation samples. The total accuracy (the accuracy of all classes) of the trained network was obtained for the testing samples, and if it was less 95%, the network was retrained with new initial conditions.

Considering the structure of Figure F. 1 for the ANN, the number of neurons (n_{ne}) in the hidden layer was varied from 5 to 50 with the step of 5 for each groups (G1, G2, and G3 in Table 2.1) and cases (TCN and TAN). The network was trained according to the above mentioned procedure, and then its accuracy was obtained for the training data of each group. Table F. 1 and Table F. 2 show the results for TCN and TAN cases respectively.

According to the results of Table F. 1 and Table F. 2, no general trends could be observed for the accuracy of each group/class and the number of neurons (n_{ne}). For example in TCN case, the accuracy of composite and noncontact classes of group G2 did not vary considerably with the number of neurons. In the TAN case, this invariability could be seen for different groups/classes such as amalgam class of group G3. On the other hand, for some values of n_{ne}, the classification accuracy enhanced significantly. For example in TAN case, the accuracy of amalgam class of G1 was increased from

Table F. 1 The Effect of Neuron Numbers in the Hidden Layer on the Classification Accuracy of TCN Case (64 features, linear scale)

		Number of Neurons [i] (n_{ne})									
Groups [ii]	**Classes** [iii]	**5**	**10**	**15**	**20**	**25**	**30**	**35**	**40**	**45**	**50**
	T (579) [v]	80 [iv]	84	79	78	80	81	79	80	80	80
G1	C (225)	87	85	84	80	84	80	82	84	83	81
	N (1021)	79	88	90	92	86	90	92	83	85	91
	T (608)	55	63	62	66	64	59	62	63	59	61
G2	C (338)	95	96	96	94	97	98	95	97	97	96
	N (1047)	94	97	97	97	97	97	97	97	97	97
	T (567)	94	93	91	90	91	93	86	95	93	92
G3	C (283)	63	59	63	73	78	63	79	66	67	61
	N (1055)	94	88	94	95	94	91	94	90	93	92

[i]: Number of neurons (n_{ne}) in the hidden layer of the artificial neural network (Figure F. 1)

[ii]: Different types of training/testing groups are defined in Table 2.1

[iii]: The classes are: T = Tooth, C = Composite, N = Noncontact

[iv]: The accuracy percentage of each group/class and number of neurons

[v]: The number of test samples for each group/class is given in the parenthesis

47% ($n_{ne} = 10$) to 89% for $n_{ne} = 25$ and $n_{ne} = 30$. However, this observation did not mean increasing the number of neurons could increase the accuracy, because for instance the maximum accuracy of tooth in G1 was occurred for $n_{ne} = 5$ (97%). These conclusions were also true for TCN case. For example the least number of neurons ($n_{ne} = 5$) could result in both maximum (87%, composite class of G1) and minimum (55%, tooth class of G2) accuracies.

Considering all the training/testing groups, the accuracy of TCN and TAN classifiers were computed for each number of neurons, and are plotted in Figure F. 2 and Figure F. 3.

Table F. 2 The Effect of Neuron Numbers in the Hidden Layer on the Classification Accuracy of TAN Case (32 features, normal scale)

		Number of Neurons [i] (n_{ne})									
Groups [ii]	**Classes** [iii]	**5**	**10**	**15**	**20**	**25**	**30**	**35**	**40**	**45**	**50**
	T (579) [v]	97 [iv]	88	91	70	51	62	79	60	62	87
G1	A (368)	55	47	51	88	89	89	77	69	85	69
	N (922)	68	98	92	98	98	99	97	99	99	98
	T (608)	83	83	87	83	85	79	87	84	84	83
G2	A (284)	98	99	100	97	97	95	96	95	97	93
	N (911)	95	95	94	94	95	94	95	95	96	97
	T (567)	92	97	98	98	98	98	98	98	98	98
G3	A (293)	96	95	95	95	95	96	95	95	96	96
	N (1003)	81	80	82	83	86	88	86	91	93	85

[i]: Number of neurons (n_{ne}) in the hidden layer of the artificial neural network (Figure F. 1)

[ii]: Different types of training/testing groups are defined in Table 2.1

[iii]: The classes are: T = Tooth, A = Amalgam, N = Noncontact

[iv]: The accuracy percentage of each group/class and number of neurons

[v]: The number of test samples for each group/class is given in the parenthesis

In the TCN case as Figure F. 2 shows, the ANN approach resulted in the highest classification accuracy for noncontact class. The next most accurate class was composite, and the tooth had the least classification accuracy among all. To choose the best number of neurons in using the ANN approach, the total accuracy among all groups/classes was considered. The maximum of the total accuracy in the TCN case was 88% that was obtained for $n_{ne} = 20$.

In the TAN case as Figure F. 3 indicates, a distinct order of classification accuracies could not be observed for different classes (similar to what was seen in the TCN case); however for high–values of n_{ne} (i.e. $n_{ne} \geq 35$), there was an order of high to low accuracies for noncontact, amalgam, and tooth respectively.

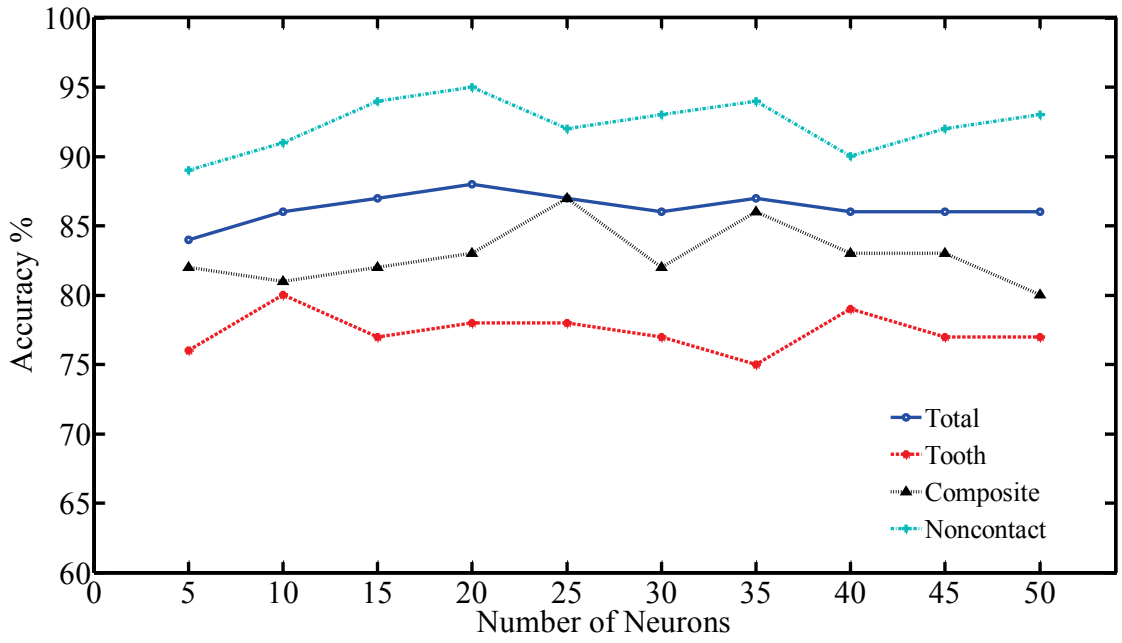

Figure F. 2 ***The effect of the neuron numbers in the hidden layer on the classification accuracy of TCN case considering all the training/testing groups (64 features, linear scale)***

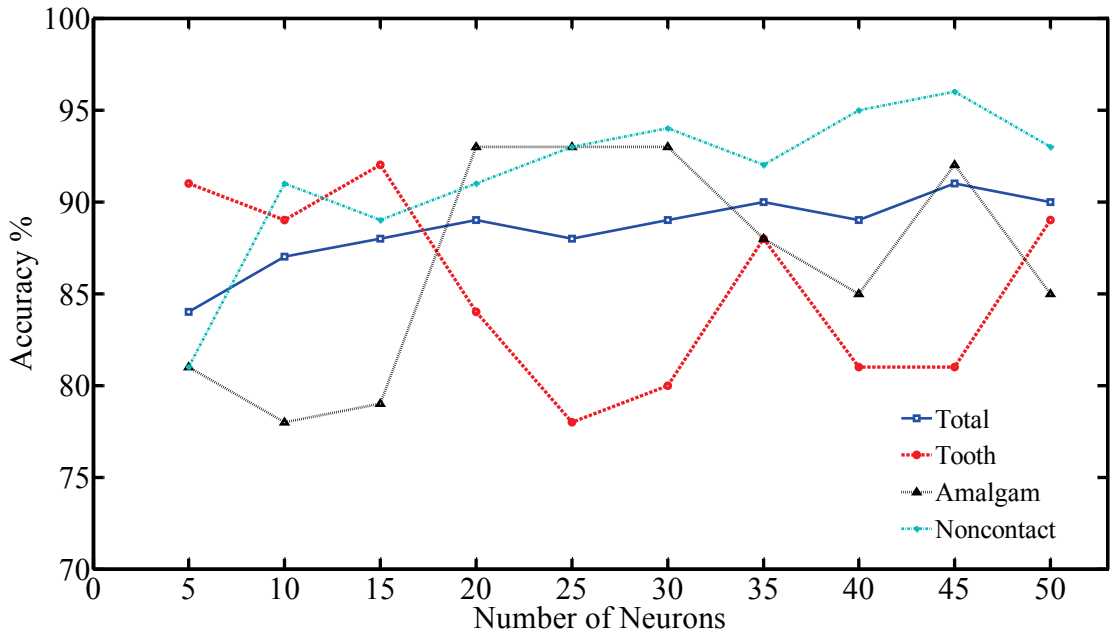

Figure F. 3 ***The effect of the neuron numbers in the hidden layer on the classification accuracy of TAN case considering all the training/testing groups (32 features, normal scale)***

Similar to the previous case, the total accuracy among all groups/classes was selected to find the best number of neurons. The maximum of the total accuracy in the TAN case was 91% that was obtained for $n_{ne} = 45$.

Considering $n_{ne} = 20$ for TCN and $n_{ne} = 45$ for TAN, the ANN classifier was trained for each case. Table F. 3 (TCN case) and Table F. 4 (TAN case) indicate the accuracy of the trained ANN classifiers on the testing data of each group, and compare the results with the SVM approach.

Table F. 3 The Comparison between the Artificial Neural Network (ANN) and the Support Vector Machine (SVM) Classifiers for TCN Case (ANN: 64 features, linear scale, 20 neurons in the hidden layer; SVM: 64 features, RBF kernel, linear scale)

		Groups [iii]		
Classifiers [i]	**Classes** [ii]	**G1**	**G2**	**G3**
Artificial Neural Network	T	78 (579) [iv]	66 (608)	90 (567)
	C	80 (225)	94 (338)	73 (283)
	N	92 (1021)	97 (1047)	95 (1055)
Support Vector Machine	T	93 (579)	74 (608)	98 (567)
	C	88 (225)	91 (338)	80 (283)
	N	84 (1021)	97 (1047)	89 (1055)

[i]: Artificial neural network and Support vector machine are depicted Figure F. 1 and Figure 2.6 respectively.

[ii]: The classes are: T = Tooth, C = Composite, N = Noncontact

[iii]: Different types of training/testing groups are defined in Table 2.1

[iv]: The classification accuracy percentage of each class/group/classification scheme. The number of testing samples is shown in the parenthesis.

According to Table F. 3 for TCN case, SVM had better results than ANN in the tooth class of all groups. On the other side, ANN was more accurate than SVM for the noncontact class of groups G1 and G3 (for G2, the accuracies were equal). In the composite class, except for group G2, SVM had a better accuracy than ANN. The maximum difference between the accuracies of both classifiers were for the tooth class of G1, in which SVM was 15% (93%–78%) more accurate than ANN.

Table F. 4 The Comparison between the Artificial Neural Network (ANN) and the Support Vector Machine (SVM) Classifiers for TAN Case (ANN: 32 features, normal scale, 45 neurons in the hidden layer; SVM: 32 features, linear kernel, normal scale)

		Groups [iii]		
Classifiers [i]	**Classes** [ii]	**G1**	**G2**	**G3**
Artificial Neural Network	T	62 (579) [iv]	84 (608)	98 (567)
	A	85 (368)	97 (284)	96 (293)
	N	99 (922)	96 (911)	93 (1003)
Support Vector Machine	T	96 (579)	92 (608)	97 (567)
	A	83 (368)	92 (284)	97 (293)
	N	85 (922)	95 (911)	92 (1003)

[i]: Artificial neural network and Support vector machine are depicted Figure F. 1and Figure 2.6 respectively.

[ii]: The classes are: T = Tooth, A = Amalgam, N = Noncontact

[iii]: Different types of training/testing groups are defined in Table 2.1

[iv]: The classification accuracy percentage of each class/group/classification scheme. The number of testing samples is shown in the parenthesis.

As Table F. 4 shows for TAN case, in the tooth class SVM had better results in groups G1 and G2. For the amalgam class, ANN was more accurate than SVM in groups G1 and G2. In the noncontact class, the accuracy of ANN for G1 was near perfect (99%), and for other groups ANN and SVM classifiers had almost a similar performance. The maximum difference between the accuracies of both classifiers was for the tooth class of G1, in which SVM was 34% (96%–62%) more accurate than ANN. Table F. 5 (TCN) and Table F. 6 (TAN) represent the classification accuracy range and average of each class for ANN and SVM classifiers.

As Table F. 5 shows for TCN case, SVM had a better accuracy average for tooth and composite classes while the classification average of the noncontact class was more accurate in the ANN approach. Regarding the accuracy average, the performance of SVM was higher for the tooth class, while ANN had a higher minimum range for the noncontact class. In the composite class, SVM resulted in a more accurate minimum range while ANN had a higher maximum accuracy range.

Table F. 5 ***The Classification Accuracy Range and Average of the Artificial Neural Network (ANN) and the Support Vector Machine (SVM) Classifiers for TCN Case (ANN: 64 features, linear scale, 20 neurons in the hidden layer; SVM: 64 features, RBF kernel, linear scale)***

	Classifiers [i]			
Classes [ii]	**ANN (Range)**	**ANN (Average)**	**SVM (Range)**	**SVM (Average)**
T	66–90	78	74–98	88
C	73–94	83	80–91	87
N	92–97	95	84–97	90

[i]: Artificial neural network (ANN) and Support vector machine (SVM) are depicted in Figure F. 1 and Figure 2.6 respectively

[ii]: T = Tooth, C = Composite, N = Noncontact

[iii]: The percentage of accuracy range and average for each case/class/classification scheme

Table F. 6 ***The Classification Accuracy Range and Average of the Artificial Neural Network (ANN) and the Support Vector Machine (SVM) Classifiers for TAN Case (ANN: 32 features, normal scale, 45 neurons in the hidden layer; SVM: 32 features, linear kernel, normal scale)***

	Classifiers [i]			
Classes [ii]	**ANN (Range)**	**ANN (Average)**	**SVM (Range)**	**SVM (Average)**
T	62–98	81	92–97	95
A	85–97	92	83–97	90
N	93–99	96	85– 95	91

[i]: Artificial neural network (ANN) and Support vector machine (SVM) are depicted in Figure F. 1 and Figure 2.6 respectively

[ii]: T = Tooth, A = Amalgam, N = Noncontact

[iii]: The percentage of accuracy range and average for each case/class/classification scheme

In the TAN case as Table F. 6 indicates, ANN had a better accuracy average for amalgam and noncontact classes while the classification average of the tooth class was more accurate for the SVM approach. Regarding the accuracy average, the performance of ANN was higher for the noncontact class, while SVM had a higher minimum range for the tooth class. In the amalgam class, the accuracy range of both methods was almost similar to each other.

Considering the results of Table F. 5, the total accuracy of TCN case for the ANN and SVM classifiers was 88%, and 89% respectively. According to the results of Table F. 6 the total accuracy of TAN case for the ANN was 91% whereas for the SVM classifier it was 92%.